ABSTRACT

Title of Thesis: EVALUATION OF THE THERMAL PERFORMANCE OF FIRE FIGHTER PROTECTIVE CLOTHING WITH THE ADDITION OF PHASE CHANGE MATERIAL

Lee K. McCarthy, Master of Science, 2010

Thesis directed by: Professor and Chair, Marino di Marzo
Department of Fire Protection Engineering

Fire fighters rely on fire fighter protective clothing (FFPC) to provide adequate protection in the various hazardous environments they may encounter during operations. FFPC has seen significant advancement in technology over the past few decades. The addition of phase change material (PCM) to FFPC is a new technology with potential to enhance the thermal protection provided by the FFPC. To explore this technology, data from bench-scale experiments involving FFPC with PCMs are compared with a theoretical finite difference heat transfer model. The results demonstrate an effective method to mathematically model the heat transfer and provide insight into the effectiveness of improving the thermal protection of FFPC. The experiments confirm that the latent heat absorbed during the phase change reduces temperatures that might be experienced at the fire fighter's skin surface, advancing the high temperature performance of FFPC.

EVALUATION OF THE THERMAL PERFORMANCE OF FIRE FIGHTER PROTECTIVE CLOTHING WITH THE ADDITION OF PHASE CHANGE MATERIAL

By

Lee K. McCarthy

Thesis submitted to the Faculty of the Graduate School of the
University of Maryland, College Park, in partial fulfillment
of the requirements for the degree of
Master of Science
2010

Advisory Committee:

Professor Marino di Marzo, Chair
Professor James Quintiere
Professor Peter Sunderland

Acknowledgements

Gratitude is extended to the staff members of the Building and Fire Research Lab at NIST. In particular, the technical guidance and or assistance from Nelson Bryner, Dr. George Braga, Dr. Rick Davis, Dr. Francine Amon, Dan Madrzykowski, Roy McLane, Christopher Kyle Smith, and members of the Fire Fighting Technology Research Group were invaluable resources during this research. This work was partially funded by the U.S. Department of Homeland Security (DHS) and the National Institute of Standards and Technology (NIST).

The author is greatly indebted to Dr. Marino di Marzo, Professor and Chair of the Fire Protection Engineering department at the University of Maryland, for guiding me through this process and to Dr. James Quintiere and Dr. Peter Sunderland for participating in the advisory committee.

Finally, the author would like to express his most sincere appreciation to his family for their continued support and especially to his grandfather, Dr. George Frank Pittman, for his unwavering guidance and encouragement throughout the author's education and lifetime. You are truly an inspiration.

Table of Contents

List of Tables

List of Figures

Nomenclature

c_p	specific heat capacity	$[kJ/kg{\cdot}K]$
F_o	finite difference form of the Fourier number $= \frac{\alpha \Delta t}{\Delta x^2}$	
k	thermal conductivity	$[kW/m{\cdot}K]$
l	total thickness	$[m]$
L	latent heat of fusion	$[kJ/kg]$
q	energy	$[kJ]$
SA	surface area	$[m^2]$
t	time	$[s]$
T	temperature	$[K]$
x	distance from front boundary position	$[m]$
α	thermal diffusivity $= \frac{k}{\rho \ c_p}$	$[m^2/s]$
Δx	thickness	$[m]$
Δt	time step	$[s]$
ΔT	temperature change	$[K]$
ρ	density	$[kg/m^3]$

Subscripts

batting	batting layer
face_cloth	face cloth layer
in	into control volume of interest
m	melting
n	at or associated with control volume n
out	out of control volume of interest
PCM	phase change material layer

PCM-1	associated with 1 control volume prior to PCM layer
PCM-2	associated with 2 control volumes prior to PCM layer
PCM+1	associated with 1 control volume after PCM layer
PCM+2	associated with 2 control volumes after PCM layer
r	range
stored	stored in control volume of interest
total	total thermal liner (face cloth and batting) layer
1	low temperature of melting range
2	high temperature of melting range

Superscripts

N	next time step
"	per unit area
‴	per unit volume
•	rate (per time)

Chapter 1: Introduction

When fire fighters go to work they are exposed to wide variety of thermal environments. Fire fighters can be exposed to radiant heat fluxes that range from relatively low values in small fires and routine activities to much higher, more extreme radiant heat fluxes experienced during the onset of flashover. Even with the significant improvement to fire fighter protective clothing, burns still rank among the top three categories for fire fighter injuries and fatalities [1, 2].

Incorporating phase change materials (PCMs) into fire fighter protective clothing is a new technology thought to improve the thermal performance of fire fighter protective clothing. Although this technology has recently gained the interest of some researchers, limited performance data or analysis has been completed to date. Initial publications on the topic present encouraging results and indicate potential for significant improvements in thermal performance.

This study used bench-scale experiments to examine the use of several different PCMs embedded in fire fighter protective clothing specimens. The specimens were exposed to different heat fluxes and durations in an attempt to simulate realistic fire fighting conditions. Experimental results of specimens with the PCMs were compared to standard fire fighter protective clothing specimens. This provided insight to the additional thermal performance of fire fighter protective clothing provided by PCMs.

To more fully understand the performance envelop of PCMs, a theoretical model was created, which predicted temperatures between different layers of the fire fighter protective clothing. This model allows the simulation of thermal performance over a wide range of conditions and configurations. It uses a finite difference scheme that extended previous research to incorporate the effects of PCM. The model displayed excellent agreement with the experimental data, and demonstrated an effective method of modeling the effects of PCM in fire fighter protective clothing. Results from this study improve the understanding of the new technology, and demonstrate of the potential benefits of using PCMs in fire fighting protective clothing.

1.1 Previous Research

Research to better understand the heat transfer and safe use limits for fire fighter protective clothing has been conducted by a wide range of organizations. The development of NFPA 1971 *Standard on Protective Ensembles for Structural Fire Fighting and Proximity Fire Fighting* [3], which was first adopted by the National Fire Protection Association (NFPA) in 1975, has helped to drive the improvement of protection provided for fire fighters. Significant research efforts focused on fire fighter protective clothing have been made by several institutions and universities including the Building and Fire Research Lab (BFRL) at the National Institute of Standards and Technology (NIST) [4], the Center for Research on Textile Protection and Comfort (T-PACC) at North Caroline State University (NCSU) [5], and the National Personal Protective Technology Laboratory (NPPTL) at the National Institute for Occupational Safety and Health (NIOSH) [6].

Recently, the addition of PCM to thermal protective clothing has become an area of increasing interest. Initial research efforts have begun to create mathematical models of PCM performance in textiles, as well as some models for fire fighter protective clothing with heat exposures that fire fighters might experience. Preliminary results indicate that PCM technology could enhance the performance of fire fighter protective clothing, but further research and technology development is necessary.

1.1.1 Fire Fighter Protective Clothing

Fire fighter protective clothing is designed to provide the fire fighter a limited level of protection from various exposures to thermal environments. Research is ongoing to understand the limits of the thermal performance of fire fighter protective clothing and the factors that contribute to fire fighter burn injuries and fatalities. Many factors such as air gaps, moisture, stored energy, previous heat exposures, degradation, age and other phenomena contribute to the complexity of the heat transfer.

Researchers at NIST have published several reports examining the thermal performance of fire fighter protective clothing [7 - 10]. A computer program was developed to predict the performance of fire fighter protective clothing. This research has greatly increased the understanding of the heat transfer through fire fighter protective clothing and provided insight into the thermal limits.

Some additional research has focused on improving the current testing standards used to evaluate the performance of fire fighter protective clothing [11, 12]. These efforts not only increase understanding, but drive innovation of new technology. NIOSH, NIST and NCSU collaborated on a recent report investigating a new test technique to capture the effect of stored thermal energy in fire fighter protective clothing [13]. Additional studies on improving test standards have been completed and continue to be topics of research [14].

Numerous other publications have contributed to understanding the thermal performance and modeling the heat transfer in fire fighter protective clothing [15-17]. One particular study by Spangler [18] is the basis for the model created in this report. The model used a multiple layer finite difference scheme that was solved with a tridiagonal matrix algorithm. This model allowed simulations of thermal performance to compare with empirical data.

1.1.2 Phase Change Materials

Phase change material typically refers to a material that has a high heat of fusion. This heat of fusion allows the PCM to store or release a large amount of energy during the phase change (Figure 1.1). PCMs have been developed and used in many applications. Some of these applications include protection of instruments and astronauts in space from the extreme temperature fluctuations, improvement to building component insulation in construction, cooling packs, and a variety of outdoor apparel such as ski wear, hunting clothing, boots, gloves, ear warmers, etc. [19 - 24].

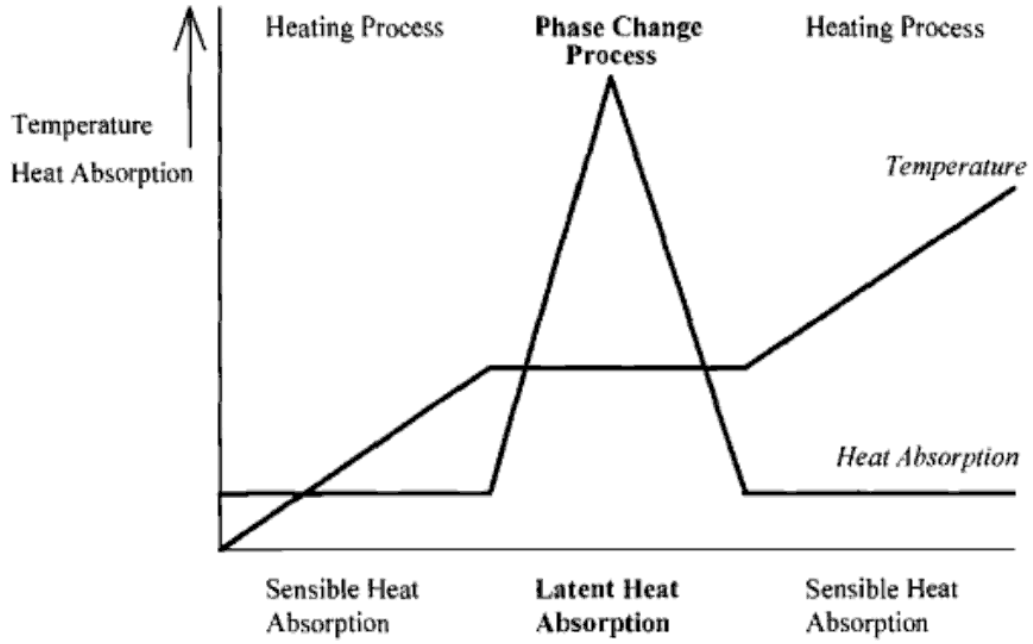

Figure 1.1: Phase Change Effect. Reproduced from [25].

There are known to be more than 500 natural and synthetic PCMs [26]. Although the type of PCM used with fire fighter protective clothing could be a future concern due to flammability or other considerations, these factors were not considered in this research. Rather, focus was placed on gaining additional understanding of the potential thermal benefits of the technology. During the phase change, the PCM changes from a solid to a liquid. This is often undesirable for practical applications because the PCM could melt and drip away. To combat this, often the PCM is bound, micro-encapsulated or macro-encapsulated [27, 28]. This prevents the PCM dissolution, contains the material, resists mechanical actions, and often maintains the same form with little volumetric expansion [25].

Interest in applying the use of PCMs to aid fire fighters has recently gained attention by some researchers. Some of this research has focused on using PCMs to actively cool fire fighters after exiting a thermal environment in order to reduce the heat stress [29]. Other researchers have begun to look at the potential benefit of adding PCM to the fire fighter protective clothing for improved heat protection and thermal performance. The potential benefits of using PCMs to passively cool fire fighters, is the focus of this report. Previous models have explored heat transfer with phase change material [30 - 33], but until recently, modeling of PCM in fire fighter protective clothing was not examined.

In 2005, Rossi and Bolli [34] published an article on a study of fire fighter protective clothing with PCM that was exposed to heat fluxes of 5 and 10 kW/m². The study predicted temperatures with a simple thermal model that considered the steady-state heat flux. The study concluded that PCM offers a good means of increasing the heat protection of fire fighter protective clothing.

In 2007, Mercer and Sidhu [35] demonstrated a method to mathematically model the heat transfer through fire fighter protective clothing with PCM. They chose to model fire fighter protective clothing for two scenarios that they described as a flash fire scenario (82.3 kW/m² for 3 s) and low intensity fire fighting (1.2 kW/m² for 5 min). The results of their model showed significant improvement in the thermal protection with the addition of PCM.

1.2 Problem Statement

Each year in the U.S. approximately 100 fire fighters die in the line of duty, and more than 80,000 are injured [36, 2]. Although not the leading cause of fatalities, burns were the third largest category of fatalities in 2008 accounting for approximately 7% of the fire fighter deaths [2]. For the period between 2003 and 2006 burns were the third largest category of minor injuries accounting for 11% of the minor injuries and the second largest category of moderate to severe injuries accounting for 9% of those injuries [1]. Advancing the technology and understanding of fire fighter protective clothing may reduce some of the fatalities and injuries.

As previously acknowledged, research on phase change material incorporation into fire fighter protective clothing is in the development stage. Early studies have indicated great promise of thermal improvement with the incorporation of PCM technology. While there have been some studies on mathematical models [35] and some studies with experimental data [34], no existing study creates a model specific to fire fighting clothing, uses the model to simulate realistic conditions, and compares the results to empirical data.

This study provides an effective method, authenticated by bench-scale experimental data, to mathematically model the heat transfer through fire fighter protective clothing that includes PCM. The modeling of the phase change properly captures the effect of the PCM, and demonstrates the potential for improved thermal performance of fire fighter protective clothing with the addition of PCMs.

Chapter 2: Bench-Scale Experiments

A series of bench-scale experiments were conducted to examine how PCM impacts the thermal protection provided by fire fighter protective clothing. These experiments included fire fighter protective clothing specimens both with and without the addition of phase change material. The protective clothing specimens were initially exposed to three different heat fluxes and exposure durations (Table 2.1).

Table 2.1: Thermal Exposures for Experiments

Series	Exposed Heat Flux (kW/m^2)	Duration of Heat Exposure (min)	Duration of Cooling (min)
LF (low flux)	2.5	15	10
MF (medium flux)	10	5	10
HF (high flux)	20	0.5	10

The thermal exposures were derived from previous work defining thermal classes by Donnelly et al. [37] as well as previous published work on typical fire fighter exposures and working environments [38]. The experiments were designed to approximate the recommended thermal classes II, III, and IV [37]. For the thermal class IV, which was not strictly defined, a 20 kW/m^2 heat flux was chosen for 30 s. This represented an exposure for less than one minute to a heat flux that is approximately the flux at the floor of a room at the beginning of flashover [38]. The intent was to subject each specimen to the three different exposures to capture the performance of fire fighter protective clothing in a range of realistic fire fighting conditions.

After an initial test series, which included all three thermal exposures, the scope of the work was isolated to the Series MF. The results from the initial test series can be found in Appendix B (Figure B-1 – Figure B-12). The temperatures displayed in those figures are an average of the three thermocouples behind each layer. When examining the behind the face cloth position graphs for each series, the temperature curve variations display the effects of the different PCMs in Series LF and MF, but little variation was observed for the Series HF.

While distinctions between the PCMs were observed for both the MF and LF exposures, Series MF was chosen for several reasons. First, the exposure was at a heat flux prior to the onset of flashover that could reasonably be assumed to cause burns to fire fighters. Fire fighters exposed to relatively low heat fluxes in typical working environments may not be burned as often, while fire fighters exposed to flashover or conditions with heat fluxes much higher than the Series MF have a small chance of survival regardless of the performance of the protective clothing. Furthermore, the Series MF heat flux is at a level that is used in other personal protective equipment standards [39].

Series MF was completed three times for each of the specimen configurations of interest. The justification for the specific specimens configurations are discussed in the *Protective Clothing Test Specimens* section below. The complete experimental matrix, with a total of thirty experiments, is displayed in Table 2.2.

Table 2.2: Experimental Matrix

Specimen Configuration	Series LF	Series MF	Series HF	TOTAL
Standard	1	3*	1	5
PCM A	1	1	1	3
PCM B	3*	3*	3*	9
PCM C	1	3*	1	5
PCM D	1	3	1	5
PCM E	1	1	1	3
				30

Indicates specimens of interest that are analyzed and compared with the theoretical model

2.1 Experiment Components

This experimental set up and apparatus have been used for research in multiple studies at NIST [7, 40 - 42]. A detailed description by Lawson and Twilley [41] was published when the apparatus was developed, as well as several other descriptions with similar experimental set ups, including that by Vettori et al. [42]. Similarly to the other experimental set ups, the major components used in this test series consisted of a radiant panel, a moving trolley assembly capable of securing the fire fighter protective clothing specimens, measurement instrumentation, and a data acquisition system (Figure 2.1 and Figure 2.2).

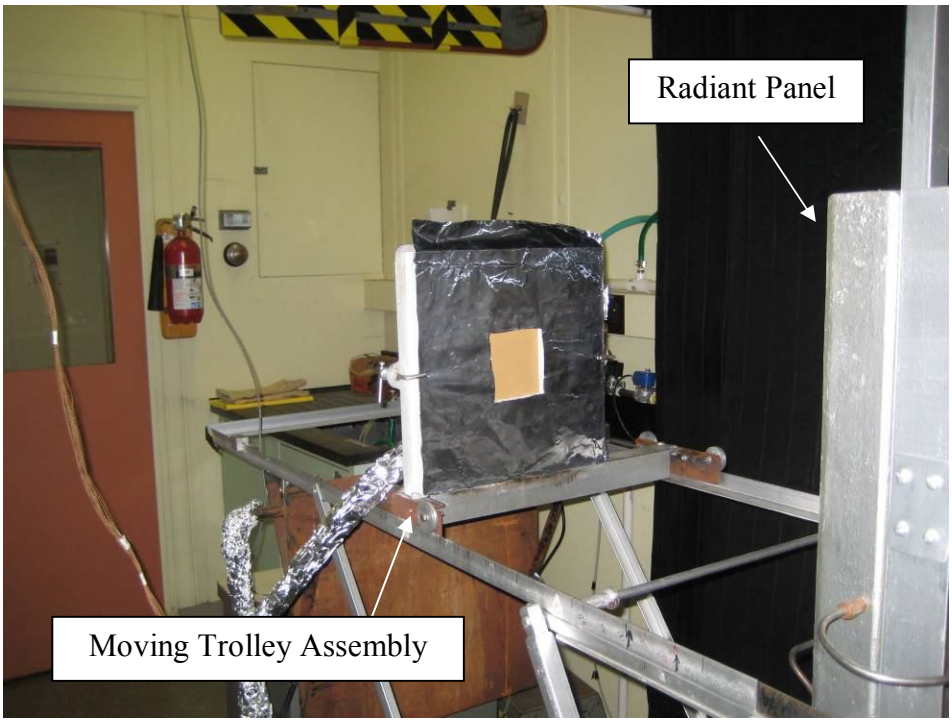

Figure 2.1: Experimental Setup View 1. Original in color.

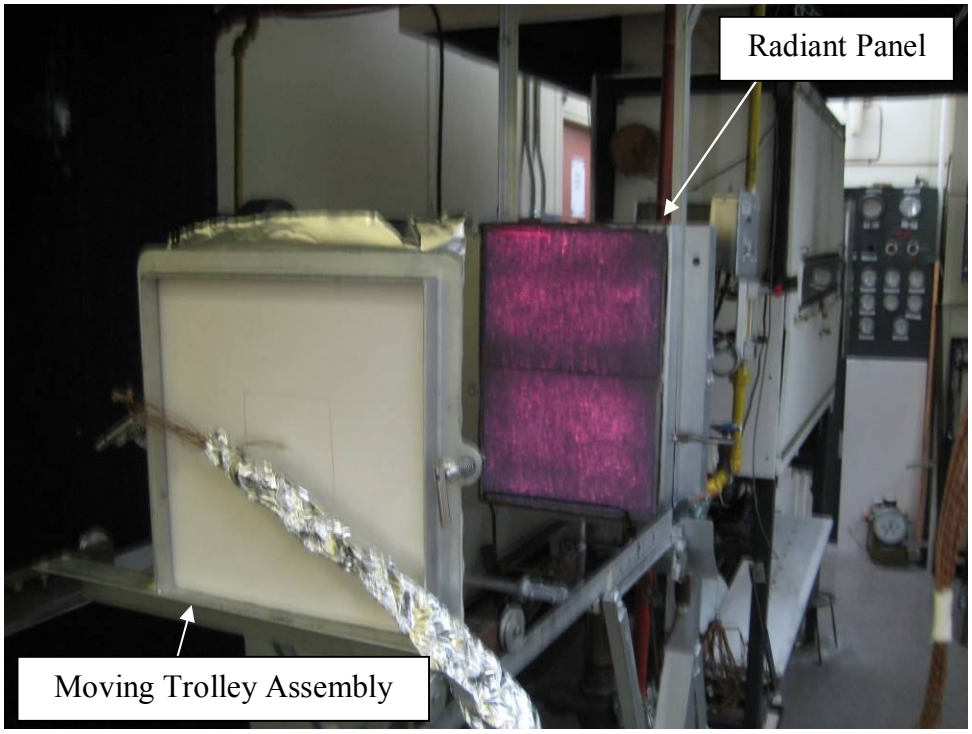

Figure 2.2: Experimental Setup View 2. Original in color.

Experimental Facility

These experiments were conducted at NIST's Building Fire and Research Laboratory Radiant Panel Laboratory. This is a controlled laboratory environment, and tests were conducted under an exhaust hood. A first level hazard assessment was completed for the laboratory space and all participants were required to complete adequate training before any experimentation commenced.

Radiant Panel

The radiant energy source for these experiments was produced by a premixed air/natural gas fueled radiant panel (Figure 2.2) with an exposure surface of 305 mm by 457 mm (12 in by 18 in). The radiant panel is specified in ASTM E162, Standard Test Method for Surface Flammability of Materials Using a Radiant Heat Source [41]. This radiant panel is normally operated at an average surface blackbody temperature of 943 K ± 4 K (1238 ± 7 °F) [42].

Protective Clothing Test Specimens

The protective clothing test specimens measured approximately 152 mm x 152 mm (6 in x 6 in) and generally consisted of three layers: the outer shell, moisture barrier, and thermal liner (Figure 2.3 and Figure 2.4). The outer shell and moisture barrier were the same for all specimens, however the thermal liners varied.

Fire fighter protective clothing thermal liners are typically comprised of a face cloth and at least one layer of batting that are sewn together [44]. All of the thermal liners included in the testing had a face cloth and only one layer of batting. The batting and face cloth were sewn together for all the specimens. Some of the test specimens had various amounts of PCM sewn in between the batting and the face cloth of the thermal liner (Figure 2.5). A complete listing of the thermal liner configurations used in this study is found in Table 2.3.

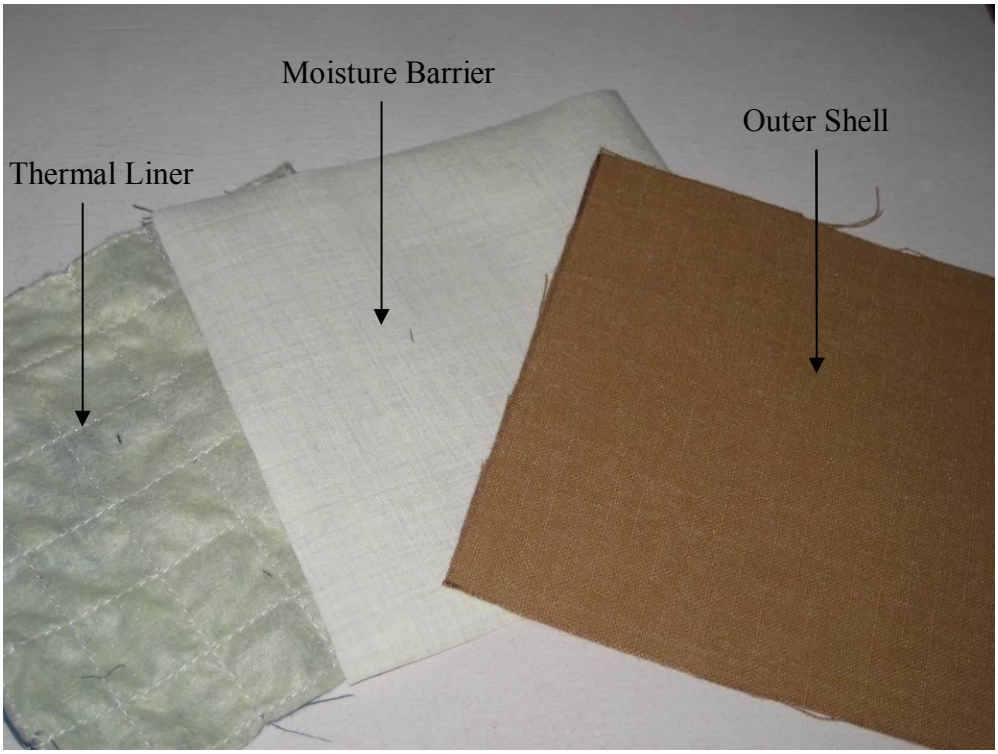

Figure 2.3: Fire Fighter Protective Clothing (outside to inside). Original in color.

Figure 2.4: Fire Fighter Protective Clothing (inside to outside). Original in color.

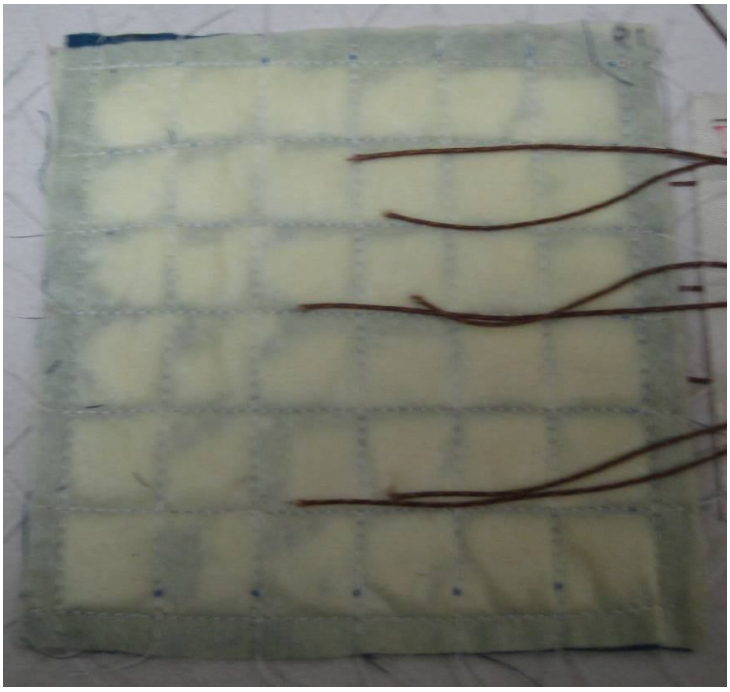

Figure 2.5: Thermal liner with PCM Sewn in. Original in color.

Table 2.3: Thermal Liner Configurations

Configuration	# of Tests	Materials Sewn Together
Standard	5	Face Cloth, 1 Layer of Batting
PCM A	3	Face Cloth, PCM_A, 1 Layer of Batting
PCM B	9	Face Cloth, PCM_B, 1 Layer of Batting
PCM C	5	Face Cloth, PCM_C, 1 Layer of Batting
PCM D	5	Face Cloth, PCM_D, 1 Layer of Batting
PCM E	3	Face Cloth, PCM_E, 1 Layer of Batting

The configurations were selected to compare various types of PCM to typical fire fighter protective clothing configurations. The amount of PCM was selected to be both an adequate amount and a multiple of the approximate mass of a 152 mm x 152 mm (6 in x 6 in) layer of batting (1.5 g ±0.1 g). Future experiments and models could compare the performance of several layers of batting to PCMs of equivalent weight or thickness. While the amount of PCM varied slightly between specimens, the average mass from a total of 50 specimens was 15 g ± 1 g.

To gain additional information for the PCMs used in this study, Differential scanning calorimetry (DSC) was performed for each material (Appendix B). This technique displays the amount of heat required (*W/g*) to increase the temperature of a material as compared to a reference material as a function of temperature. The DSC technique works on the principle that when a material undergoes a phase change, more or less heat will need to flow to that material to maintain the same temperature as the reference material. The results display similarities to Figure 1.1. All the graphs show an exponential

increase, a peak, and then an exponential decrease in the amount of heat absorbed to raise the temperature of the material. The level portions of the graphs show the sensible energy absorption, while the peak shows the latent heat absorption. Some of the DSC results showed two peaks, which is probably due to the mixture of materials in the PCM.

After the scoping experimentation, focus was placed on the PCM B configuration. This decision was based on the various melting temperature ranges for the different PCMs. It has been published that pain is felt when human skin reaches approximately 44 °C (111 °F) and second degree burns occur at approximately 55 °C (131 °F) [45]. Delaying the time lapse between when the fire fighter would experience pain and when a second degree burn might occur provides optimal protection. A schematic of the temperature gradient in fire fighter protective clothing is displayed in Figure 2.6. Although the actual temperature gradient is not strictly linear and the layer thicknesses are not to scale as depicted, the figure conveys the idea that each additional layer or air gap decreases the temperature from the outer surface. The face cloth layer, air gap, and clothes the fire fighter wears under the fire fighter protective clothing would lower the temperature beyond that of the PCM layer, so the ideal melting temperature would start somewhere above 44°C.

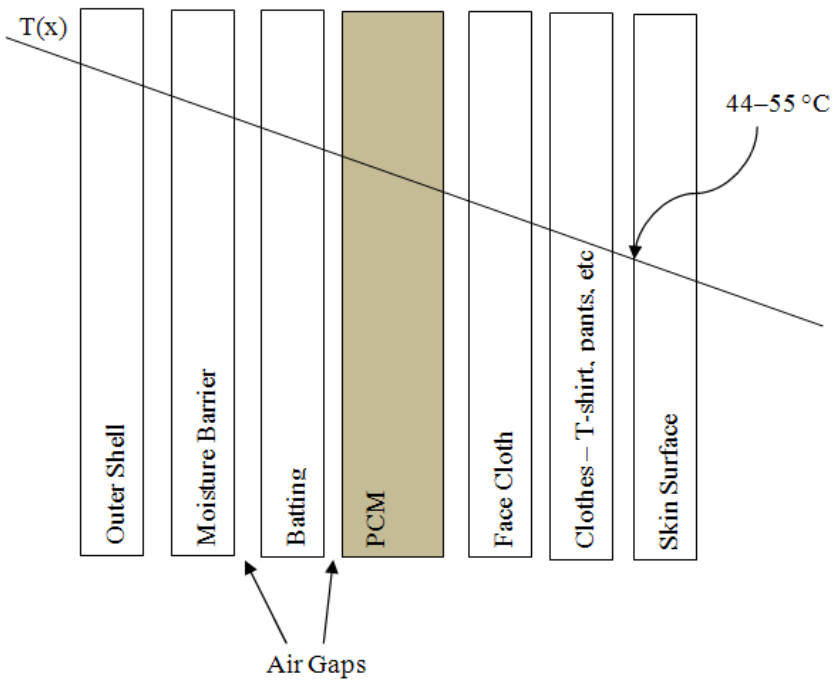

Figure 2.6: Schematic of Temperature Gradient in Fire Fighter Protective Clothing

There are numerous variables to consider when predicting the temperature difference between PCM layer and the skin surface, so a close examination was not performed in this study. Based on the results of the bench scale experiments, fire fighter protective clothing layers and air gaps indicate an estimated temperature decrease of 10–40 °C. Assuming the materials between the PCM and the skin would perform similarly, this would yield an ideal melting temperature range starting around 54–84°C. Figure 2.7 displays the melting temperatures of the different PCMs included in this study [27]. It was important to consider that for the PCM to be beneficial to the fire fighter, it must melt prior to the fire fighter receiving burns. Therefore, the best option was determined to be PCM B because its melting temperature range (44–55 °C) was close to the ideal

range while ensuring to a starting melting temperature lower than the expected temperatures that the fire fighter would receive burns.

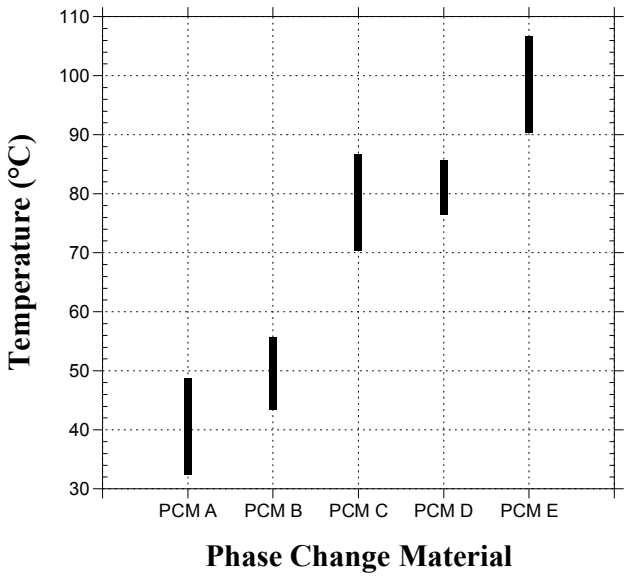

Figure 2.7: Melting Temperatures of the PCMs

Not only was the melting temperature of PCM E too high, but the material melted and dripped out of the fire fighter protective clothing during the initial Series MF. This is why the graphs in Appendix B show such dramatic effects for the PCM E temperatures. PCM E was therefore eliminated from further testing. PCM A was also eliminated from further testing because it's melting temperature range started at only 34 °C (93 °F), a temperature that could be reached in ambient air in some places on extremely hot summer days.

Although, PCM B was selected as the best option, PCMs C and D were also reasonable options. Three Series MF experiments were conducted for PCM B, C, and D. PCM D was later eliminated from analysis because the material properties were unknown and could not be obtained from the manufacturer. To gain additional data for PCM B, Series LF and HF experiments were also completed for the PCM B configuration.

All specimens were kept in a conditioning room for at least 24 hours prior to testing. This controlled environment was maintained at 19°C ±1°C (66°F ±2°F) 44% ±3% relative humidity.

Trolley Assembly

The specimens were held in place by a holder on a moving trolley assembly that was attached to the radiant heat panel test frame (Figure 2.1 and Figure 2.2). The trolley assembly allowed the specimens to be clamped between two 13 mm (½ in) thick calcium silicate boards. While the back face was a solid calcium silicate board, the front board had a 102 mm x 102 mm (4 in x 4 in) square section removed from the center. This provided the exposure area for the fire fighter protective clothing test specimen. The face of the calcium silicate board closest to the radiant panel was also covered in aluminum foil with the aim of minimizing the heat transfer to the calcium silicate boards.

The radiant panel remained at a constant temperature, so to adjust the incident heat flux imposed on the specimens the trolley assembly was positioned a calibrated distance from the panel. The distance from the radiant panel to achieve the desired heat flux was

determined by the use of a calibrated Schmidt-Boelter total heat flux tranducer, which was placed in the center of the window of the front calcium silicate board. These distances were measured and marked prior to the experimentation. Accurate heat flux positioning was not the goal for these experiments, but rather, the intent was only to compare the various fire fighter protective clothing configurations under reproducible heat exposure conditions.

Measurement Instrumentation

The Schmidt-Boelter total heat flux transducer that was used for approximating the heat flux level at the face of the fire fighter protective clothing specimen was a water cooled, thermopile type, heat flux transducer. It has a nominal range of 0 to 23 kW/m² with a sensitivity of approximately 10 mV at 23 kW/m². The time constant for this heat flux gauge is 250 ms.

Type K (Chromel-Alumel) thermocouples with a glass braid insulated wire diameter of 0.13 mm (0.005 in) and bead diameter of 0.18 mm (0.007 in) were used to obtain temperature data at several locations within the fire fighter protective clothing specimens. The diameter was selected to be approximately $^{1}/_{10}{}^{th}$ the thickness of the individual layers in an attempt to reduce additional errors due to preferred conduction through the thermocouple. Small bead size allowed for more rapid response to changes in temperature. Three thermocouples were placed behind the outer shell, moisture barrier, batting and face cloth (Figure 2.8 - Figure 2.14). To get the thermocouples behind the batting, they were pushed through the batting layer, because the thermal liners (face cloth

and batting) were sewn together. Figure 2.12 shows a close up of the thermocouples both behind and in front of the batting layer (i.e. behind the moisture barrier).

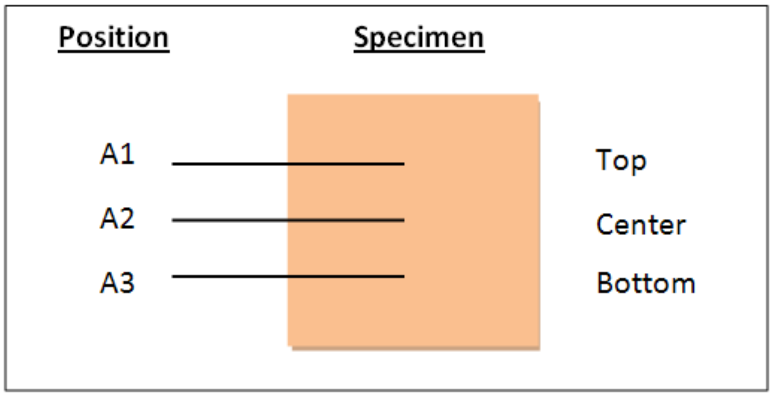

Figure 2.8: Thermocouple (TC) position for each layer.

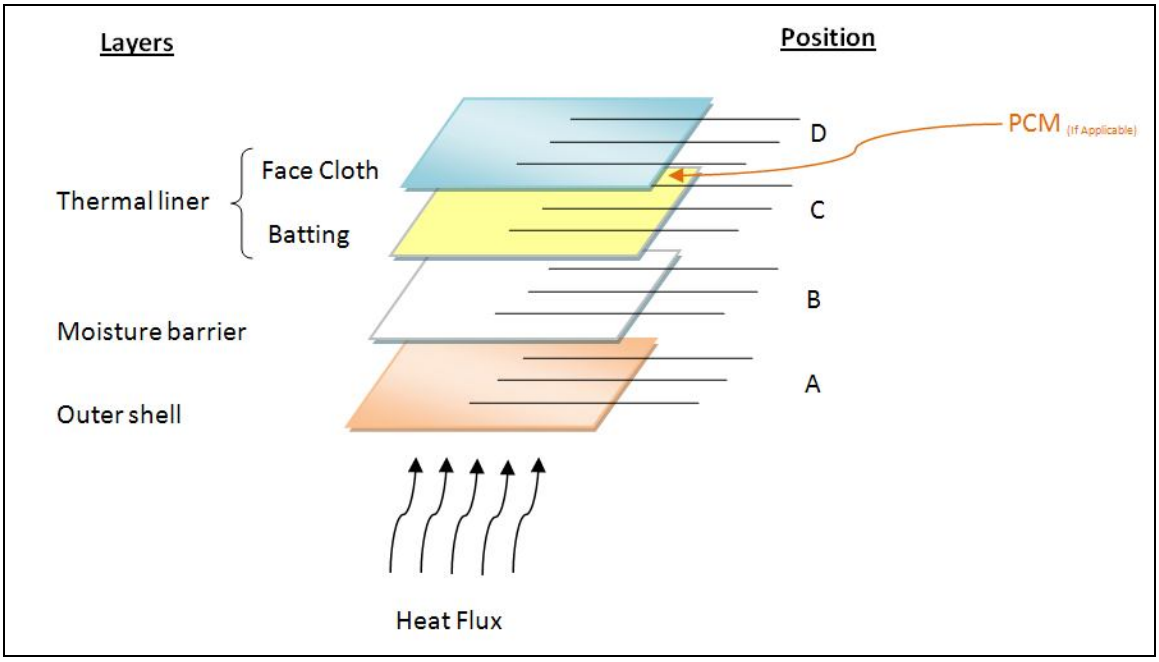

Figure 2.9: Thermocouple positions within specimens.

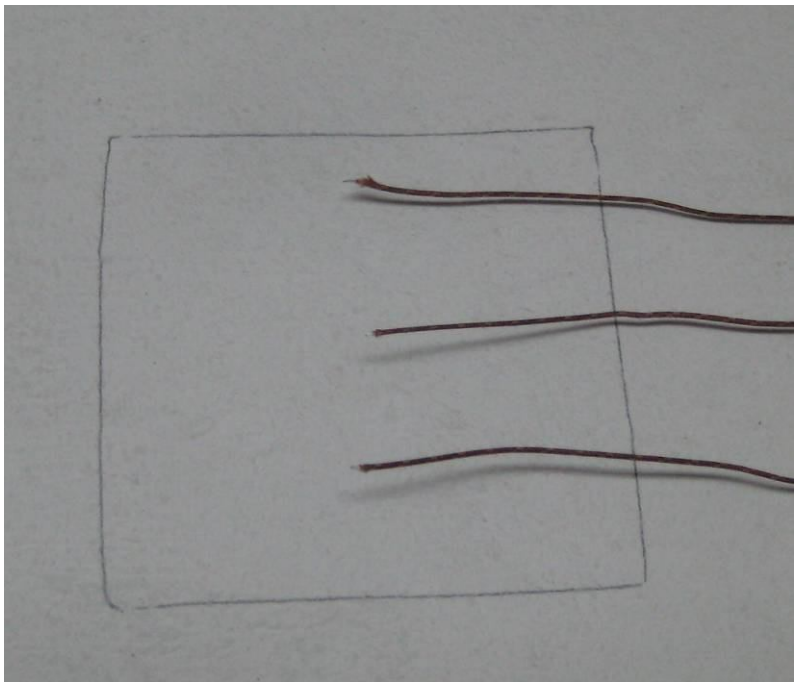

Figure 2.10: TCs behind face cloth. Original in color.

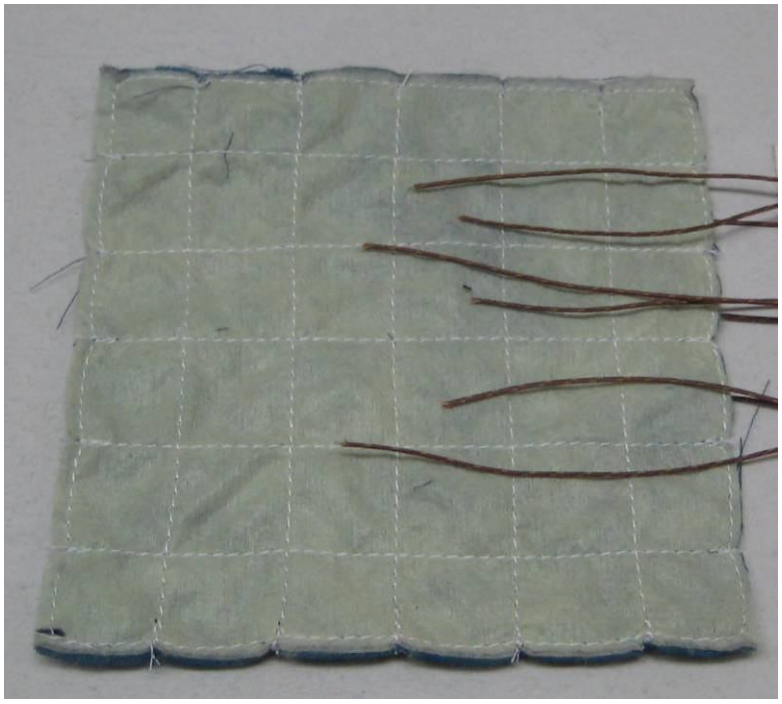

Figure 2.11: TCs behind batting and moisture barrier. Original in color.

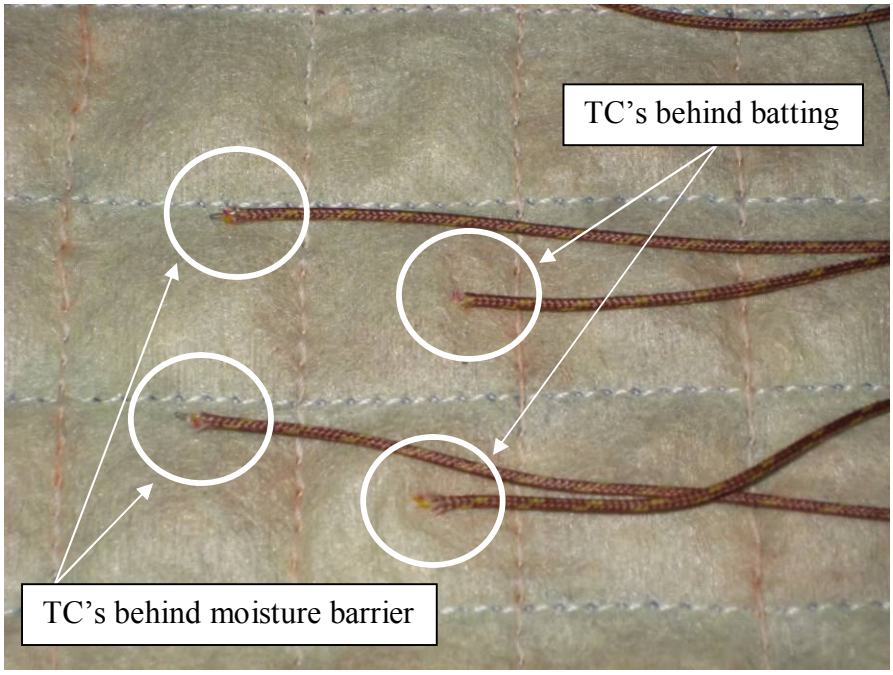

Figure 2.12: Close up of TC positions. Original in color.

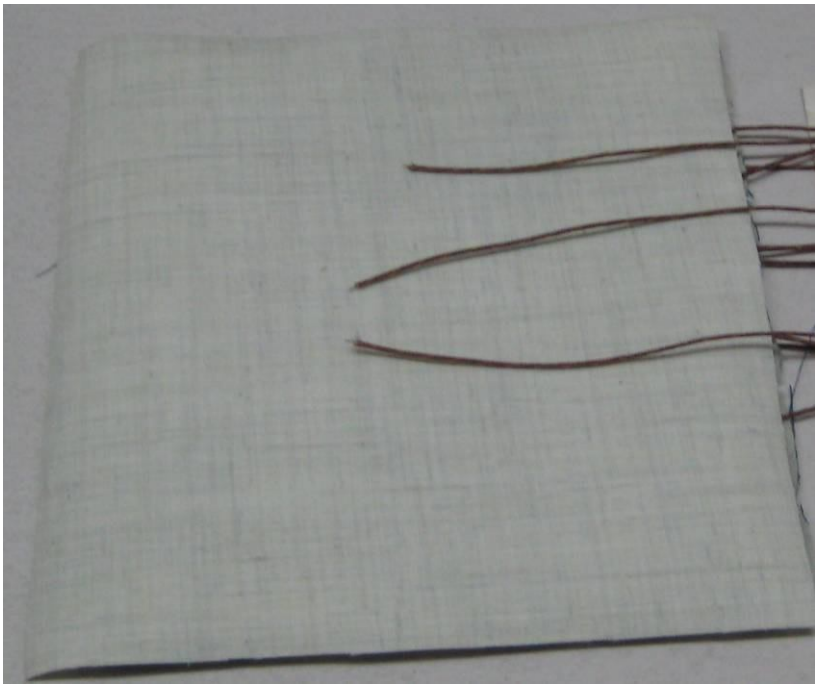

Figure 2.13: TCs behind outer shell. Original in color.

Figure 2.14: Specimen assembled with TCs in place. Original in color.

Additionally, two Type K thermocouples with a glass braid insulated wire diameter of 0.51 mm (0.020 in) and bead diameter of approximately 0.61 mm (0.024 in) were used. One was placed on the back face of the last calcium silicate board (Figure 2.15) and one measured the room temperature at a remote location.

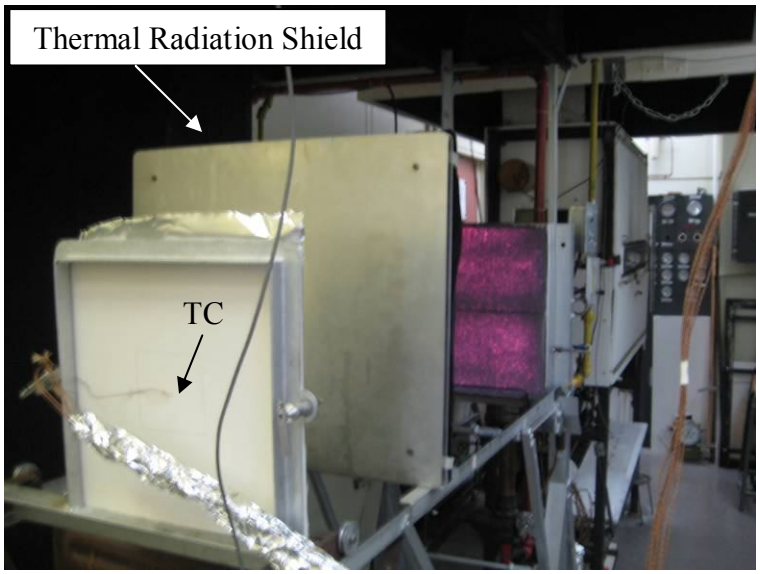

Figure 2.15: Radiant panel set-up with back face TC visible. Original in color.

Data Acquisition

A computer controlled 24-bit data acquisition system was used for recording the results. The data logger has multiple input channels, and data were recorded from each thermocouple and the heat flux transducer every second. The data logger contained a cold junction temperature compensation device for correcting test thermocouple measurements.

2.2 Experimental Procedure

The radiant panel was started 45 minutes prior to the start of any experimentation to ensure adequate time for temperature stabilization as established in previous studies. The trolley assembly distance from radiant panel was calibrated and marked on the radiant panel track for the heat flux of interest using the heat flux transducer. The individual layers of the test specimens were complied on the trolley assembly with the thermocouples positioned appropriately. A thermal radiation shield was put in place to prevent the test specimen from heating prior to the desired start time (Figure 2.15). The trolley assembly was placed into position, heat shield removed and time for the exposure began. After the desired duration (Table 2.1), the heat shield was again placed between the radiant panel and the test specimen, the trolley assembly was moved back, and assembly was allowed to cool. After cooling, the test specimen was removed and the process was repeated for each fire fighter protective clothing specimen in the testing series.

Chapter 3: Theoretical Model

The theoretical model created in this study is an extension of previous work that was mentioned in *Section 1.1.1*. The model utilizes MATLAB® to solve a Crank-Nicolson finite difference method approximation of the governing second order partial differential heat transfer equation. Several assumptions and simplifications were made prior to arriving at the final model. A detailed description of the process follows.

3.1 Initial Assumptions and Estimations

The model is an estimation of the one-dimensional heat transfer exclusively due to conduction. Previous studies and heat transfer principles have demonstrated that the effects of convection need not be considered within the fire fighter protective clothing layers [18, 46]. The Rayleigh number correlation in external free convection is much less than 1000 based on the thicknesses of the air gaps, meaning the buoyancy-driven flow is weak, and heat transfer is primarily by conduction across the fluid [18]. Other studies [7, 8] have included the radiative heat transfer between layers, but these effects were not included herein.

Boundary Conditions

In *Chapter 2*, the different test series were described in regard to the incident heat flux on the outside of the fire fighter protective clothing (Table 2.1). This was done only to convey the idea that the exposures were chosen to capture the performance of fire fighter

protective clothing in a range of realistic fire fighting conditions. This radiant heat flux was not used as the front boundary condition; rather an average of the thermocouple temperature reading from behind the outer shell was used. The heat flux could have been used, but it would have added additional complications because of radiation, convection, transmissivity and reflectivity. These would change with time as the outer shell material degrades and the surface properties change. It was not worthwhile to add these additional complications to the model, as the focus of this study was on the effect of the PCM.

In general, boundary conditions can be assigned a function to match data or actually assigned to the experimental data. Functions are often helpful if the data presents noise. Data from this study were good; therefore boundary conditions were assigned to the average thermocouple temperature readings from data at positions behind the outer shell (front boundary condition) and behind the back face (back boundary condition) for each simulation.

Material Properties

To calculate the heat transfer, material properties for each layer must be known. The properties of interest include the thickness, density, thermal conductivity, and specific heat. Strictly speaking, all of these material properties change with temperature, some more so than others. However, to simplify the calculation, it was assumed that all the properties remained constant for a particular exposure and the values were estimated at an average temperature of all the layers during the heat exposure. A complete listing of the material properties used for each model can be found in Appendix A.

The properties of air are published [46], and the properties of the calcium silicate board and phase change materials were based on manufacturers' specifications. However, the properties of the fire fighter protective clothing were unknown. To obtain a reasonable estimation, the material properties were derived using the least square equations from previous work done by Lawson et al. [47]. Based on measured thicknesses and visual inspection of the materials that were tested, they were approximated by materials that were reported in NISTIR 7282 [47]. The moisture barrier was considered to be similar to the Nomex® IIA Pajama Check® Crosstech®.

The face cloth and batting material properties required extrapolation because in NISTIR 7282 [47] the properties were not determined for the individual face cloth or batting, but rather the entire thermal liner assembly. The material properties of the face cloth were considered to be similar to the Nomex® III-Defender. Using the known thicknesses, properties for the face cloth, and properties for the total thermal liner properties from the report [47], the material properties for the batting were calculated with Equations (1 – 3).

$$\rho_{batting} = \frac{\Delta x_{total}\rho_{total} - \Delta x_{face\_cloth}\rho_{face\_cloth}}{\Delta x_{batting}} \quad \textbf{(1)}$$

$$k_{batting} = \frac{\Delta x_{batting}}{\frac{\Delta x_{total}}{k_{total}} - \frac{\Delta x_{face\_cloth}}{k_{face\_cloth}}} \quad \textbf{(2)}$$

$$\left(c_p\right)_{batting} = \frac{\left(\rho\Delta x c_p\right)_{total} - \left(\rho\Delta x c_p\right)_{face\_cloth}}{\left(\rho\Delta x\right)_{batting}} \quad \textbf{(3)}$$

3.2 Single Layer Assumption

The governing heat transfer equation, derived from the conservation of energy, for one-dimensional heat transfer without energy generation or phase change within the control volume is given by:

$$\rho c_p \frac{\partial T}{\partial t} = \frac{\partial}{\partial x}\left(k \frac{\partial T}{\partial x} \right) \qquad \textbf{(4)}$$

Prior to more complex finite difference approximations with multiple layers, a simple homogenous single-layer assumption was considered. This was based on the linear flow of heat in a solid bounded by parallel plates. It assumed fixed temperature boundary conditions, and an initial uniform temperature throughout. The homogenous assumption used an effective thermal diffusivity, α, for the entire fire fighter protective clothing specimen. Equation (4) becomes:

$$\frac{\partial T}{\partial t} = \alpha \frac{\partial^2 T}{\partial x^2} \qquad \textbf{(5)}$$

Boundary Conditions: $T = \phi_1(t)$ *when* $x = 0$

$T = \phi_2(t)$ *when* $x = l$

Initial Condition: $T = f(x)$ *when* $t = 0$

This has an exact solution as reported by Carslaw and Jaeger's book *Conduction of Heat in Solids* [48] and solves for temperature as a function of time and position:

$$T(x,t)=\frac{2}{l}\sum_{1}^{\infty}\exp\left(\frac{-\alpha n^2\pi^2 t}{l^2}\right)\cdot\sin\left(\frac{n\pi x}{l}\right)\left[\int_0^l f(x')\sin\left(\frac{n\pi x'}{l}\right)dx'+\frac{n\alpha x}{l}\int_0^t\exp\left(\frac{\alpha n^2\pi^2\lambda}{l^2}\right)\left\{\phi_1(\lambda)-(-1)^n\phi_2(\lambda)\right\}d\lambda\right] \quad \textbf{(6)}$$

This is further simplified by assigning the boundary and initial conditions to represent a normalized fixed temperature condition. Recalling that the boundary conditions were set to the temperatures behind the outer shell and the back face, this simulated the temperature behind the outer shell instantly becoming hot (1) while the temperature behind the back face remained at the initial cold temperature (0).

Boundary Conditions: $T=1 \;\; when \;\; x=0$

$T=0 \;\; when \;\; x=l$

Initial Condition: $T=0 \;\; when \;\; t=0$

Then, equation 6 becomes:

$$T(x,t)=\sum_{1}^{\infty}\left[1-\exp\left(\frac{-\alpha n^2\pi^2 t}{l^2}\right)\right]\cdot\frac{\sin\left(\frac{n\pi x}{l}\right)}{\frac{n\pi}{2}} \quad \textbf{(7)}$$

The final Equation (7) was coded in MATLAB® (Appendix C: 01_FFPC_Single_Layer.m) and results can be seen in Figure 3.1. The three lines are meant to represent the temperatures at the approximate locations of interest (behind the moisture barrier, batting and face cloth layers). For Figure 3.1 and all the graphs throughout, the label describes the layer immediately before. For example the label "Model – Moisture Barrier" is representative of the predicted temperature behind the moisture barrier.

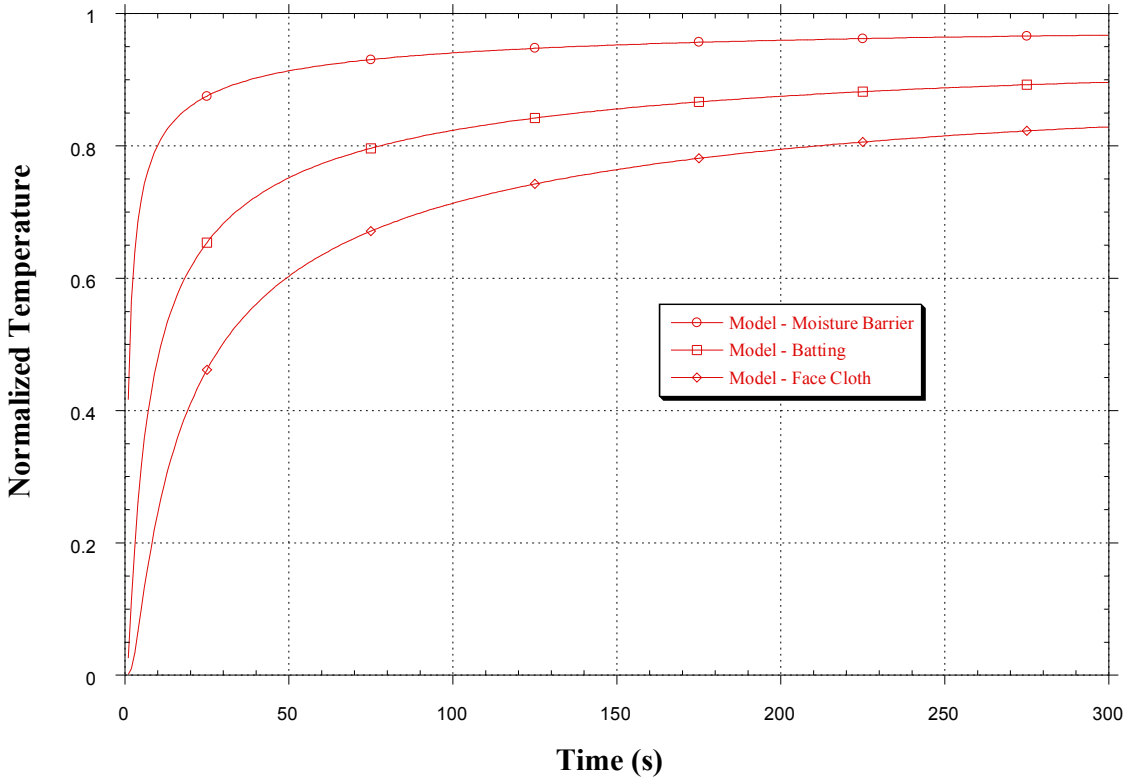

Figure 3.1: Single Layer MATLAB® Result

Finite Difference Method

A Crank-Nicolson finite difference scheme was used to obtain the solution to the multi-layered fire fighter protective clothing heat transfer. This scheme was chosen for the accuracy, stability, and computational demands. Prior to computing the multi-layer problem, the finite difference method for a homogenous, single-layer assumption was completed.

Equation (5) is approximated by the Crank-Nicolson finite difference method:

$$\frac{\partial T}{\partial t} \approx \frac{T_n^N - T_n}{\Delta t} \tag{8}$$

$$\frac{\partial^2 T}{\partial x^2} \approx \frac{\left.\frac{\partial T}{\partial x}\right|_{n+1/2} - \left.\frac{\partial T}{\partial x}\right|_{n-1/2}}{\Delta x} \tag{9}$$

Equation (9) is approximated:

$$\left.\frac{\partial T}{\partial x}\right|_{n+1/2} \approx \frac{T_{n+1} - T_n}{\Delta x} \tag{10}$$

$$\left.\frac{\partial T}{\partial x}\right|_{n-1/2} \approx \frac{T_n - T_{n-1}}{\Delta x} \tag{11}$$

$$\frac{\partial^2 T}{\partial x^2} \approx \frac{1}{2}\left[\frac{T_{n+1} - 2T_n + T_{n-1}}{\Delta x^2} + \frac{T_{n+1}^N - 2T_n^N + T_{n-1}^N}{\Delta x^2}\right] \tag{12}$$

Equation (12) and Equation (8) combine:

$$\frac{T_n^N - T_n}{\Delta t} \approx \frac{\alpha}{2}\left[\frac{T_{n+1} - 2T_n + T_{n-1}}{\Delta x^2} + \frac{T_{n+1}^N - 2T_n^N + T_{n-1}^N}{\Delta x^2}\right] \tag{13}$$

$$T_n^N - T_n \approx \frac{F_o}{2}\left[T_{n+1} - 2T_n + T_{n-1} + T_{n+1}^N - 2T_n^N + T_{n-1}^N\right] \tag{14}$$

Where Δx is the discretization distance, assigned to a value of 1 m. For the temperature terms, the subscript indicates position, while the superscript indicates time. This is visually displayed in Figure 3.2.

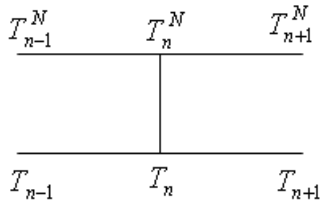

Figure 3.2 Crank-Nicolson Stencil

Finally, Equation (14) is rearranged by moving all the temperatures at the next time step to one side.

$$\left(\frac{-F_o}{2}\right)T_{n-1}^{N}+\left(1+F_o\right)T_{n}^{N}+\left(\frac{-F_o}{2}\right)T_{n+1}^{N}=\left(\frac{F_o}{2}\right)T_{n-1}+\left(1-F_o\right)T_{n}+\left(\frac{F_o}{2}\right)T_{n+1} \qquad \textbf{(15)}$$

Equation (15) can be solved with numerical linear algebra by means of the tridiagonal matrix algorithm (or Thomas algorithm). This method uses a LU factorization with backward substitution. This equation and the tridiagonal matrix algorithm were coded in MATLAB® (Appendix C: 02_FFPC_Single_layer_TriDiagonal.m) and solved for the same conditions as the single layer program for validation. As seen in Figure 3.3 the results are virtually the same as the single layer, demonstrating that the code and finite difference method are valid means of approximating the heat transfer.

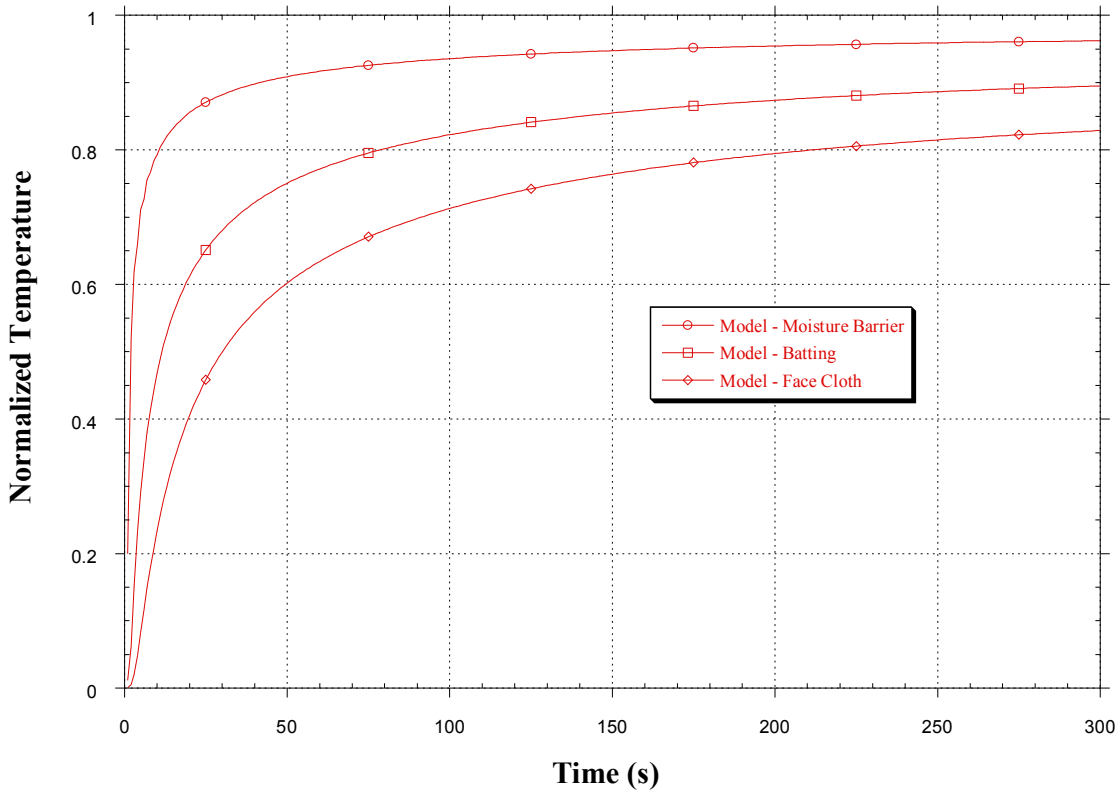

Figure 3.3: Single Layer FDM MATLAB® Result

3.3 Multi-Layered Model

After establishing a method to approximate the heat transfer in a single homogenous layer, a multi-layered model was created. Starting with Equation (1), the heat transfer is approximated with the Crank-Nicolson finite difference method while accounting for changing material properties between layers (Figure 3.4):

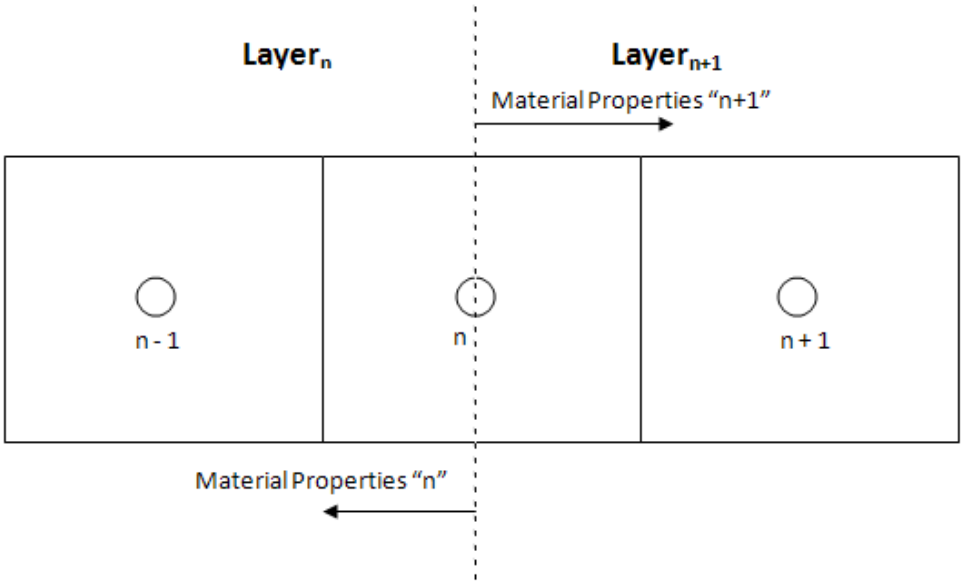

Figure 3.4: Schematic of FDM between Two Layers

$$\rho c_p \frac{\partial T}{\partial t} = \frac{\partial}{\partial x}\left(k \frac{\partial T}{\partial x}\right) \tag{1}$$

Equation (1) is approximated:

$$\rho c_p \frac{\partial T}{\partial t} \approx \overline{\rho c_p} \frac{T_n^N - T_n}{\Delta t} \tag{16}$$

$$\frac{\partial}{\partial x}\left(k \frac{\partial T}{\partial x}\right) \approx \frac{k_{n+1} \left.\frac{\partial T}{\partial x}\right|_{n+\frac{1}{2}} - k_n \left.\frac{\partial T}{\partial x}\right|_{n-\frac{1}{2}}}{\Delta x} \tag{17}$$

Equation (17) is approximated:

$$\left.\frac{\partial T}{\partial x}\right|_{n+\frac{1}{2}} \approx \frac{T_{n+1} - T_n}{\Delta x} \tag{18}$$

$$\left.\frac{\partial T}{\partial x}\right|_{n-\frac{1}{2}} \approx \frac{T_n - T_{n-1}}{\Delta x} \tag{19}$$

$$\frac{\partial^2 T}{\partial x^2} \approx \frac{1}{2\Delta x^2}\left[k_{n+1}\left(T_{n+1} - T_n\right) - k_n\left(T_n - T_{n-1}\right) + k_{n+1}\left(T_{n+1}^N - T_n^N\right) - k_n\left(T_n^N - T_{n-1}^N\right)\right] \tag{20}$$

Equation (16) is combined with Equation (20) to yield:

$$\frac{T_n^N - T_n}{\Delta t} \approx \frac{1}{\left(\overline{\rho c_p}\right)\cdot 2\cdot \Delta x^2}\left[k_{n+1}\left(T_{n+1}-T_n\right)-k_n\left(T_n-T_{n-1}\right)+k_{n+1}\left(T_{n+1}^N-T_n^N\right)-k_n\left(T_n^N-T_{n-1}^N\right)\right] \quad \textbf{(21)}$$

Where the thermal conductivity, *k*, for each node is defined by the layer it resides in, as indicated by the subscripts corresponding to the material properties in Figure 3.4. The subscripts also apply for the average ρc_p calculation:

$$\overline{\rho c_p} = \frac{\left(\rho c_p\right)_n + \left(\rho c_p\right)_{n+1}}{2} \quad \textbf{(22)}$$

The remaining notation is the same as that previously demonstrated for the homogenous, single-layer assumption. Note that if the nodes are all within the same layer, the result is the same a previously calculated in the single layer assumption (Equation 15).

Equation (21) is rearranged by moving all the temperatures at the next time step to one side:

$$\begin{aligned}&\left[\frac{-1}{2}\left(\frac{k_{n+1}\Delta t}{\overline{\rho c_p}\cdot\Delta x^2}\right)\right]T_{n-1}^N+\left[1+\left(\frac{(k_{n+1}+k_n)\Delta t}{\overline{\rho c_p}\cdot\Delta x^2\cdot 2}\right)\right]T_n^N+\left[\frac{-1}{2}\left(\frac{k_n\Delta t}{\overline{\rho c_p}\cdot\Delta x^2}\right)\right]T_{n+1}^N\\&=\left[\frac{1}{2}\left(\frac{k_{n+1}\Delta t}{\overline{\rho c_p}\cdot\Delta x^2}\right)\right]T_{n-1}+\left[1-\left(\frac{(k_{n+1}+k_n)\Delta t}{\overline{\rho c_p}\cdot\Delta x^2\cdot 2}\right)\right]T_n+\left[\frac{1}{2}\left(\frac{k_n\Delta t}{\overline{\rho c_p}\cdot\Delta x^2}\right)\right]T_{n+1}\end{aligned} \quad \textbf{(23)}$$

Equation (23) is the final equation that was implemented into MATLAB® code (Appendix C: 03_FFPC_Multi_Layer.m). Once again, to validate both the mathematics and code, the simulation was run with the same conditions. This was accomplished by fixing the boundary condition temperatures and assigning all the material layers the same thermal conductivity, specific heat and density that would approximate the previously used effective thermal diffusivity. It can be seen in Figure 3.5 that results are once again very similar to the previous calculation for the homogenous layer, providing validation.

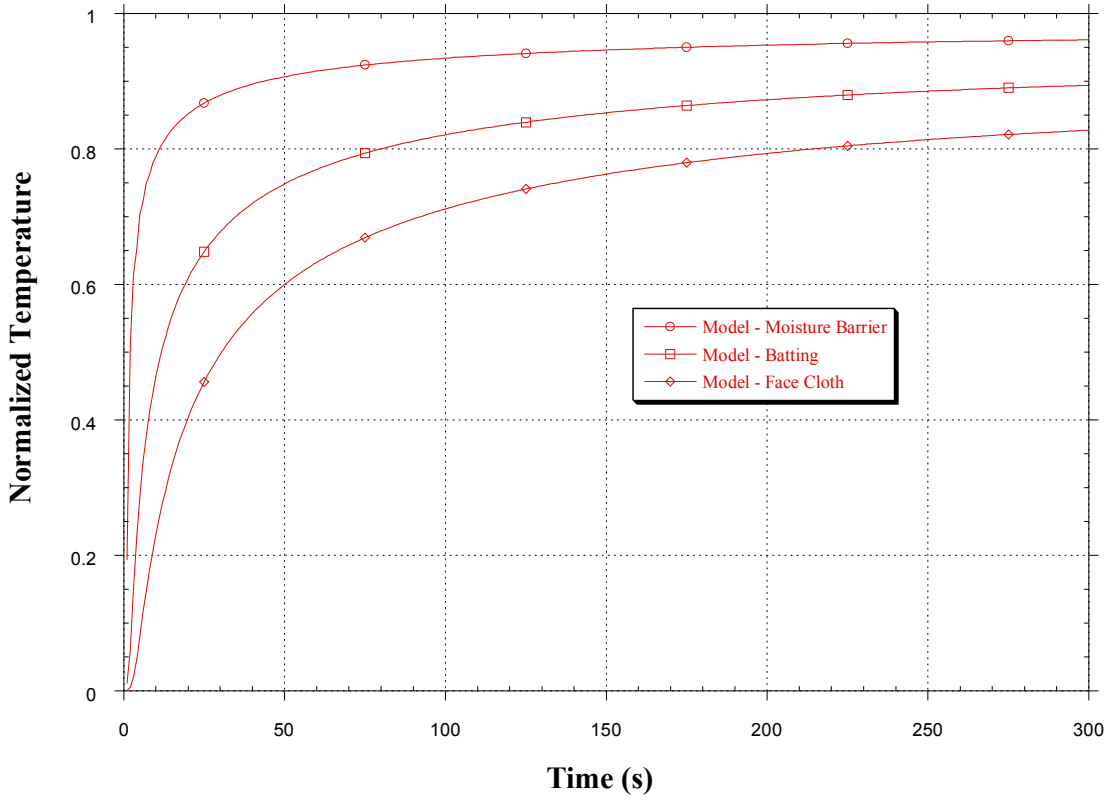

Figure 3.5: Multi Layer FDM Fixed Temp and Constant Material Properties

Up until this point, the boundary condition temperatures were fixed at 1 and 0. The next step involved inputting empirical data from experiments as boundary conditions. This provided a more realistic view of the transient heat transfer as the front surface boundary condition gradually increased in temperature, while the back surface boundary condition remained relatively constant. Plots show the predicted temperatures by the model (behind moisture barrier, batting and face cloth positions) and the experimental data boundary conditions (behind outer shell and back face); no uncertainty was displayed for the data temperatures because the values are those that were actually used for the model. To compare this result to the previous graphs, the temperatures was normalized between the minimum temperature and the maximum temperature and the results displayed in Figure 3.6 are consistent with previous results. Figure 3.7 shows the same results as Figure 3.6, but with actual temperatures.

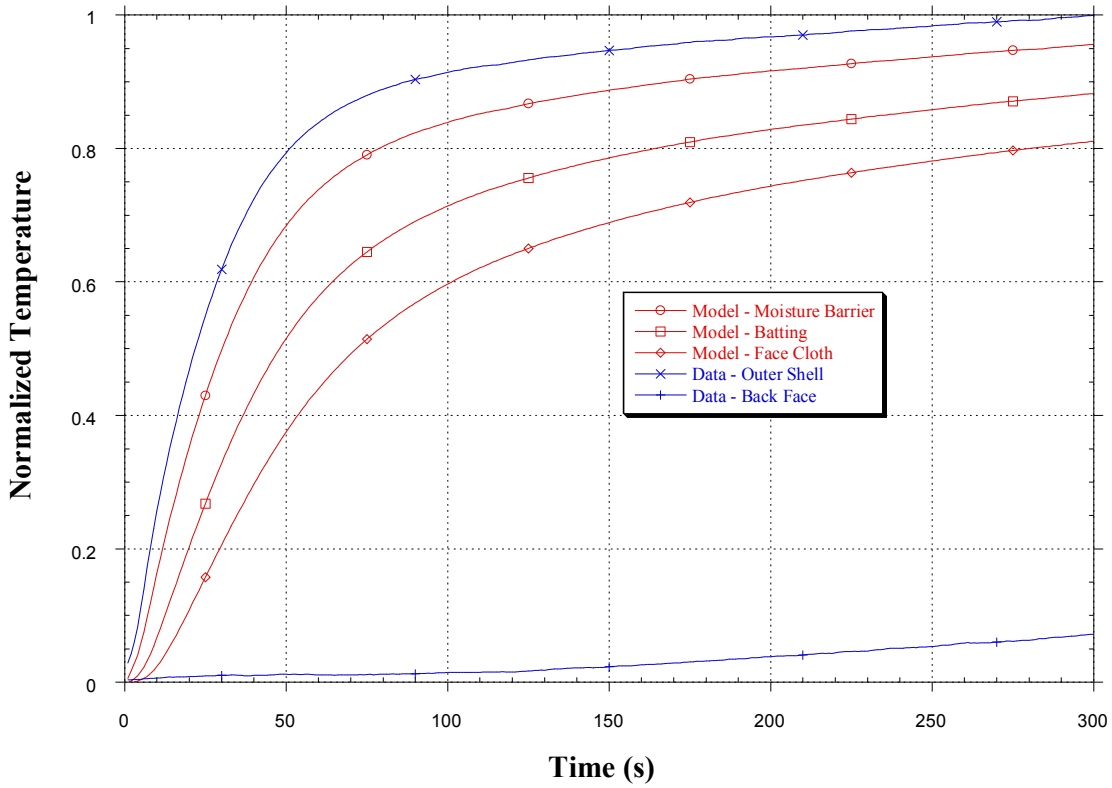

Figure 3.6: Normalized Temperatures for Multi Layer FDM with BC Input

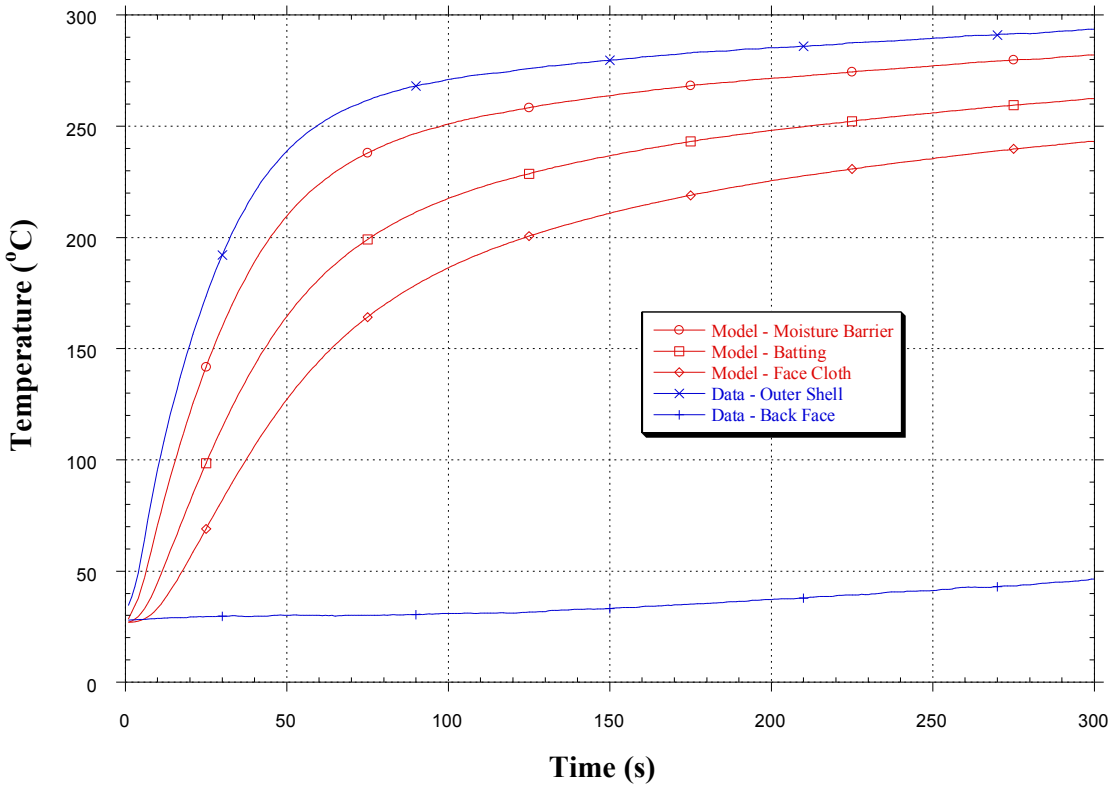

Figure 3.7: Multi Layer FDM with Boundary Condition Input

The final refinement of the multi-layer model without including the phase change material was to implement the estimated individual material properties and adjust the air gaps to match the empirical data. The air gaps were estimated based on measurements and comparing the model to the Series MF experiments with fire fighter protective clothing without PCM (Standard Configuration). The result can be seen in Figure 3.8 and is compared with empirical data in the *Results* section.

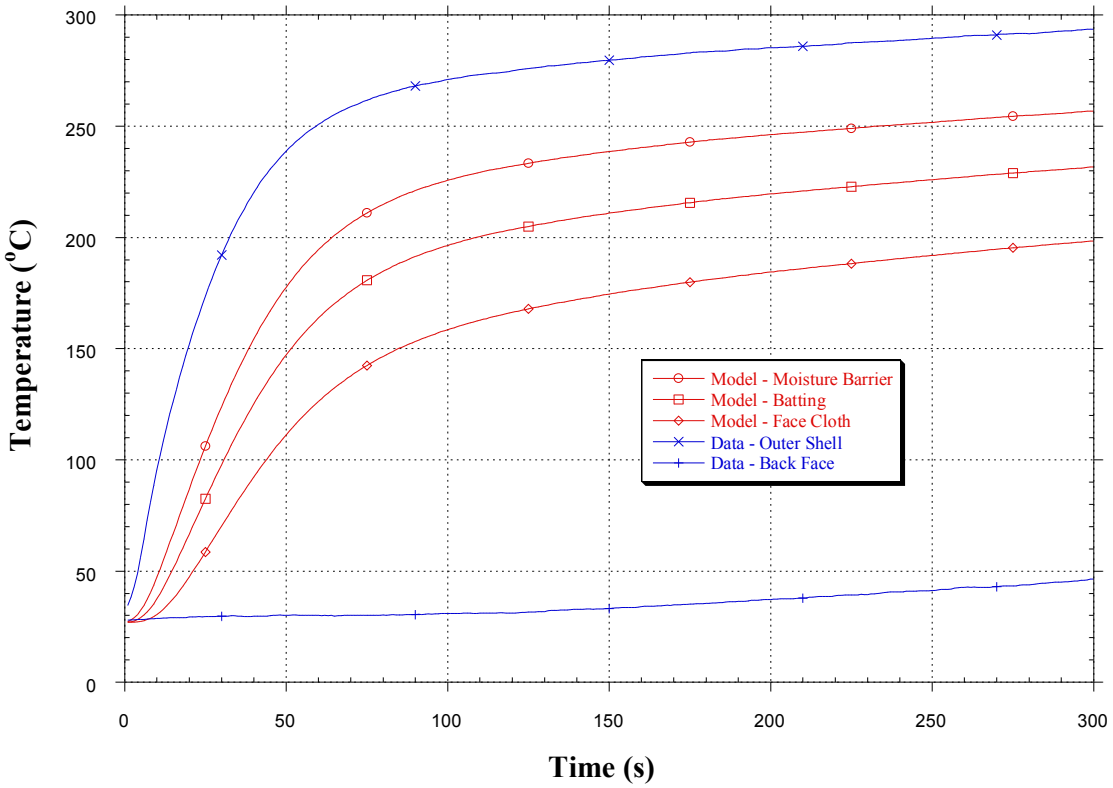

Figure 3.8: Final Multi Layer FDM Approximation

3.4 Phase Change Material

To account for the latent energy in the phase change material layer, an additional term is required in the governing heat transfer equation:

$$\rho c_p \frac{\partial T}{\partial t} = \frac{\partial}{\partial x}\left(k \frac{\partial T}{\partial x}\right) - \dot{q}''' \qquad \textbf{(24)}$$

This $\dot{q}'''$ term accounts for latent energy that is absorbed during the phase change. The PCMs used in the experiments were mixtures, so there was not an exact melting point but rather a temperature range in which the material melted (Table 3.1). It was unrealistic to

expect to know exactly where and how much of the phase change material was melting within the layer. Therefore a function was created for this volumetric energy absorption rate. The function only applied for nodes within the PCM layer, and temperatures within the melting range.

A Guassian error function was used to estimate the amount of latent energy absorbed based on the temperature of the node (Figure 3.9). This accounted for the approximation within the finite difference method, where the entire control volume is assumed to be the same temperature when the actual temperature within the control volume would be expected to have a gradient.

$$\dot{q}''' = \frac{\rho\ L}{\Delta t}(1.4)\left[1 - erf\left(\left|\frac{T_n - T_m}{T_r}\right|\right)\right] \qquad \textbf{(25)}$$

Where: $T_m = \frac{T_1 + T_2}{2}$ = Approximate melting temperature [$°C$]

$T_r = T_2 - T_1$ = Melting temperature range [$°C$]

Table 3.1: Modeled Phase Change Melting Temperatures

Material	Melting Temperature (°C)	T_1 (°C)	T_2 (°C)	T_m (°C)
PCM_B	44 - 55	44	55	49.5
PCM_C	71 - 86	71	86	78.5

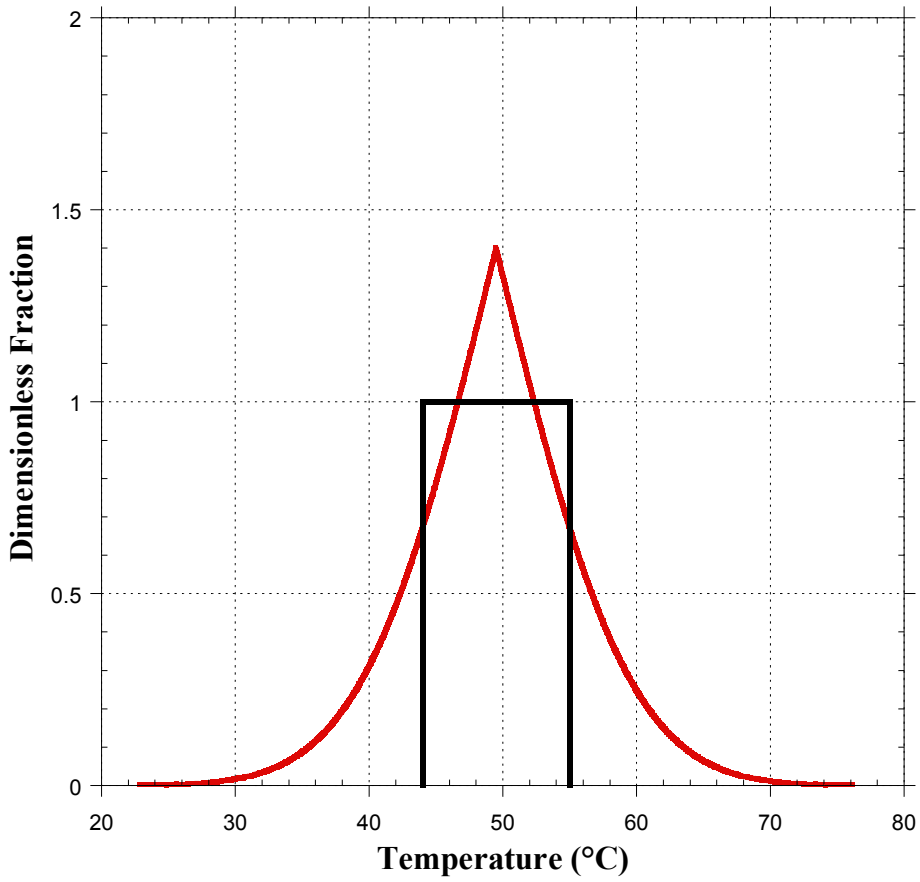

Figure 3.9: Latent Energy Temperature Function

The rate that the volumetric energy absorption function absorbed energy was assigned a maximum value of 60 % of the transient conduction term (Equation 26). This was estimated based on an overall energy balance, and comparisons to the experimental results. The energy balanced was based on the assumption that, at best, the phase change could absorb enough energy to keep the temperature constant. This would make the left hand side of Equation (24) go to zero, and the volumetric energy absorption would be

equal to the transient conduction. When this was run in the model and compared to the experimental data, it appeared that the rate was too high. However, scaling the term to sixty percent provided good agreement with the data. This is reasonable, as some portion of the transient heat transfer could be increasing the temperature of the layer.

$$\dot{q}'''_{\max} = 0.6 \cdot k \cdot \frac{T_{n-1} - 2T_n + T_{n+1}}{\Delta x^2} \quad \textbf{(26)}$$

When Equation (24) is solved using the finite difference scheme described in previous sections, each term on the right hand side is multiplied by $\frac{\Delta t}{\rho c_p}$ to solve for the temperature difference. Consistently, this was done to the terms described above for the volumetric energy absorption function prior to implementing them into code. The MATLAB® code can be seen for the PCM B configuration in Appendix C (04_FFPC_Multi_Layer_PCMB.m) and the results are shown below (Figure 3.10).

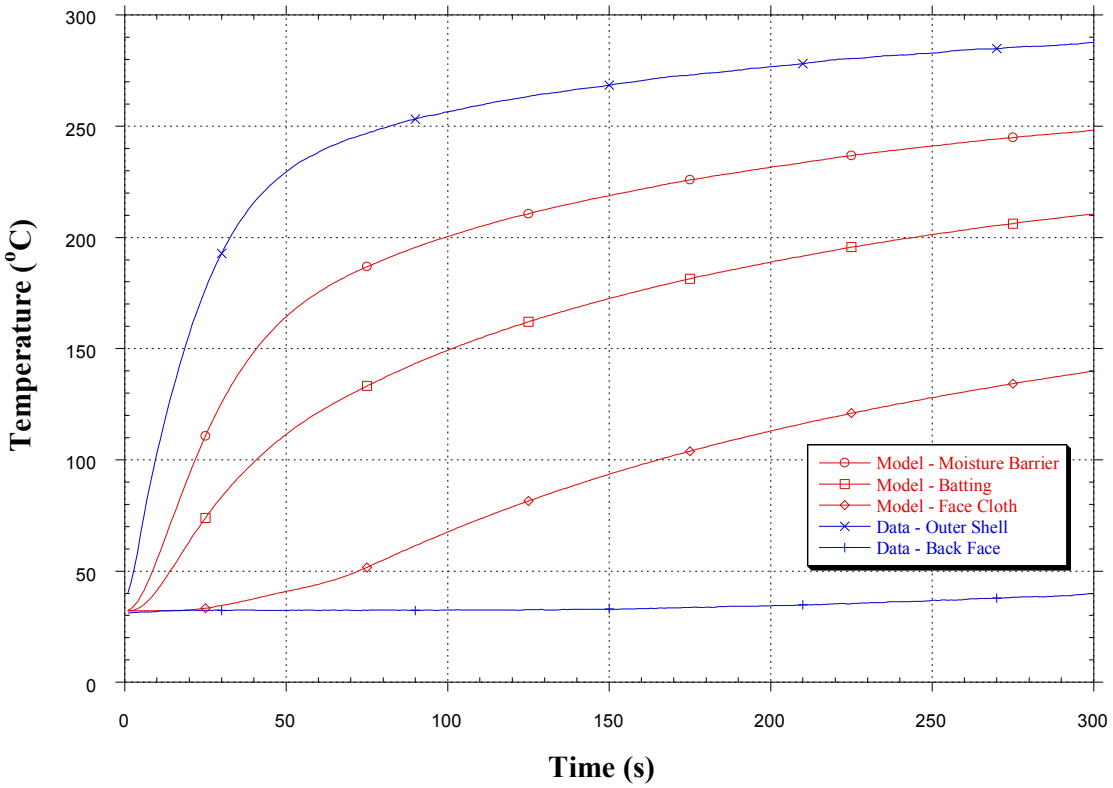

Figure 3.10: Series MF Multi Layer FDM Approximation PCM B Configuration

Chapter 4: Uncertainty

Inherent to any measurement is a certain level of uncertainty. Attempts were made to minimize the measurement uncertainties in this study. However, there were three major contributions to the uncertainty. These included the measured temperatures, specimen assembly, and material properties.

There are a few factors that are responsible for the uncertainties in the measured temperatures. First, the thermocouples have an intrinsic uncertainty of ± 1% that is published by the manufacturer [49]. Additionally, there is no easy method for attaching a thermocouple to a surface that ensures a true surface temperature. When placing the thermocouples, both between the fire fighter protective clothing layers and on the back face of the calcium silicate board, it was difficult to determine how firmly the sensor was touching the material. Variances in the pressure exerted by the sensor on the protective clothing could change the contact area between the sensor and protective clothing, thereby changing the heat transfer characteristics. The presence of the thermocouple alone will cause a perturbation of the temperature distribution at the point of contact. Heat transfer is therefore due to conduction across the actual contact area, as well as conduction or radiation across the gap. The size of the thermocouples was chosen in an attempt to minimize this uncertainty while still maintaining practicality for the experiments. Finally, the majority of the temperature measurement uncertainty lies in the position of the thermocouple within the specimen. While attempts were made to ensure the sensors were consistently placed and touching the back face of the layer of interest, it

was difficult to know if the sensor was touching the back face of the layer, the front face of the next layer, both layers, or neither. This was particularly difficult for the batting layer, due to the means of placing the thermocouples as described in *Chapter 2*. A sample plot of the different temperature readings behind the batting for the Series MF Standard configuration tests is shown below (Figure 4.1). Three tests were conducted with three thermocouples behind the batting for a total of nine different temperature readings.

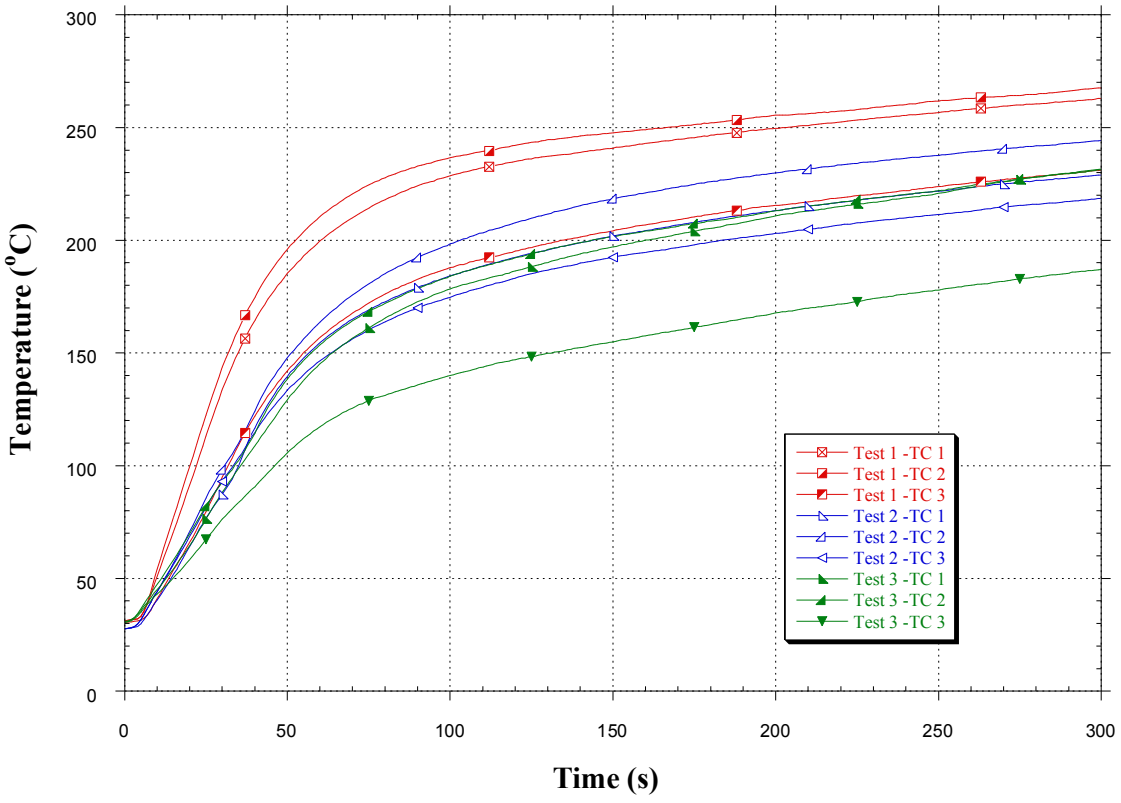

Figure 4.1: Sample Thermocouple Temperature Readings – Behind the Batting

Similarly, the plots in the *Results* section represent the average temperatures from three experiments, each with three thermocouples per position for a total, averaged temperature among nine thermocouple readings. Standard deviations are presented for some of the data points. As anticipated, the uncertainty of the temperature reading behind the batting layer was consistently greater than the other locations. Also expected, the uncertainty for the back face thermocouple reading was the lowest because it was the easiest thermocouple to position consistently.

Included in the specimen assembly were uncertainties for the measured layer thicknesses and estimated air gaps. Measurements for the thickness of the layers were difficult, particularly for the thermal liners with PCM sewn within. Several measurements were made for each layer and the average value was used in the model. Air gaps were initially estimated to be approximately the diameter of the glass braid insulation on the thermocouples between layers for each specimen. However, once the specimen was actually placed in the moving trolley assembly it was challenging to determine the exact size of the air gaps. Therefore, air gaps were ultimately estimated based on a comparison to the experimental data. The air gap measurements taken prior to assembly were only used to ensure that the values used in the model were within reason. Figure 4.2 displays the various average thicknesses and their associated standard deviations. It is clear that the uncertainty for the thermal liners with PCMs sewn within was much greater than the other measured thicknesses.

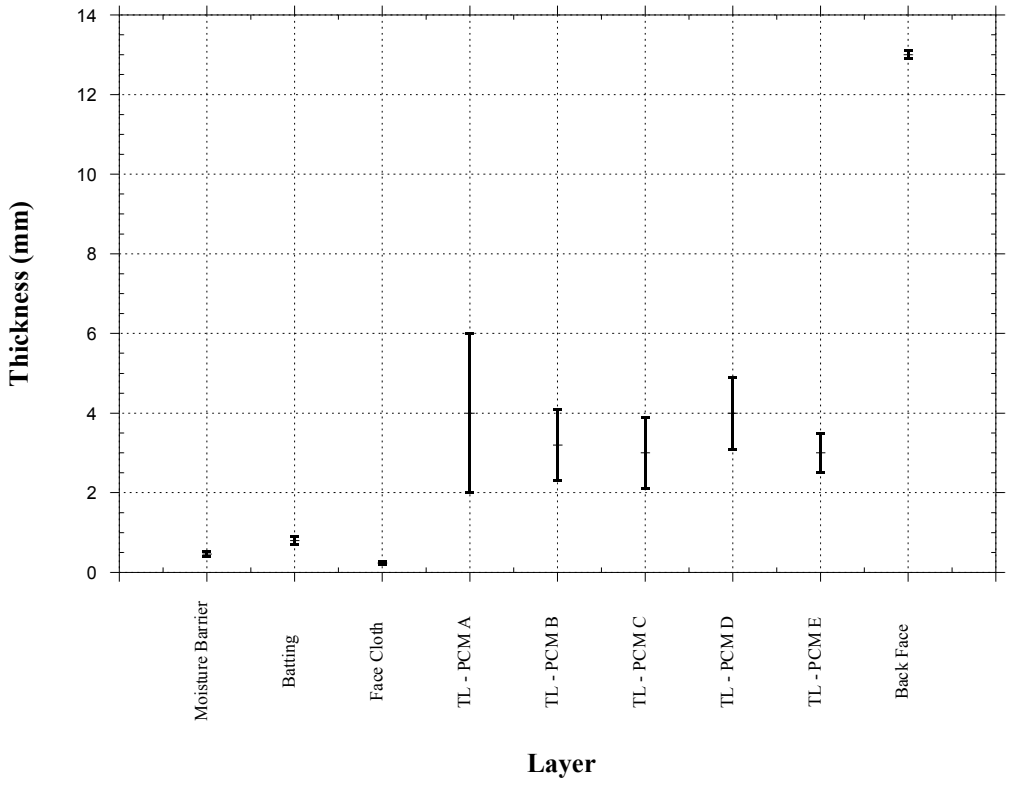

Figure 4.2: Thickness Measurements

Material properties were taken from the published values that were provided by the manufacturer or as described in Section 3.1. The information for density, thermal conductivity, and specific heat that was obtained from Lawson et al. [46] published combined standard uncertainties of ± 5%, ± 6 % and ± 27 % respectively. While the exact material properties as a function of temperature were not incorporated in the model, it is reasonable to assume that the actual material properties were not significantly different from those used.

Chapter 5: Results

As described in *Chapter 2*, a total of thirty experiments were completed during this study, but focus was placed on Series MF and PCM B. This section presents and analyzes the experimental results of the PCM B configuration for thermal exposure Series LF, MF, and HF as well as the PCM C and Standard specimen configurations for the Series MF exposure. The complete experimental matrix was displayed *Chapter 2* (Table 2.2). Furthermore, each of the previously mentioned tests were simulated with the theoretical model and compared to the experimental results.

General observations during the experiments were fairly consistent throughout. Figure 5.2 presents the observed appearance of the specimens after the Series HF heat exposure. Similar observations were made during the Series MF experiments (Figure 5.2). There was no visual damage observed for Series LF (Figure 5.3). During the Series MF and HF experiments, off gassing was observed during the heat exposure. The discolorations of the specimen and off gassing observations are probably indications of material degradation. Often, even after allowing the specimens to cool, the configurations with PCM embedded within still felt warm to the touch after the heat exposure.

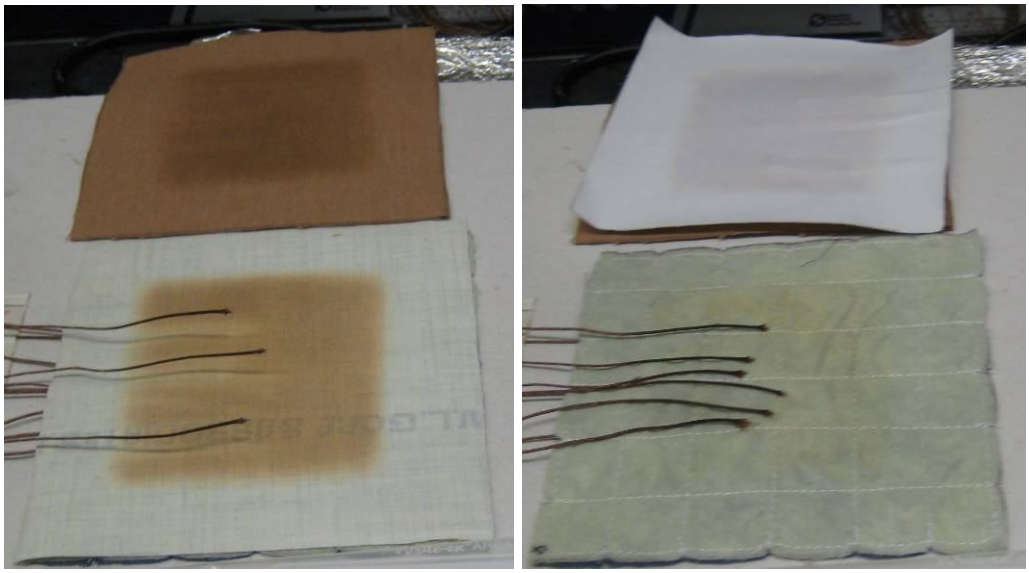

Figure 5.1: Series HF Post Exposure Specimen Pictures. Original in color.

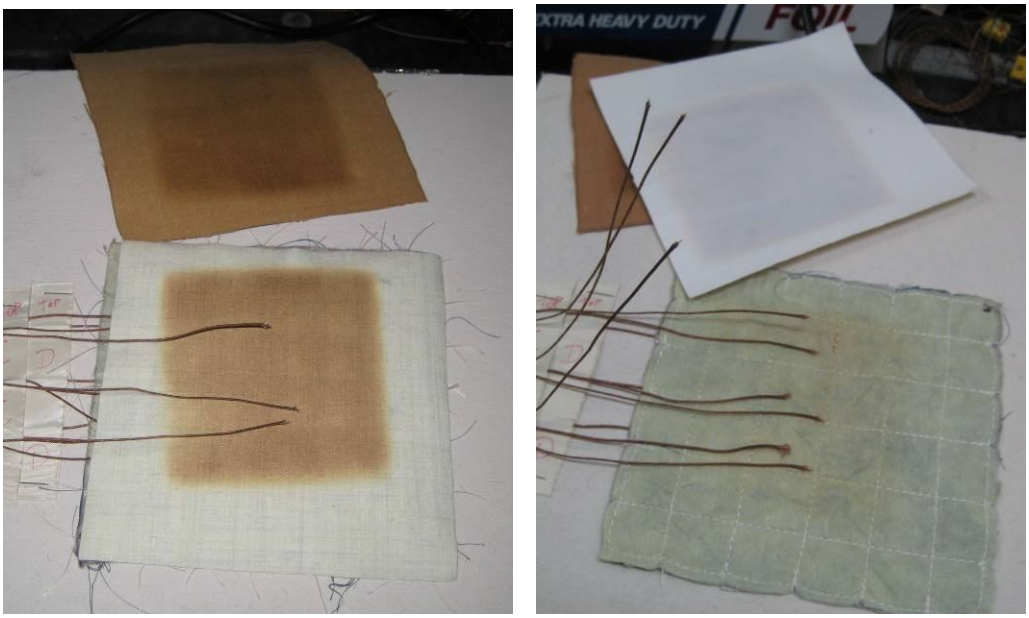

Figure 5.2: Series MF Post Exposure Specimen Pictures. Original in color.

Figure 5.3: Series LF Post Exposure Specimen Pictures. Original in color.

5.1 Experimental Data

The results from the Series MF standard configuration are shown in Figure 5.4. In Figure 5.4 it is observed that each layer and air gap combination reduces the temperatures between 25 °C and 40 °C. Temperatures behind the outer shell reach approximately 300 °C, while temperatures seen behind the face cloth only reach close to 200 °C. It is also noted that the uncertainty is the greatest for the batting layer. As mentioned in *Chapter 4*, this was expected due to the difficulty in consistently placing the thermocouples in the already sewn together thermal liner.

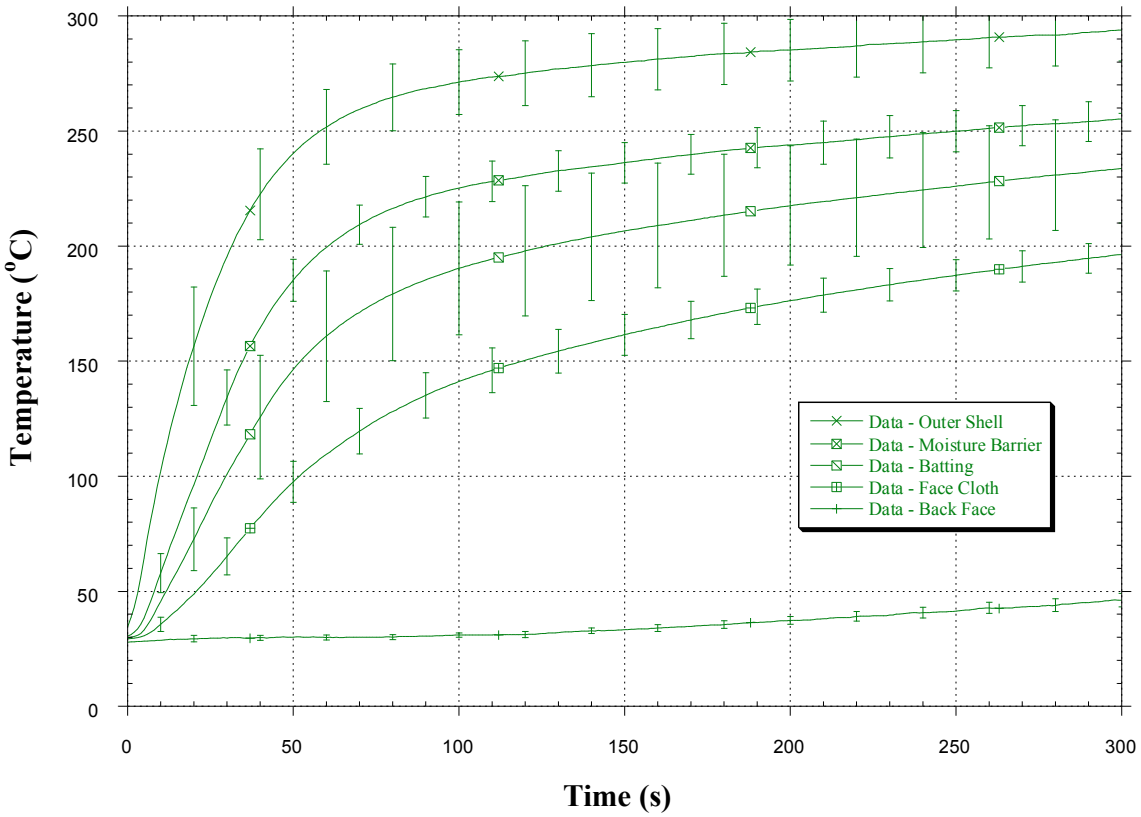

Figure 5.4: Series MF – Standard Configuration

The results from the Series MF, PCM B configuration are shown in Figure 5.5. Each layer and air gap combination reduces the temperatures by approximately 40 °C. The maximum temperature seen behind the face cloth is approximately 50 °C less than that of the standard configuration. The lower temperatures are expected due to both the addition of the material and the energy absorbed during the phase change. During the first 100 s of the exposure, the temperature differences are much greater than near the end, when the system is approaching steady state.

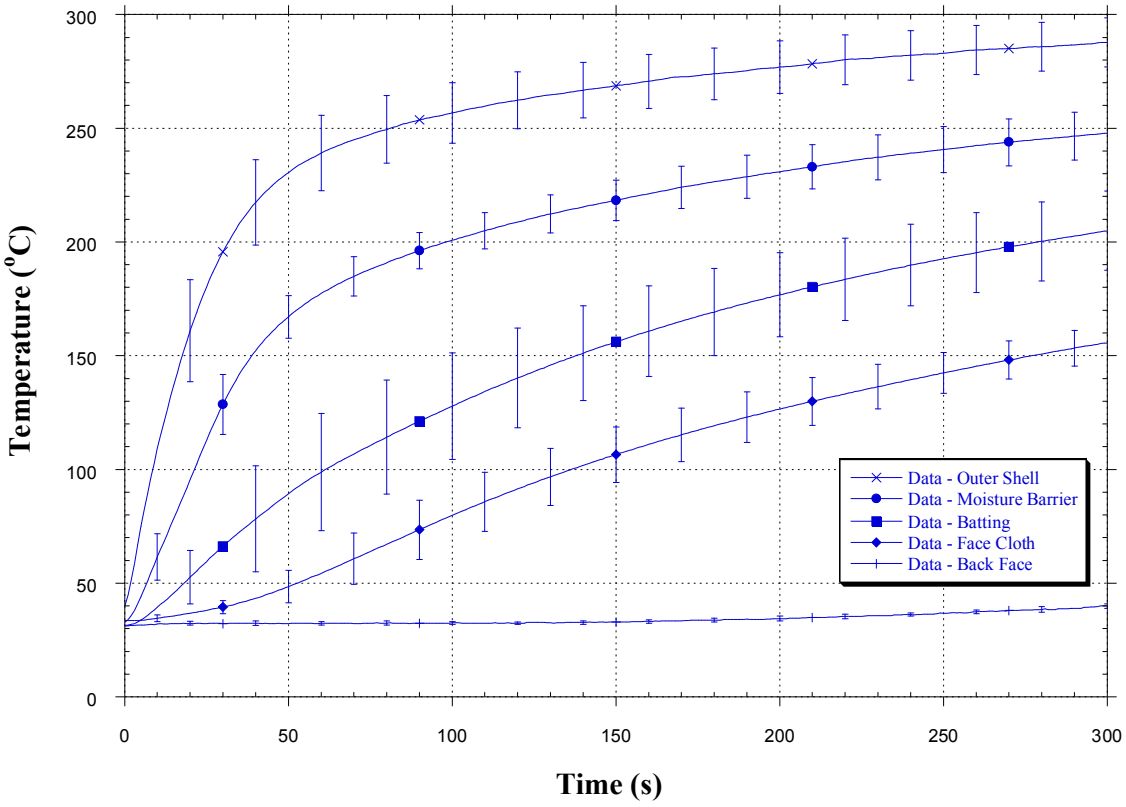

Figure 5.5: Series MF – PCM B Configuration

Figure 5.6 displays a comparison of the PCM B configuration and the standard configuration for the Series MF exposure. The plot focuses on the changes seen in the beginning 125 s of the exposure. It is observed that the temperatures of the outer shell and moisture barrier for the PCM B configuration follow closely to the standard configuration until about 35 s, when they begin to diverge. This is likely due to the initiation of the phase change.

Examining the temperatures behind the batting and face cloth layers illustrates that the temperatures are significantly lower for the PCM B than the standard configuration. This is largely due to the additional material. Close examination near the melting temperatures of the PCM B (44–55 °C) reveals a change in slope of the temperature curves for behind the face cloth. All the other curves display a consistent concave shape, but the PCM B face cloth curve exhibits a convex shape between approximately 20 and 60 s. This is an indication that there is latent energy absorption taking place.

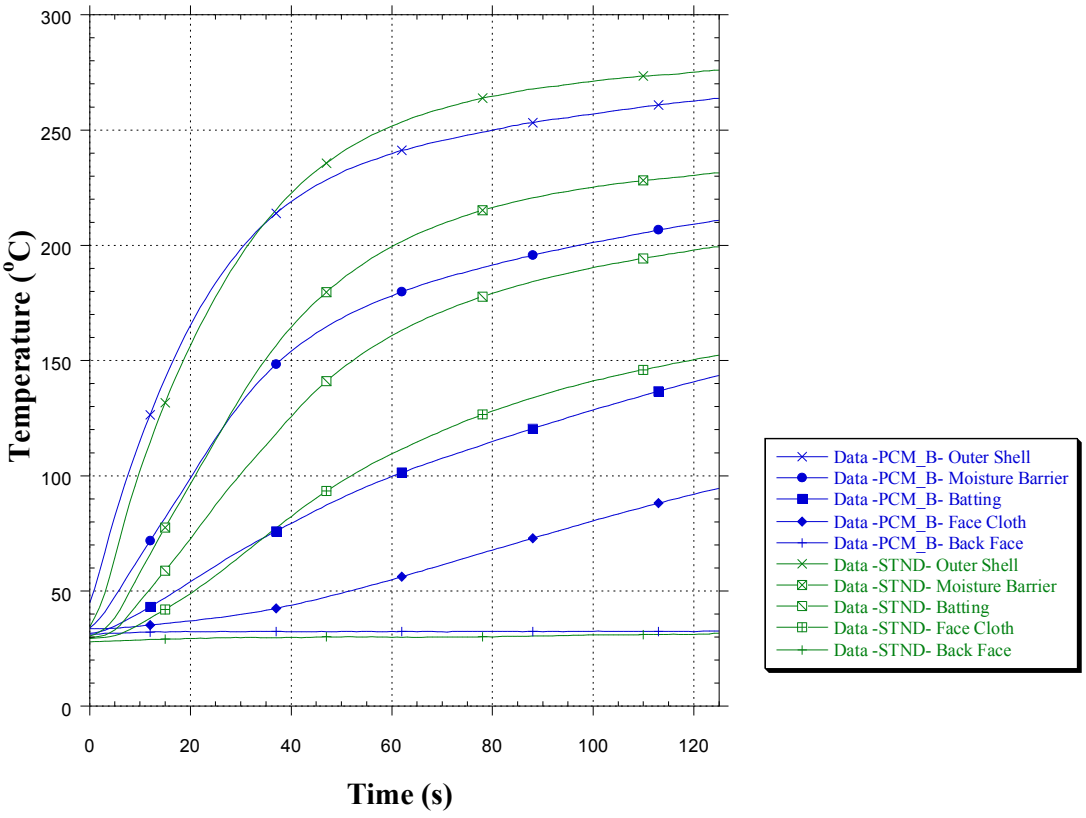

Figure 5.6: Series MF – Comparison of PCM B and Standard Configuration

The results from the Series MF PCM C configuration are similar to those of the PCM B configuration (Figure 5.7). Each layer and air gap combination reduce the maximum temperatures by about 40 °C and even more so where the PCM layer lies. The maximum temperatures reached for PCM C configuration were slightly above those with the PCM B.

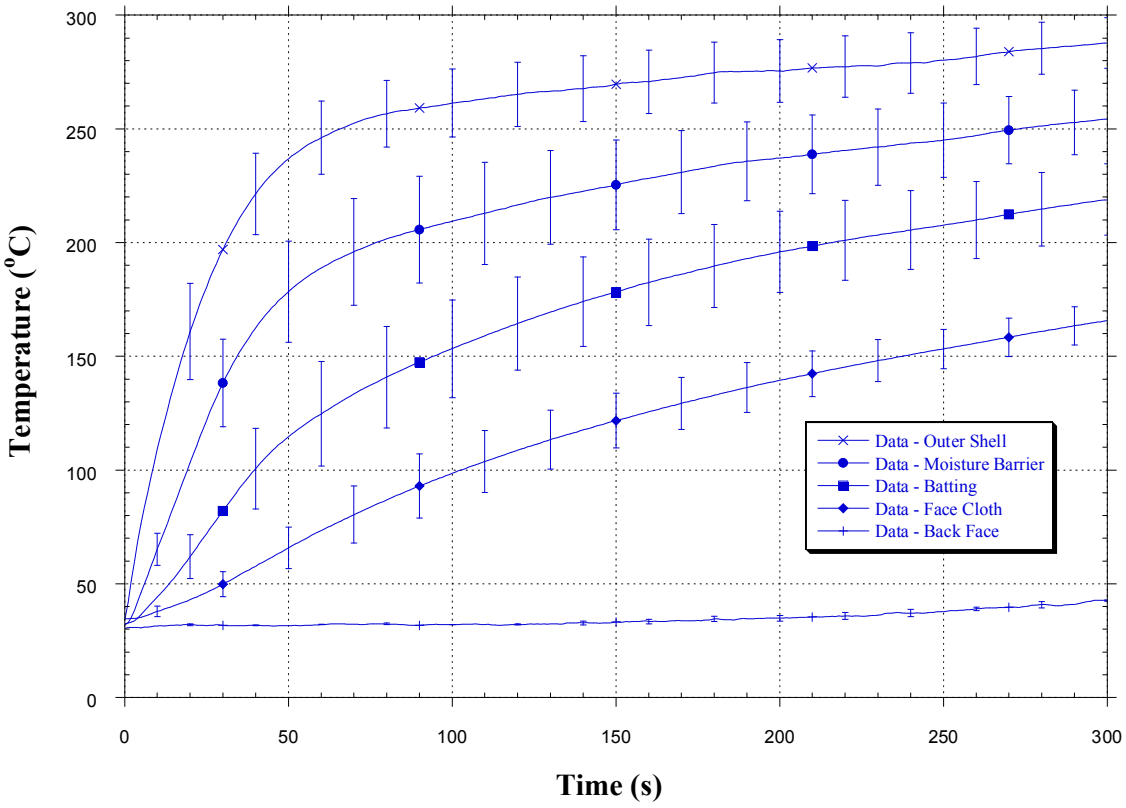

Figure 5.7: Series MF – PCM C Configuration

Figure 5.8 shows a comparison of PCM C to the standard configuration during the first 125 s of the exposure. Again, the results display similarities that were observed with the PCM B comparison. Both the outer shell and moisture barrier of the PCM C configuration match closely to the standard configuration until about 40 s, once again indicating phase change. It is logical for the PCM C curves to start to diverge slightly after the PCM B because the melting temperature for the PCM C is higher. Close examination of the temperatures behind the face cloth layer for the PCM C configuration show a slight change in slope around 20 s, but it is not as pronounced as the PCM B configuration.

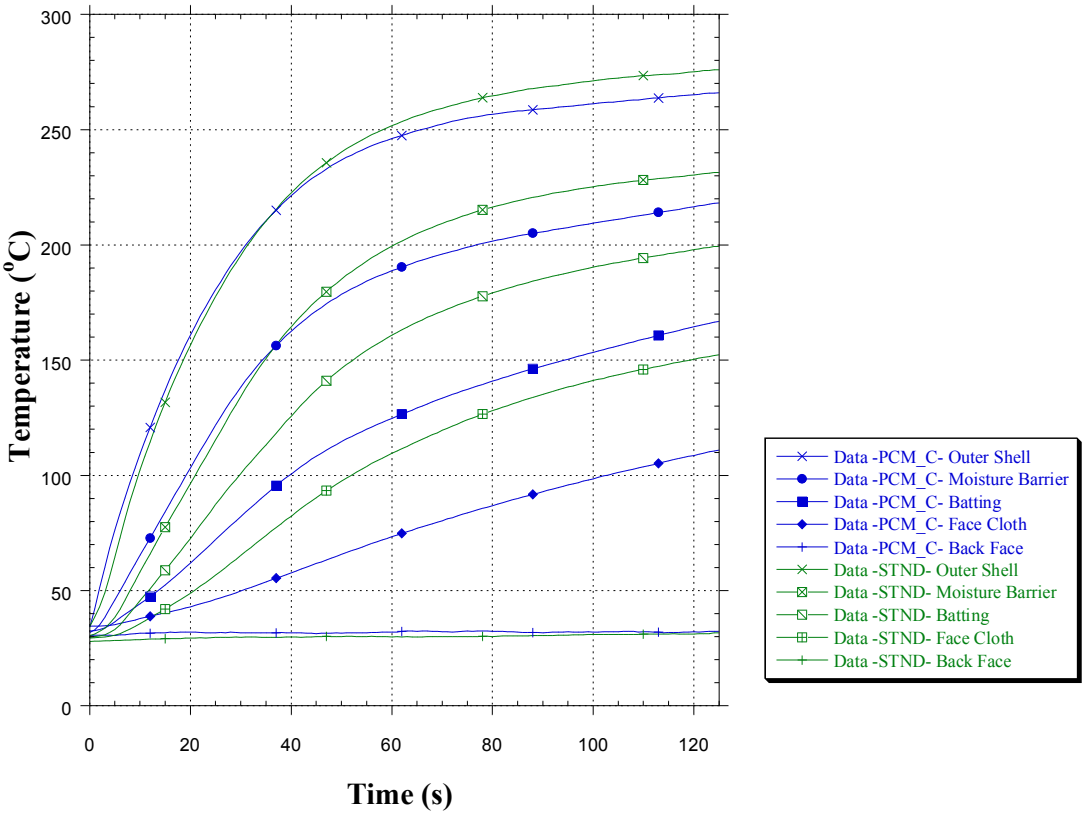

Figure 5.8: Series MF – Comparison of PCM C and Standard Configuration

Figure 5.9 displays the results from the Series LF experiments with the PCM B configuration. This was a much longer exposure (900 s) at a lower heat flux (2.5 kW/m²), and the results show a more gradual increase in temperature and significantly lower maximum temperatures. The maximum temperature reached behind the outer shell was less than half that reached during the Series MF exposure. Each layer and air gap combination decreased the temperature by approximately 10 °C, with the face cloth reaching almost 100 °C. In addition, the slight change of slopes that were observed for the Series MF PCM B and C configurations are even more pronounced for the Series LF. This is understandable as the lower heat flux keeps the PCM within its melting temperature longer. A changing slope in the batting and face cloth temperatures is observed between 50 and 250 s. The temperature differences between the layers are greatest around 200 s, where the change in slope is evident.

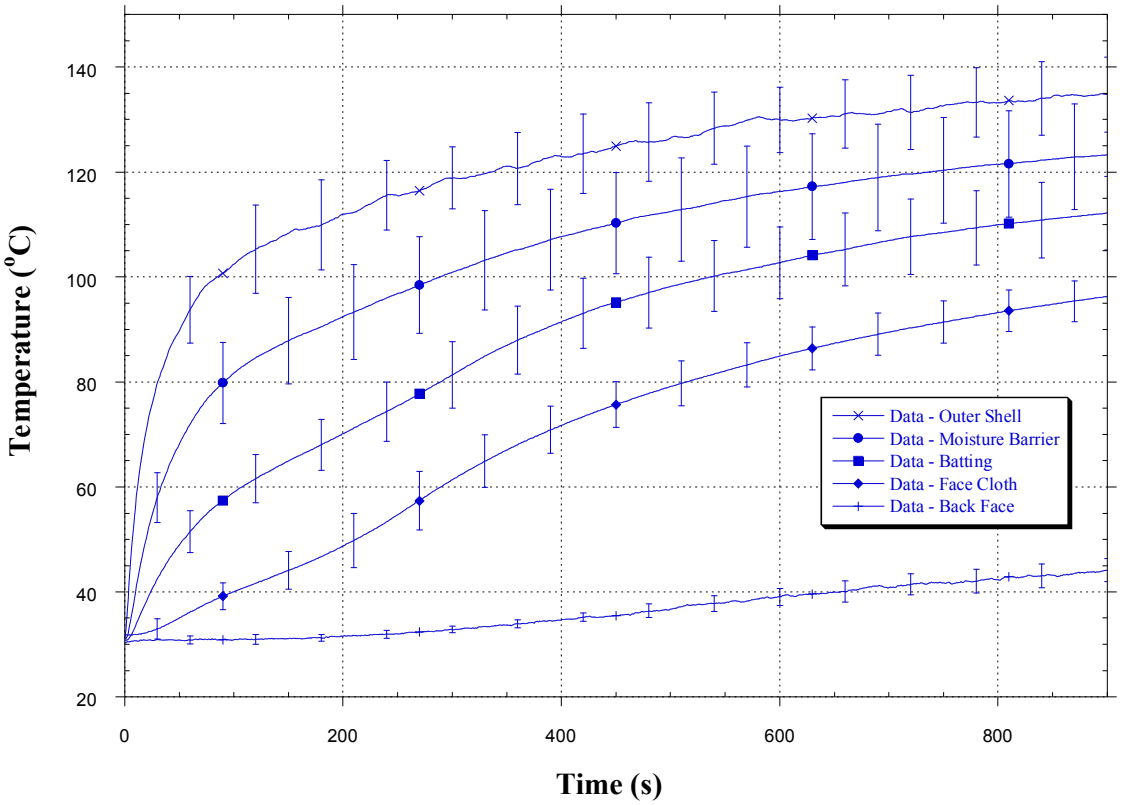

Figure 5.9: Series LF – PCM B Configuration

Finally, Figure 5.10 displays the results from the Series HF, PCM B configuration experiments. This exposure time was so short (30 s) that it was difficult to make any clear observations regarding the PCM. With such an intense heat flux (20 kW/m²), even extremely short durations present good probabilities of fire fighter protective clothing degradation. Browning and initial indications of damage to the fire fighter protective clothing was observed with the 30 second exposure. The effects of the degradation would have added unwanted complications that could be a topic of research in itself. For these reasons, a longer duration at for Series HF was not considered.

Even with the short duration, one can observe that the temperature increase behind the outer shell is much more rapid than the other exposures and a maximum is reached in 30 s that is greater than was observed in the other exposures. Moreover, the difference in the temperatures between layers is not as uniform. This is probably influenced by the short duration and more extreme transient heat transfer condition.

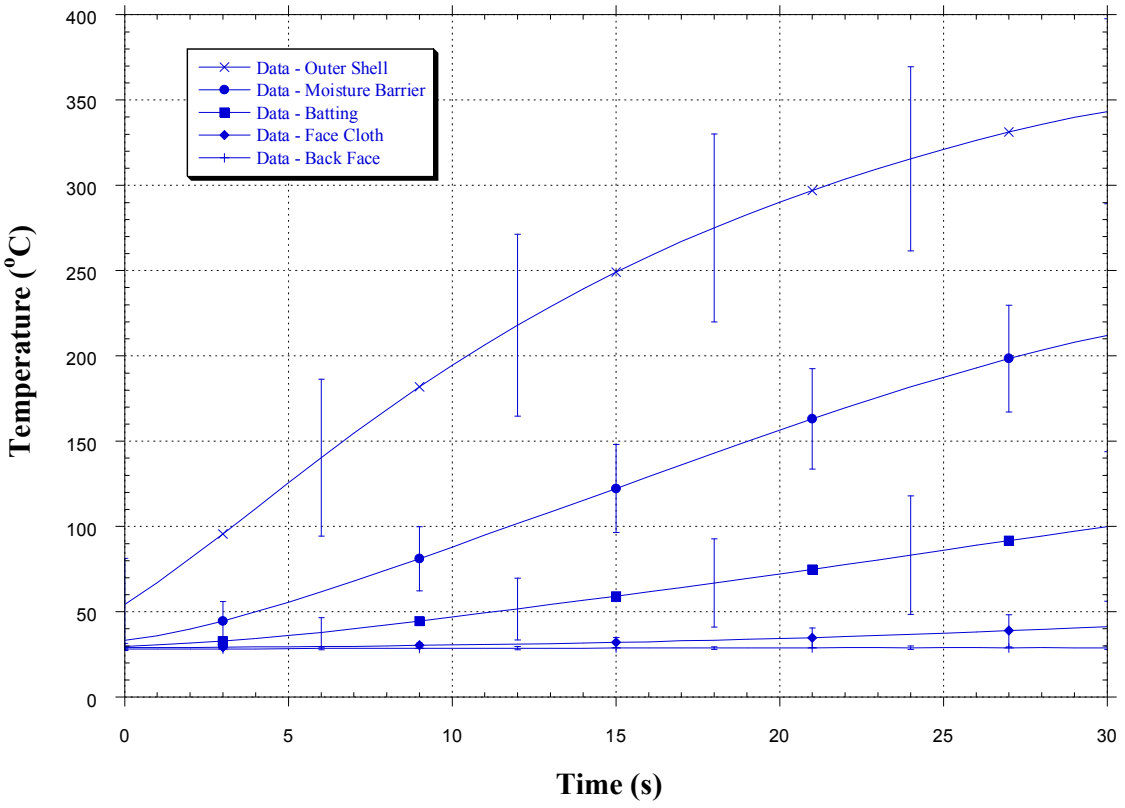

Figure 5.10: Series HF – PCM B Configuration

5.2 Model

The theoretical heat transfer model was created as described in *Chapter 3*. The results for the standard configuration and PCM B configuration were displayed in Figure 3.8 and Figure 3.10 respectively. The rest of the tests are modeled and compared to experimental data in the next section. The focus of this section is to demonstrate how the model was able to capture the effect of the latent energy absorbed by the PCM. This was accomplished by comparing the temperature curves, specifically behind the face cloth layer, of the model (Model) and the model excluding the volumetric energy absorption term (No LH Model).

Figure 5.11 displays the temperature differences behind the face cloth for the Series MF, PCM B configuration. At about 15 s the model predicts that the PCM layer reaches its melting temperature range (44–55 °C) and lower temperatures are predicted in the model that includes the latent heat. A maximum difference in temperature of almost 7 °C at is observed at approximately 75 s and temperatures remain lower for the remainder of the heat exposure. Far removed from the melting range of the PCM, the models predict similar temperatures with temperature differences approaching only slightly above 1°C.

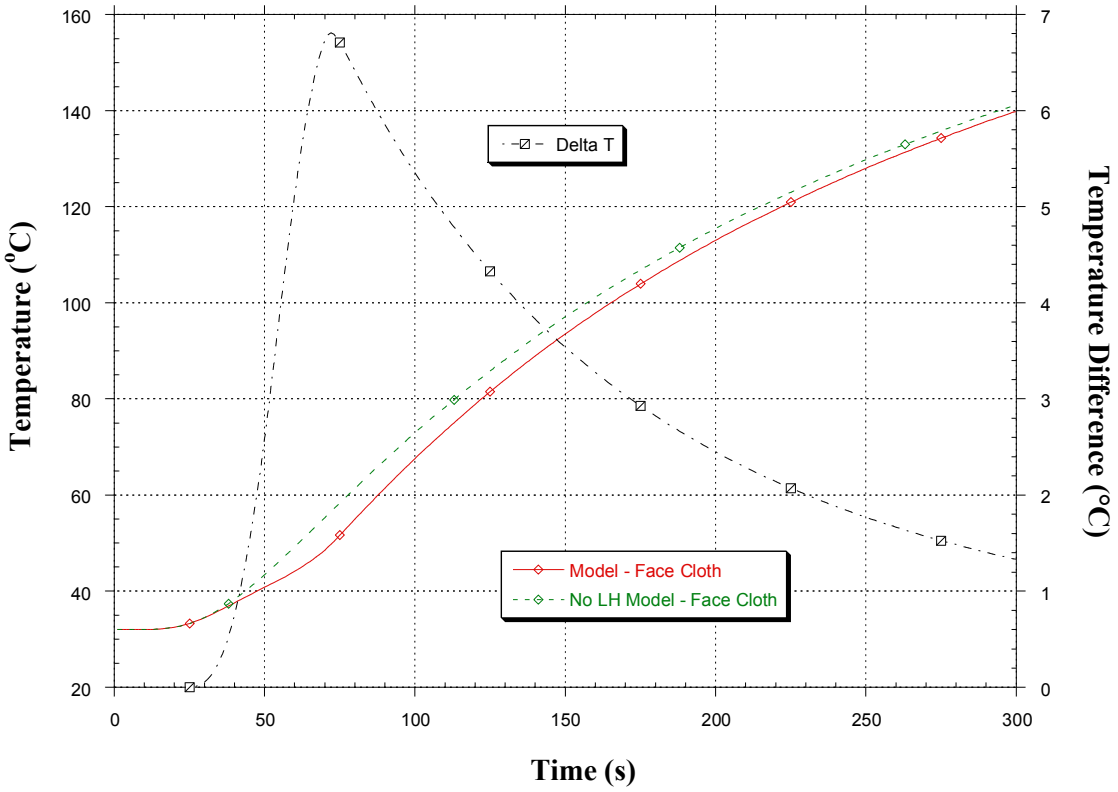

Figure 5.11: Series MF – PCM B Configuration Model vs. No LH Model

Figure 5.12 examines the predicted temperature differences behind the face cloth layer for the Series MF, PCM C configuration. Results are similar to the PCM B configuration. At approximately 25 s the model predicts that the PCM layer heats up to within the PCM's melting temperature range (71–86 °C) and the predicted lower temperatures for model that includes the latent heat. It is sensible that the PCM C, with a higher melting temperature, starts melting later than the PCM B. The maximum difference in temperature is almost 8.5 °C at about 100s s and temperatures remain lower for the remainder of the heat exposure. After the temperatures have surpassed melting

range of the PCM, the models predict similar temperatures with differences converging to as little as 1.5 °C.

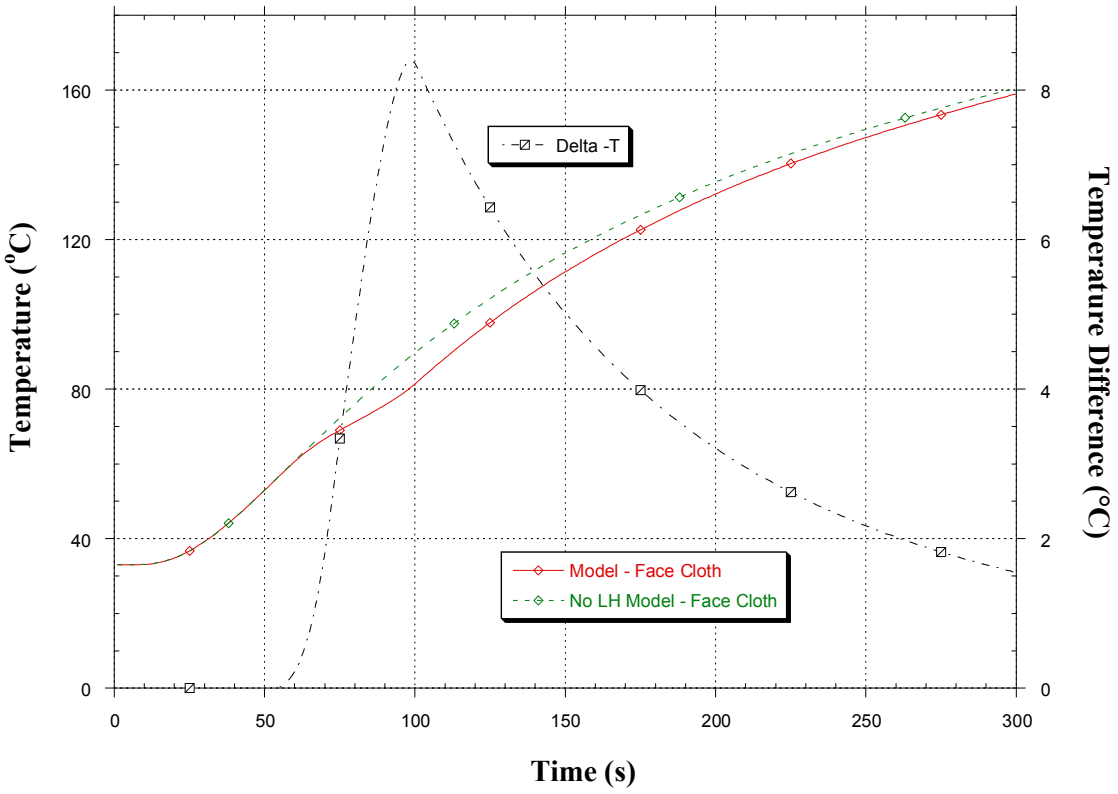

Figure 5.12: Series MF – PCM C Configuration Model vs. No LH Model

Figure 5.13 shows the predicted temperature differences behind the face cloth layer for the Series LF, PCM B configuration. Again, the effect of the PCM is more prominent for the lower heat flux. The maximum difference in temperature reaches slightly above 6 °C just after 200 s and temperatures remain lower for the remainder of the heat exposure. As

the temperatures diverge from the melting range of the PCM, the models predicts differences as little as 0.3 °C at 900 s.

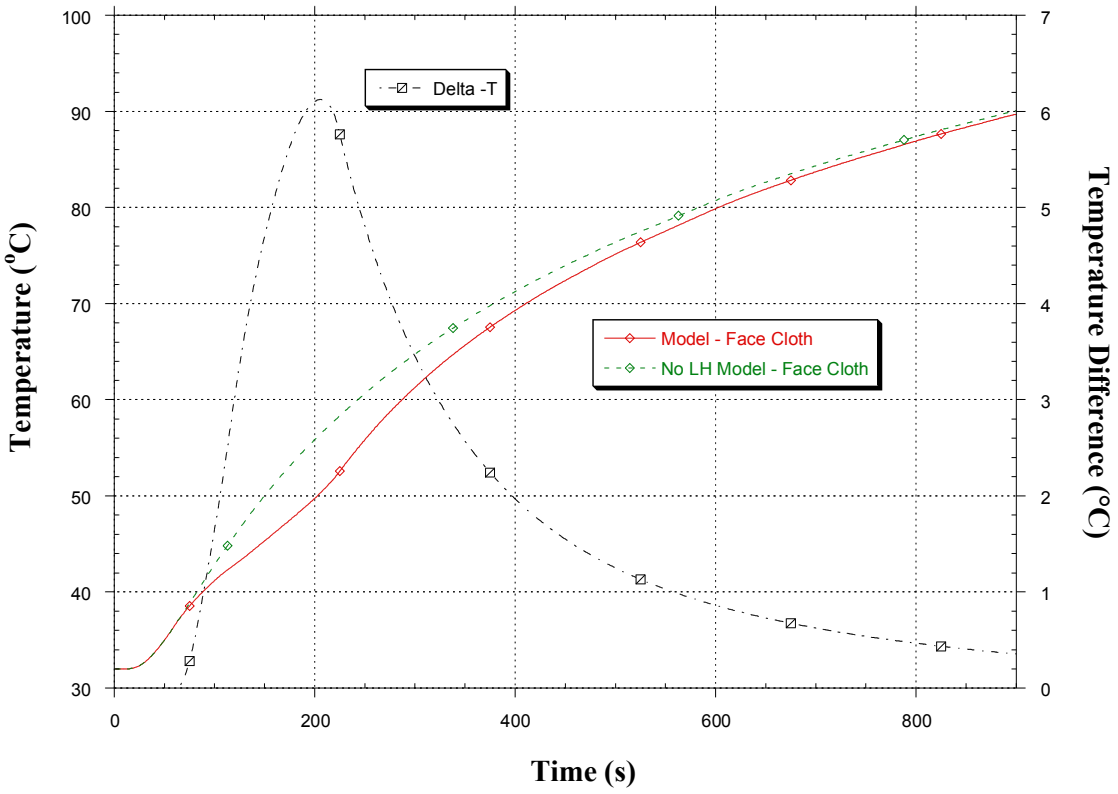

Figure 5.13: Series LF – PCM B Configuration Model vs. No LH Model

Finally, Figure 5.14 displays the behind the face cloth layer temperature comparison for the Series HF, PCM B configuration. The models predict that the effect of the latent heat is very little, with a maximum difference in temperature of only 0.5 °C. The continual increase of the Delta-T curve in Figure 5.14, indicates that that PCM has not yet had time to complete the phase change. The PCM doesn't start melting until approximately 20 s

into the heat exposure and is still just beginning to absorb the latent energy by the 30 second mark. The exposure time was too short to see the entire effects of the PCM.

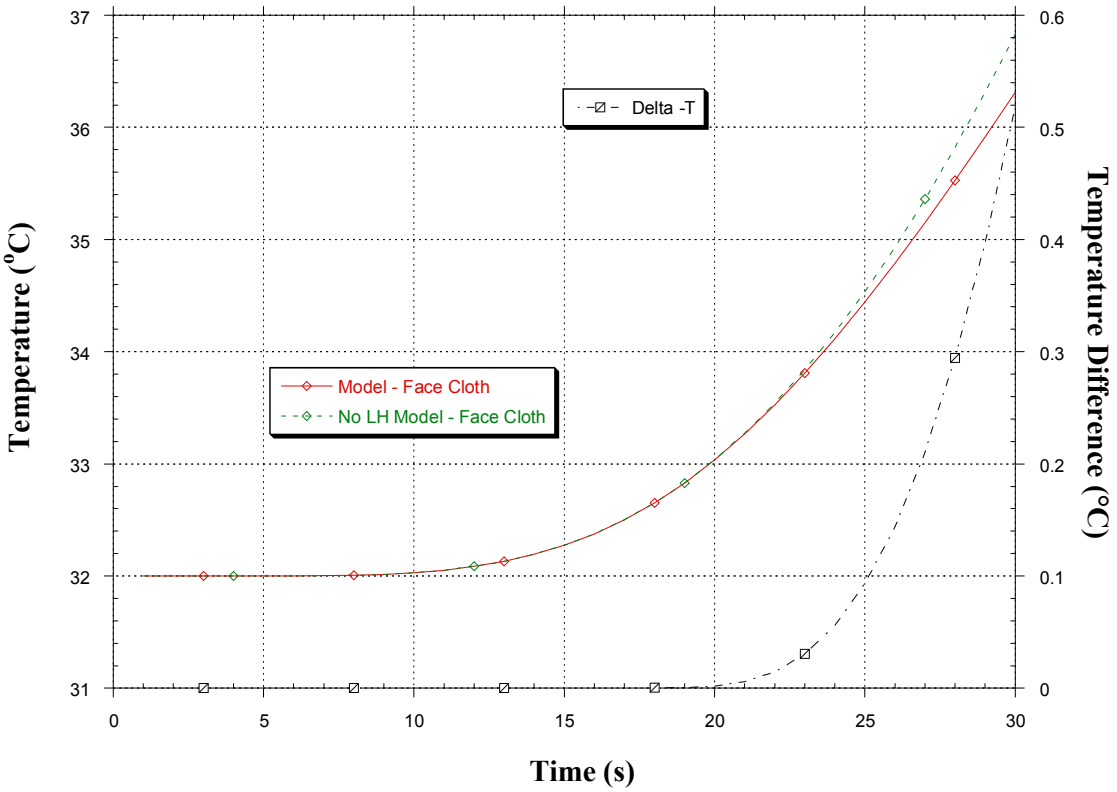

Figure 5.14: Series MF – PCM B Configuration Model vs. No LH Model

To further quantify the effect of the PCM, an energy balance was examined for the Series MF, PCM B configuration. The amount of energy stored in the PCM layer per unit area is given by Equation (27):

$$q''_{PCM} = \Delta x \cdot \rho \cdot c_p \Delta T + \Delta x \cdot \rho \cdot L \qquad \textbf{(27)}$$

The $\Delta x \cdot \rho \cdot c_p \Delta T$ term in Equation (27) represents the sensible energy, while the $\Delta x \cdot \rho \cdot L$ term represents the latent energy. The theoretical model was used to determine the amount of energy was stored in the PCM layer per unit area (Figure 5.15). This was determined by estimating the energy that was stored for each time step:

$$q''_{stored} = q''_{in} - q''_{out} \quad \textbf{(28)}$$

$$q''_{stored} = \frac{\left[k_{batting}\left(T_{pcm-2} - T_{pcm-1}\right) - k_{face\_cloth}\left(T_{pcm+1} - T_{pcm+2}\right)\right]}{\Delta x} \quad \textbf{(29)}$$

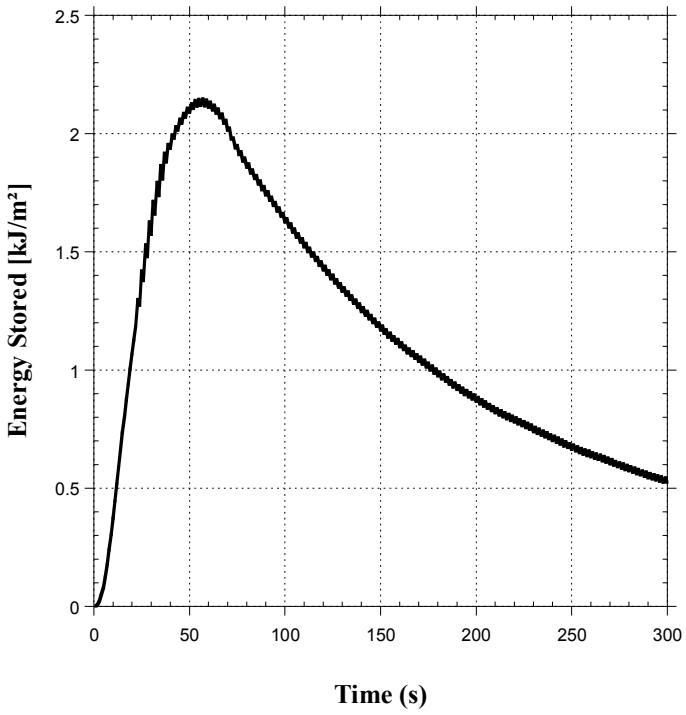

Figure 5.15: Energy Storage in PCM B Layer – Series MF

The sensible energy term from Equation (27) was then estimated based on the overall change in temperature from the initial temperature to the final temperature for each node within the PCM layer. The sum of the sensible energy per unit area for this test was calculated to be 319 *kJ/m²*. The stored energy calculated from Equation (29) in the model was summated to 347 *kJ/m²* and compared with Equation (27) to determine the amount of latent energy absorbed. Setting, q''_{PCM} equal to q''_{stored} and solving for the latent energy term yields:

$$\Delta x \cdot \rho \cdot L = \sum \left[\frac{k_{batting}}{\Delta x} \left(T_{pcm-2} - T_{pcm-1} \right) - \frac{k_{face\_cloth}}{\Delta x} \left(T_{pcm+1} - T_{pcm+2} \right) \right] - \sum \Delta x \cdot \rho \cdot c_p \Delta T \quad \textbf{(30)}$$

$$Latent\_Energy = 347 - 319 = 28 \ \ kJ/m^2$$

For the entire 300 s test, the latent heat accounted for approximately 8% of the energy absorbed, while the sensible energy accounted for the other 92%. As expected, the percentages change over time. A plot of the percentage of latent energy absorbed versus time is displayed below (Figure 5.16), and it is observed that the latent heat accounted for as much as 30% of the energy absorption. These values were calculated every 30 s using the same method described above. This demonstrates that the PCM material is able to absorb more energy for the same amount of mass than a material that doesn't change phase. The PCM material would perform particularly well if the fire fighter were to leave the heat exposure immediately after the change of phase was complete.

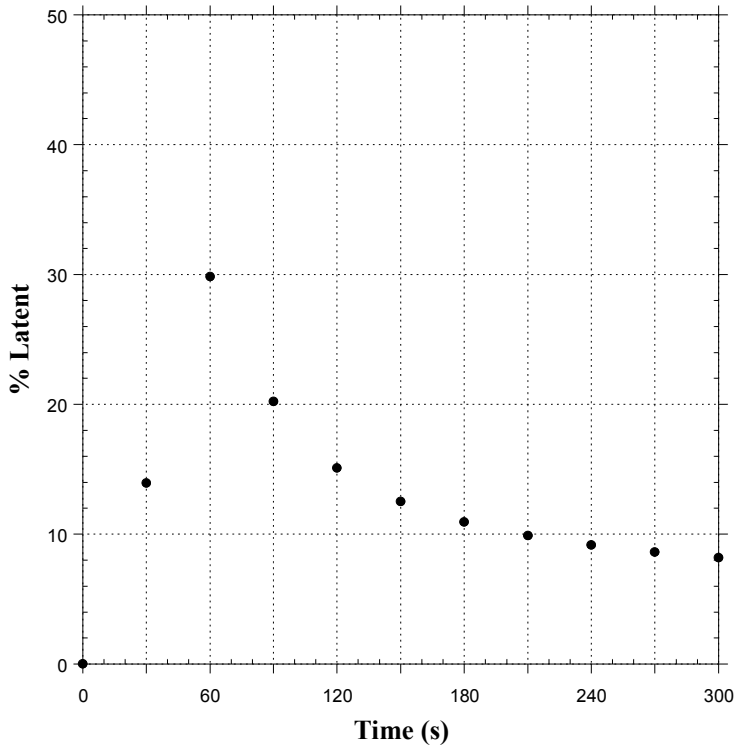

Figure 5.16: Percentage of Latent Energy Absorption vs. Time

5.3 Model Compared with Experimental Data

The theoretical heat transfer model was run and compared with the previous experimental results. Figure 5.17 displays the comparison for the standard configuration. The model demonstrates excellent agreement with the empirical data and is within the uncertainty for the majority of the measurements. The overall shape of the temperature curves are close to those seen by the experiments. The predicted temperatures behind the moisture barrier and batting are more consistent with the empirical data than the temperature behind the face cloth in the middle of the heat exposure. The model predicts slightly

higher temperatures behind the face cloth, which could be due to several factors including the positioning of the thermocouple, the air gaps and the assumed material properties. As the time nears the end of the exposure, the accuracy of the model improves, which is consistent with what one might expect as the heat transfer approaches steady-state.

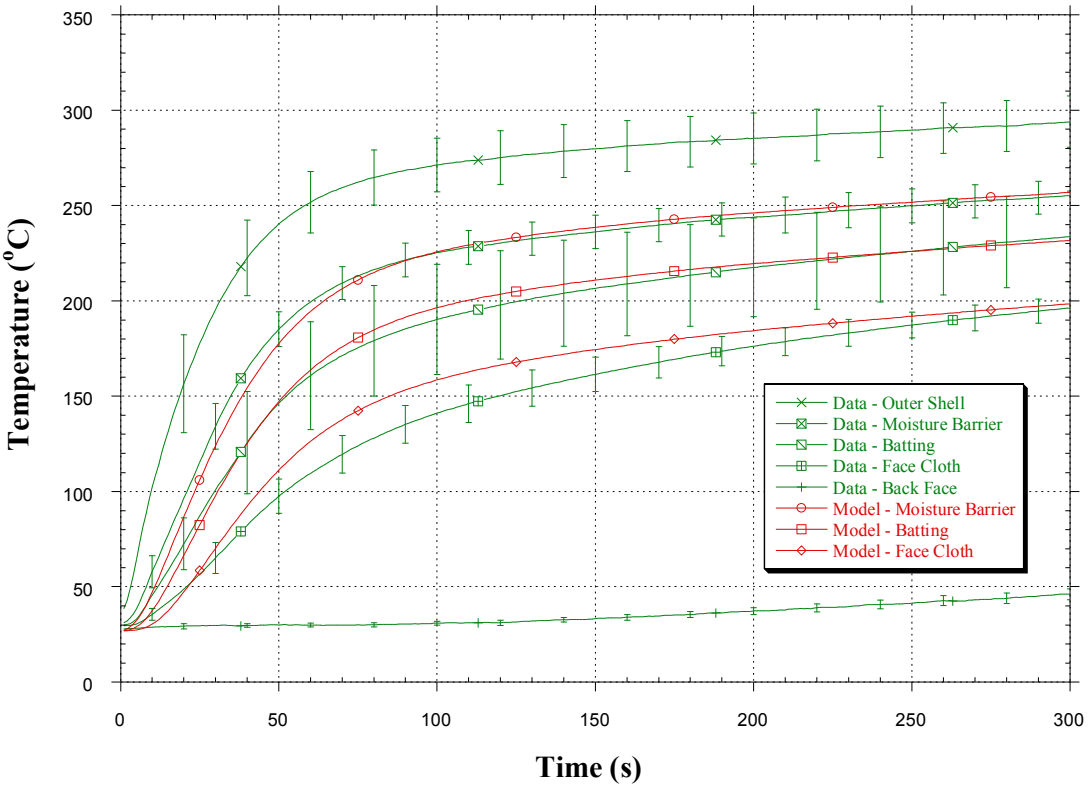

Figure 5.17: Series MF – Standard Configuration Model vs. Experimental Data

Figure 5.18 displays the Series MF PCM B configuration comparison between the model and the data. Once again the overall shape of the predicted temperature curves are consistent with those that were measured, and the model results are close to the measurement uncertainty. The model over-predicts the temperatures behind the batting

layer, while under-predicting the temperatures behind the face cloth. Explanations for this could include the positioning of the thermocouples and material properties. Particularly, the measured thickness for the thermal liners embedded with PCM carried significant uncertainty. Not only was it difficult to measure, but the amount of PCM in each pocket that was sewn into the thermal liner were not perfectly uniform (Figure 2.5). Furthermore, thermocouples behind the batting had the most uncertainty. These thermocouples could have been in contact with the PCM, reading lower temperatures.

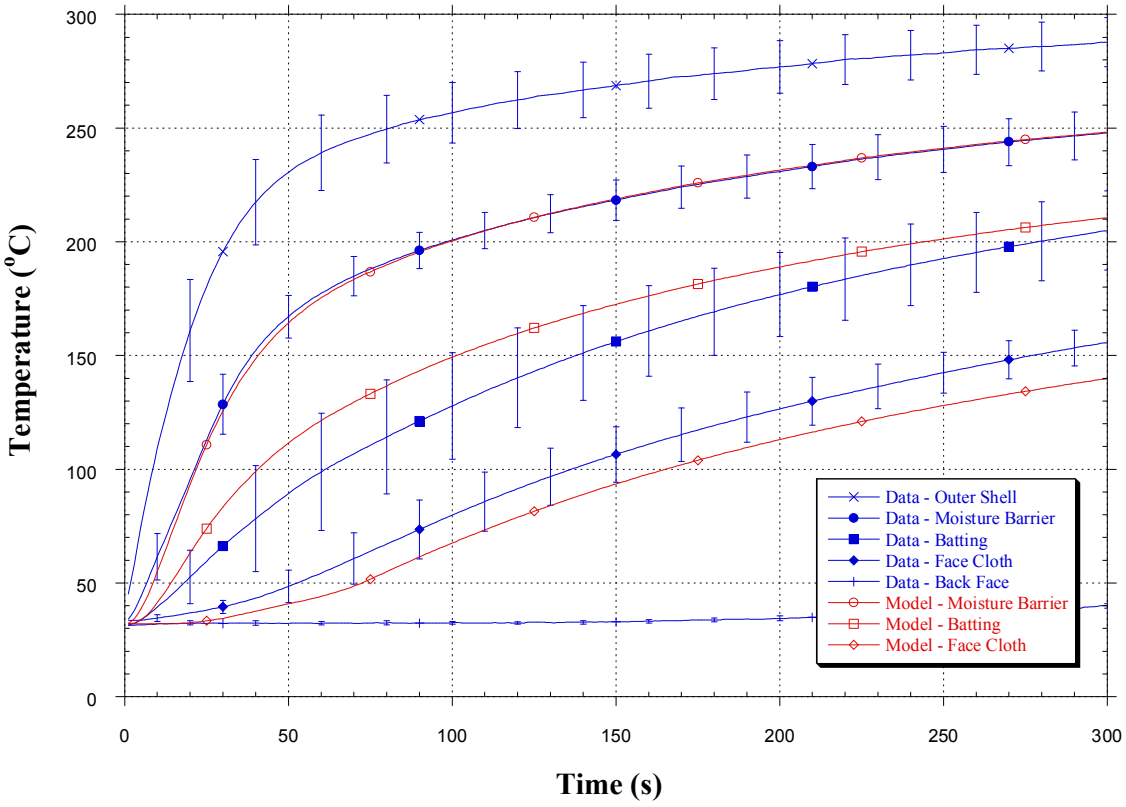

Figure 5.18: Series MF – PCM B Configuration Model vs. Experimental Data

Figure 5.19 displays the PCM C configuration comparison for the same Series MF exposure. There is an even greater concurrence between the model and data for the PCM C than there was for the PCM B. There are differences between the predicted temperatures by the model and the empirical data, but these differences are very close to or within the measurement uncertainty. Explanations of the differences are consistent with those previously explained for the PCM B.

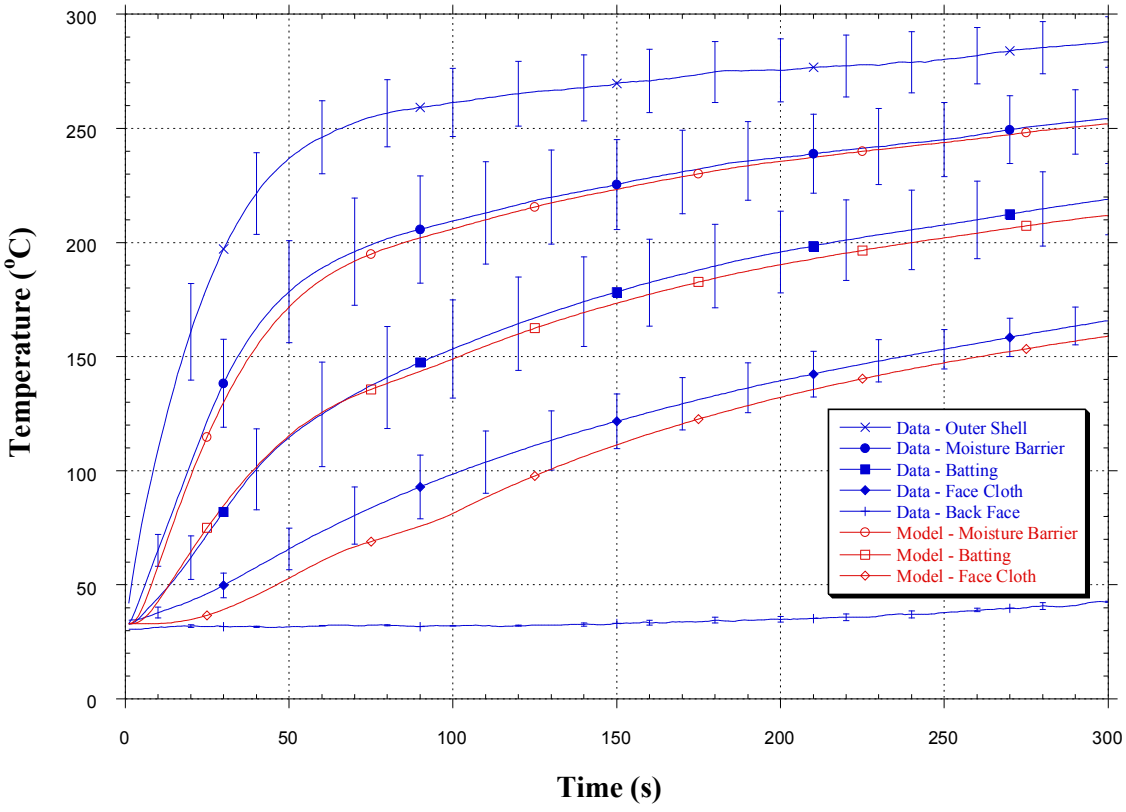

Figure 5.19: Series MF – PCM C Configuration Model vs. Experimental Data

Figure 5.20 shows the results for the PCM B configuration from the Series LF exposure as compared with the theoretical model. Consistent with the previous results, the model does an excellent job at predicting the temperatures behind the moisture barrier, yet loses some accuracy behind the face cloth. The predicted temperatures from the model are still within the measurement uncertainty for the majority of the time. Justifications for the inconsistencies remain similar to the previous discussions. One noted difference for the Series LF is the increased difference seen for the temperature behind the face cloth close the end of the exposure. The temperatures predicted by the model fall just outside the standard deviation of the temperature measurements. In addition to the previously mentioned areas for uncertainty with thermocouple placement and material properties, this could be explained by the initial temperature of the calcium silicate board being higher than predicted. During the longer exposures, it was observed that the calcium silicate board stored more heat. Time was allotted between experiments for cooling, but it is reasonable to assume that the board could have not cooled completely to room temperature. This would add additional energy in the experiment that was not accounted for in the model.

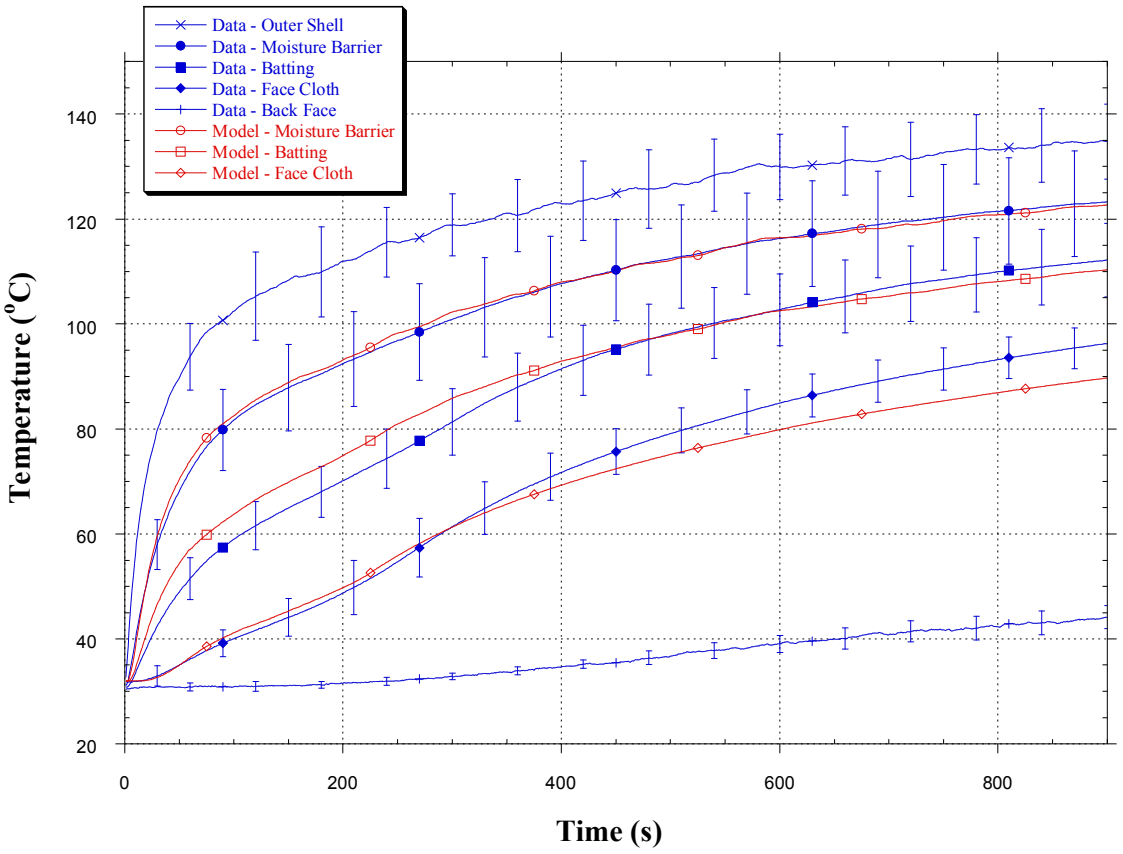

Figure 5.20: Series LF – PCM B Configuration Model vs. Experimental Data

Figure 5.21 displays the same comparisons for the PCM B configuration, but at the Series HF exposure. As mentioned previously, the short duration of this exposure makes it difficult to observe the effect of the PCM. The early transient heat transfer is generally more difficult to predict than conditions closer to steady state. Even so, Figure 5.21 illustrates that the theoretical model still predicts the temperatures within reason, and all the temperatures are within the measurement uncertainty.

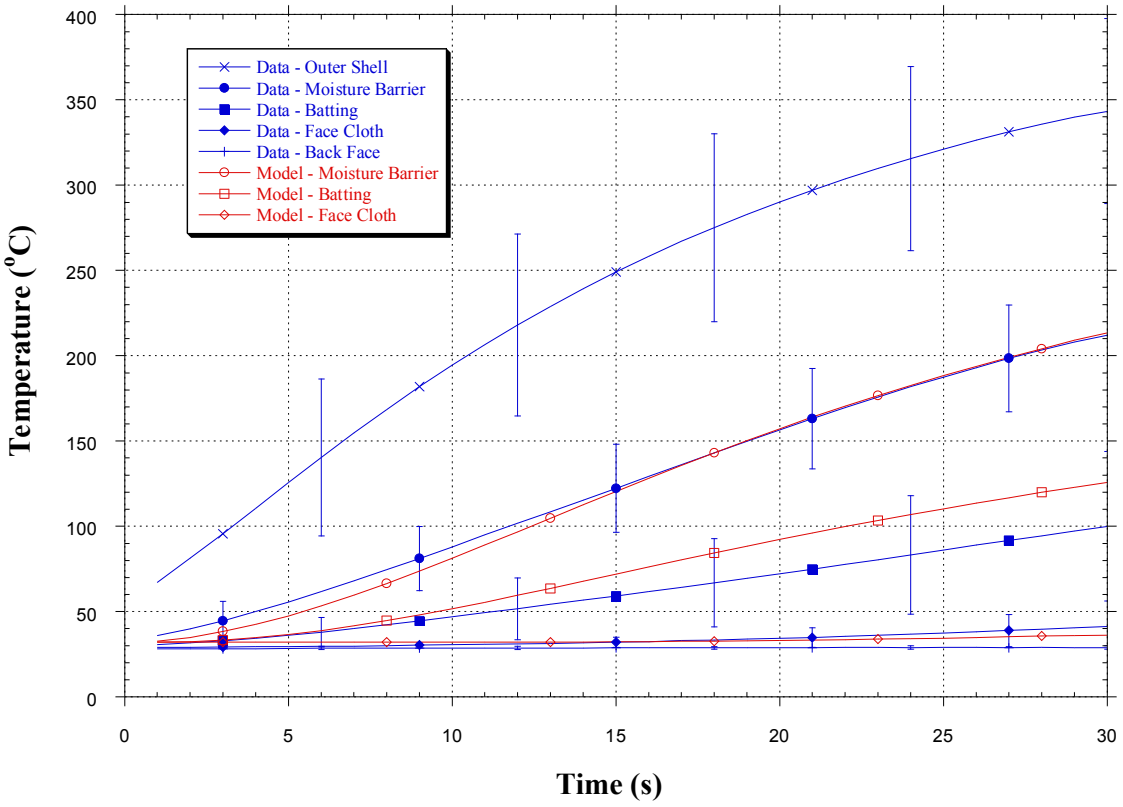

Figure 5.21: Series HF – PCM B Configuration Model vs. Experimental Data

Chapter 6: Conclusions

6.1 Conclusions

Bench-scale experiments were conducted for a range of radiant heat exposures to simulate realistic fire fighting conditions. Results displayed lower overall temperatures for the specimens with PCMs than those without. The temperature differences were largely due to the additional material, but there was some effect caused by the phase change. Close examination of the temperature plots for the layers near the PCM displayed a change of slope, indicating latent heat absorption. The effects of the latent heat were more evident in the lower heat flux exposure than the higher heat flux exposures.

To further investigate the effect of the PCMs, a mathematical model of the heat transfer through fire fighter protective clothing was created that incorporated the phase change material. The model was compared to the experimental data and predicted temperatures with excellent agreement. Using the theoretical model the phase change effect was able to be estimated, properly capturing the effect of the PCM. The model provides an excellent tool that can be used to quantify the effect of the PCM, as well as compare the results to numerous specimen configurations and exposures without the expense of experimentation.

For the Series MF experiments in this study, the model predicted a reduction in temperature by as much as 8.5 °C (15 °F) due to the absorption of latent heat. Moreover, the model predicted that the latent energy absorption accounted for as much as 30% of the total energy absorbed in the PCM layer, thus indicating that the PCM was able to absorb more energy per mass than a material that doesn't change phase. These maximum values are representative of the end of the phase change. This would be the ideal time for the fire fighter to exit the heat exposure environment because the heat transfer no longer contributes to the latent energy, and the benefit of the PCM has expired. Predicted temperatures near the end of the exposure, far removed from the phase change, were only about 1 °C lower due to the latent energy absorption.

The results of this work provided insight into the effectiveness of adding PCM to fire fighter protective clothing, yet further research and analysis is required before making concrete conclusions in regard to the practical application. The overall goal of advancing the technology and understanding of fire fighter protective clothing is to reduce fire fighter fatalities and injuries. While it is understandable that continuing to improve the thermal performance alone will not reduce these statistics, this study demonstrates that there are potential benefits from the use of PCMs in fire fighter protective clothing.

6.2 Future Research

The physiological effects of the added weight of PCM to the fire fighter protective clothing should be explored and a cost-benefit analysis conducted. During fire fighting activities, fire fighters have thermal influences both externally from the fire environment and internally from heat stress related to physical exertion. Additional weight can add to the internal heat stress by increasing the physical exertion. This research was focused on the externally induced heat flux, leaving room for improvement if physiological impacts are fully considered as well. Applications of PCM could be applied only to specific areas where fire fighters are typically burned to maximize the benefit without adding significant weight.

Additional research into the cooling phase of the PCM is another area that deserves some attention. This study examined the heat exposure and ability of the PCM to delay the heat transfer through the fire fighter protective clothing. The delay of heat transfer during an exposure provides a benefit to the fire fighter. After the exposure, however, delaying the release of this energy could keep the fire fighter warmer and contribute to heat stress or burns. Although it may not be possible, an ideal material would delay heat transfer to the fire fighter but release that energy quickly when removed from the exposure environment.

As mentioned to in the previous section, there are many factors other than the thermal performance of fire fighter protective clothing that contribute to the number of fire fighter burns injuries and fatalities. One important factor is the responsibility of the users of fire

fighter protective clothing to understand its safe use limits. Traditionally this knowledge is passed down from experienced fire fighters to those that are inexperienced. However, it would be ideal to be able to effectively convey this information to the fire service, without the fire fighters' risk of getting burned by a trial and error method. Future work to create computer simulations, DVDs or other means of portraying this vital information to fire fighters would be beneficial to reducing those statistics.

Appendix A

Table A.1: Series LF and HF Material Properties

Properties taken at ~100°C **Material**	**Thermal Conductivity (W/m-K)**	**Density (kg/m³)**	**Specific Heat (kJ/kg-K)**	**Thickness (mm)**
Air Gap	0.034	0.87	1.01	*
Moisture Barrier	0.084	316.8	2.29	0.46
Batting	0.059	54	2.4	0.80
Face Cloth	0.09	316.9	2.33	0.24
Calcium Silicate Board	0.12	737	1.17	13.02

* Air Gap thickness varies

Table A.2: Series MF Material Properties

Properties taken at ~200°C **Material**	**Thermal Conductivity (W/m-K)**	**Density (kg/m³)**	**Specific Heat (kJ/kg-K)**	**Thickness (mm)**
Air Gap	0.041	0.70	1.03	*
Moisture Barrier	0.134	316.8	2.75	0.46
Batting	0.088	54	3.4	0.80
Face Cloth	0.14	316.9	3.51	0.24
Calcium Silicate Board	0.12	737	1.26	13.02

* Air Gap thickness varies

Table A.3: Phase Change Material Properties

Material	Thermal Conductivity (W/m-K)	Density (kg/m³)	Specific Heat (kJ/kg-K)	Latent Heat (kJ/kg)	Thickness (mm)	Melting Temperature (°C)
PCM_A	0.2	750	1.5	64	4	33-48
PCM_B	0.1	640	1.6	105	3.2	44-55
PCM_C	0.2	750	1.5	70	2.8	71-86
PCM_D	-	830	-	149	3.9	77-85
PCM_E	0.2	940	1.8	168	2.9	91-106

Appendix B

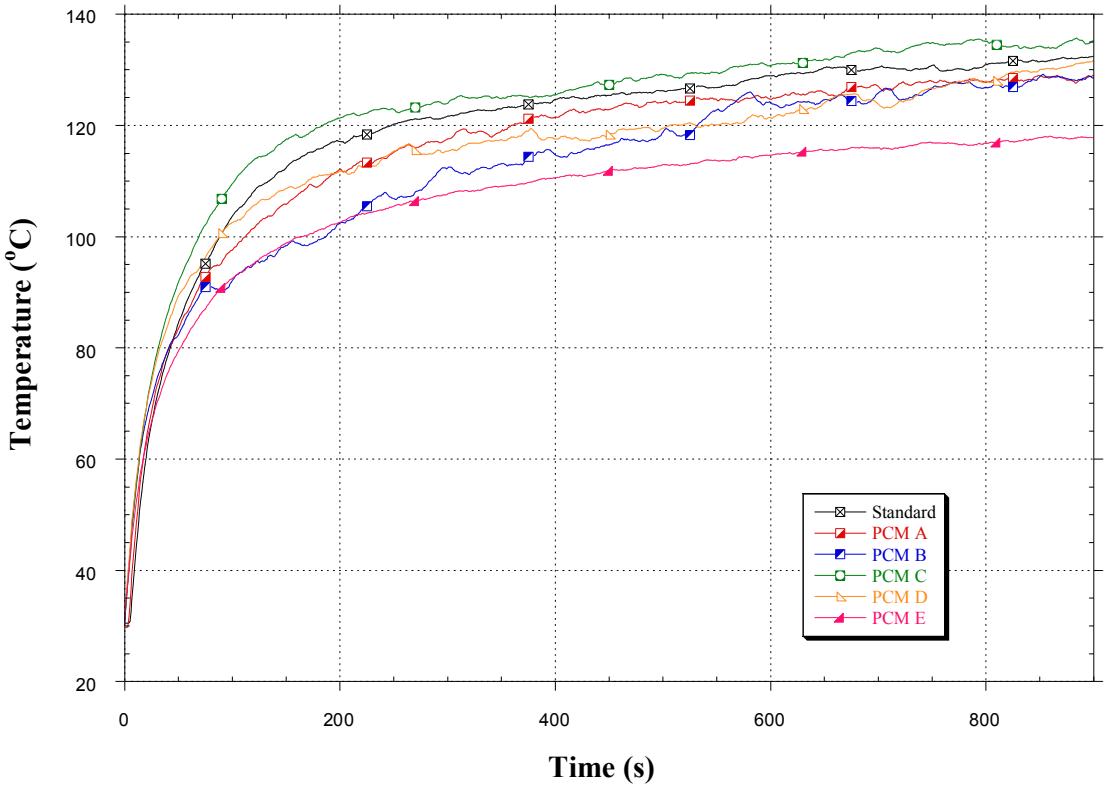

Figure B-1: Series LF – Behind Outer Shell TC Position

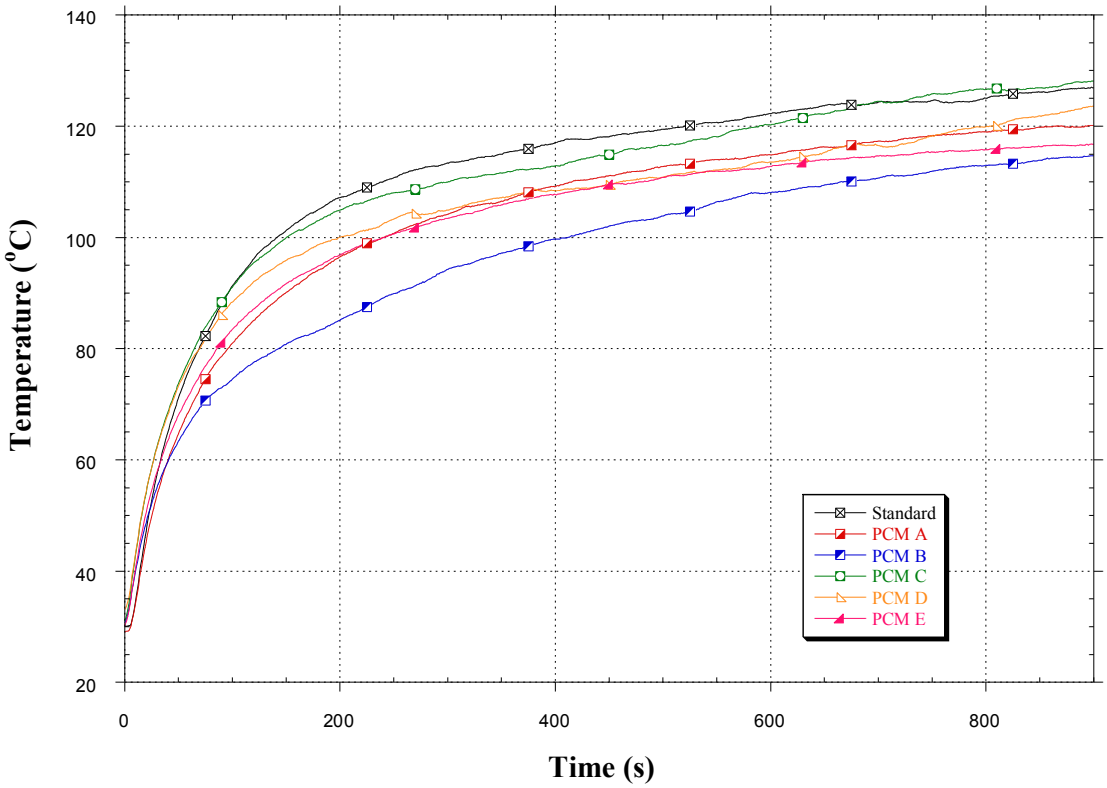

Figure B-2: Series LF – Behind Moisture Barrier TC Position

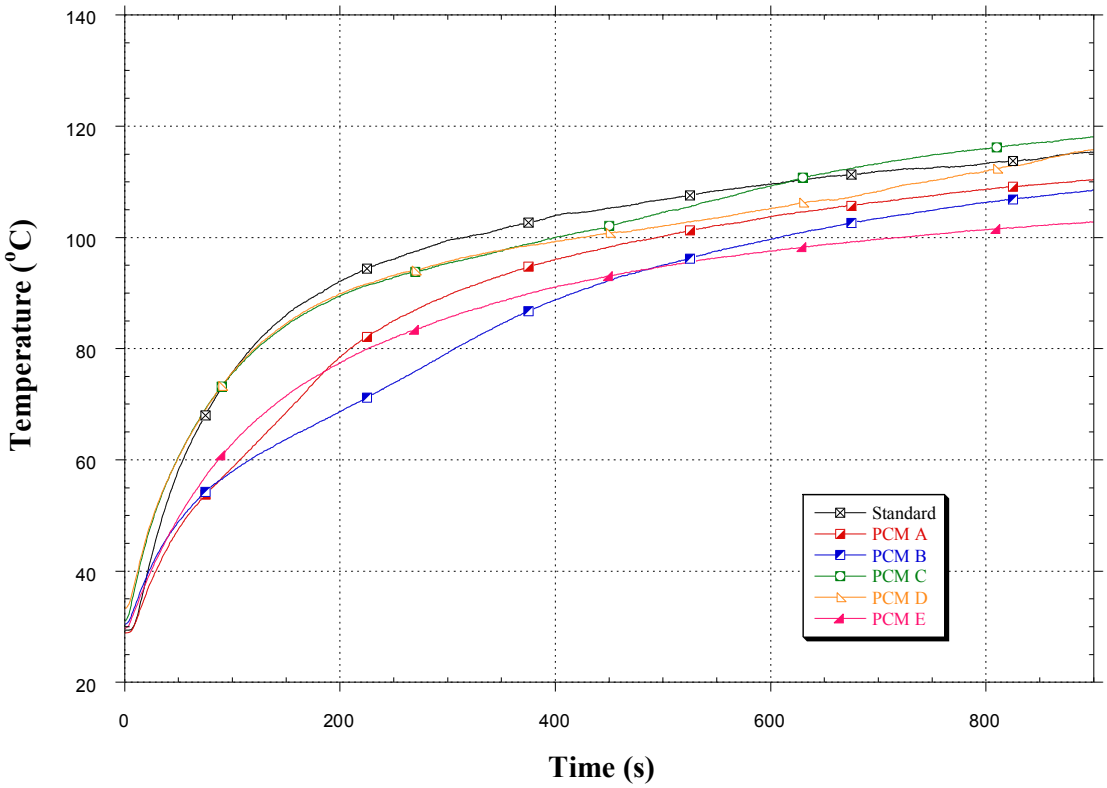

Figure B-3: Series LF – Behind Batting TC Position

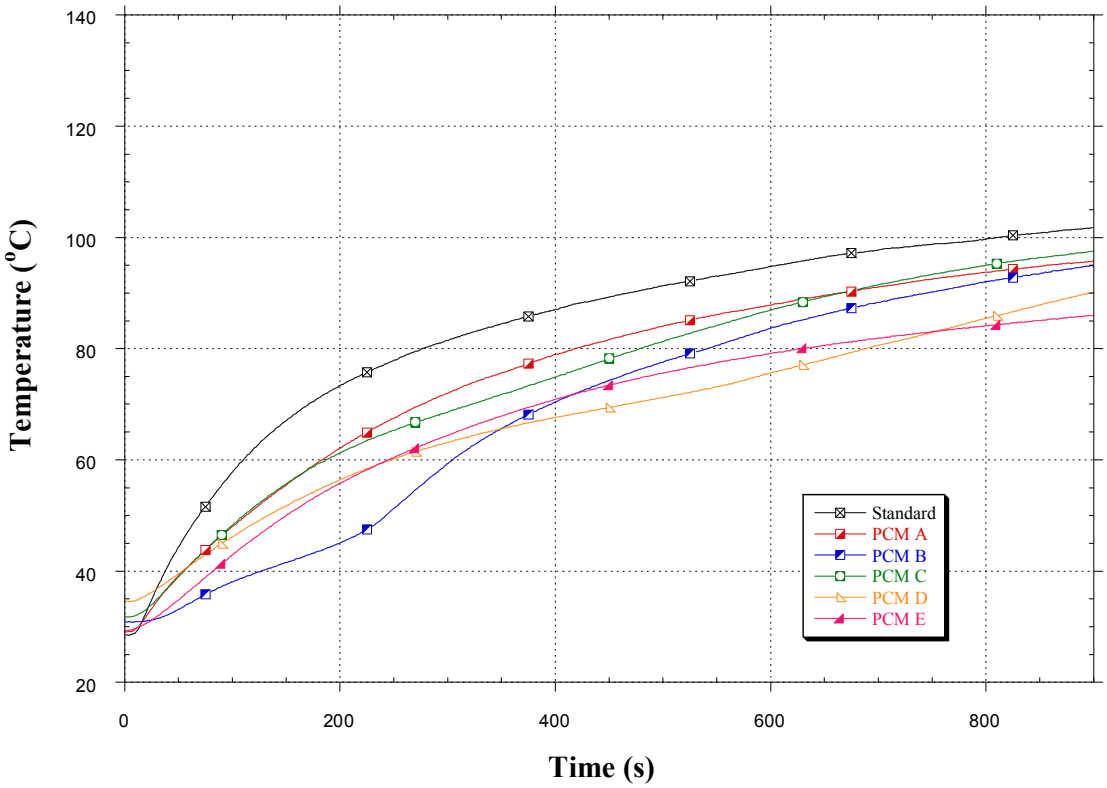

Figure B-4: Series LF – Behind Face Cloth TC Position

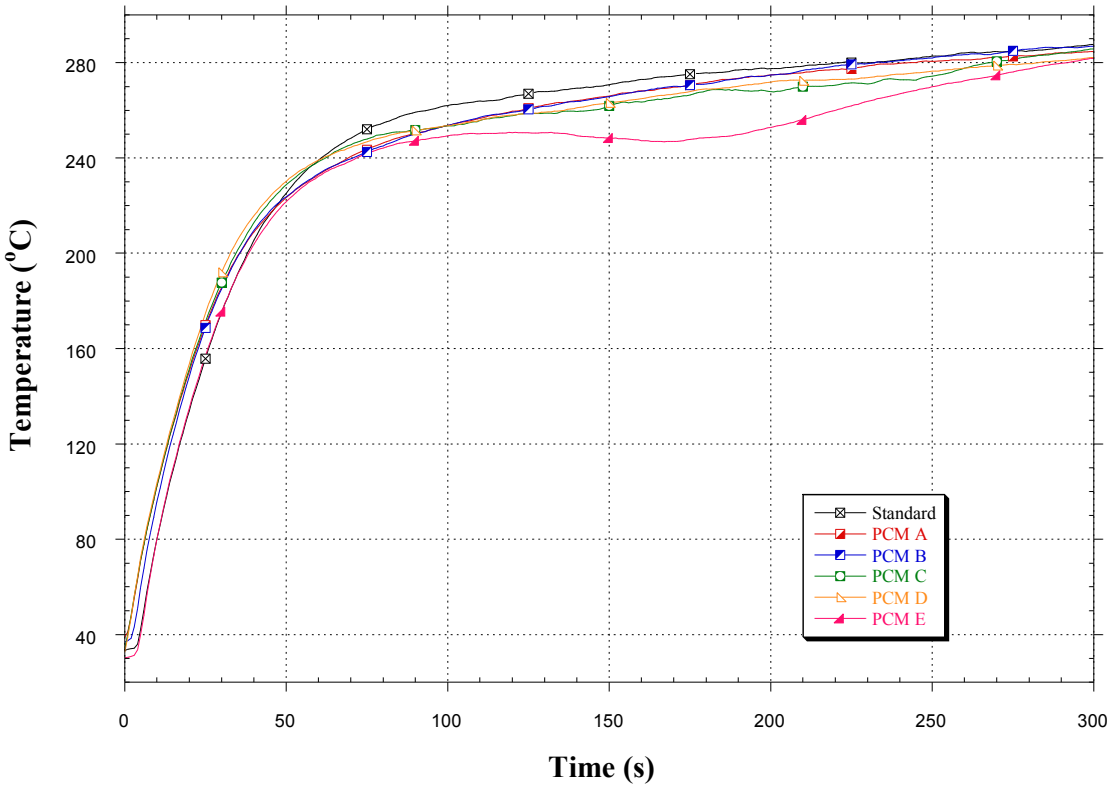

Figure B-5: Series MF – Behind Outer Shell TC Position

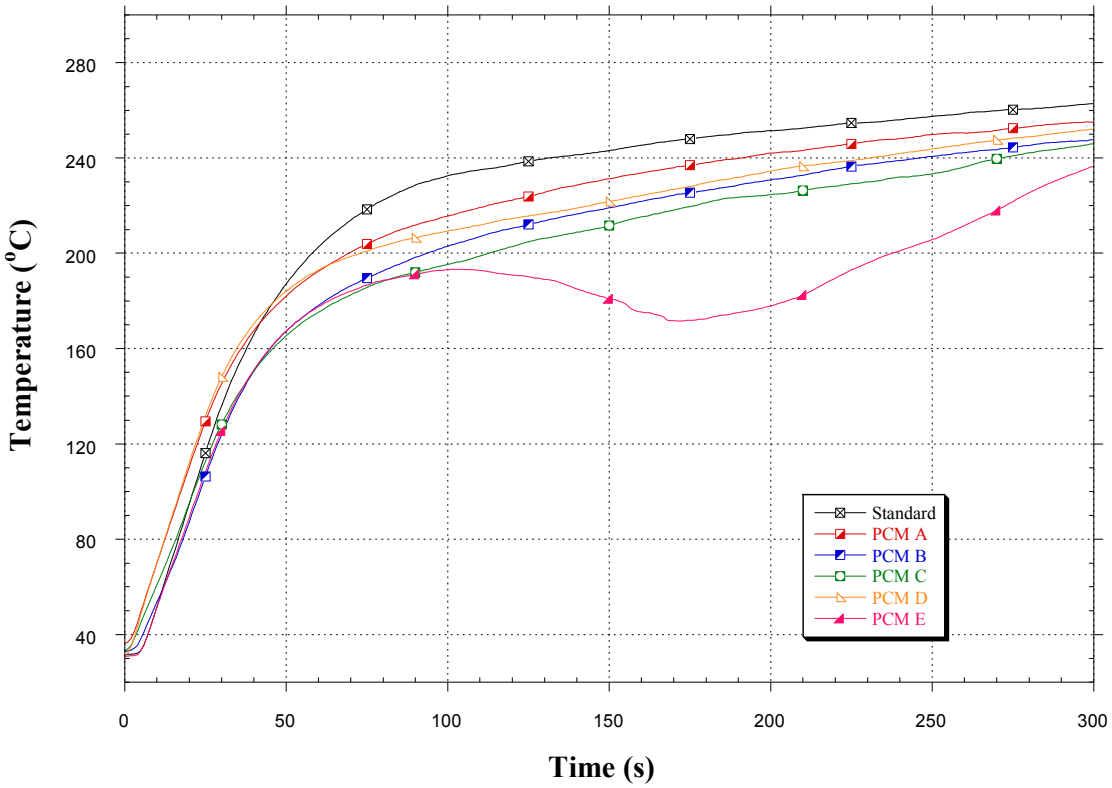

Figure B-6: Series MF – Behind Moisture Barrier TC Position

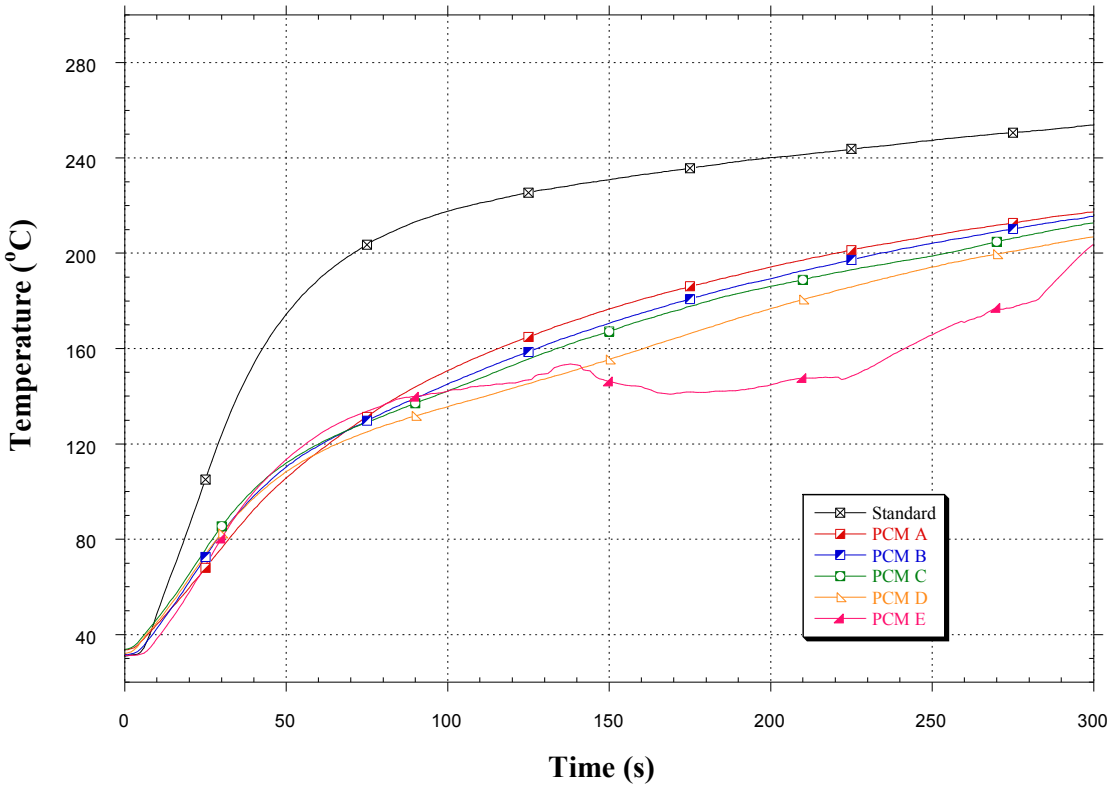

Figure B-7: Series MF – Behind Batting TC Position

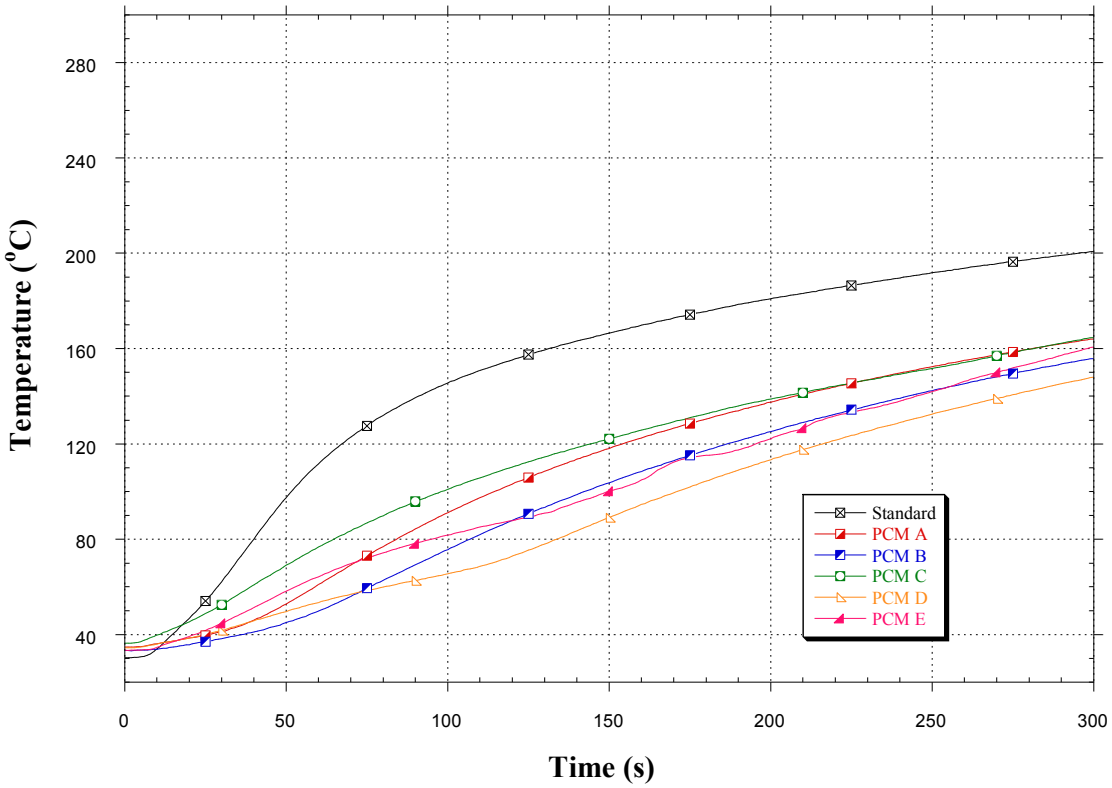

Figure B-8: Series MF – Behind Face Cloth Position

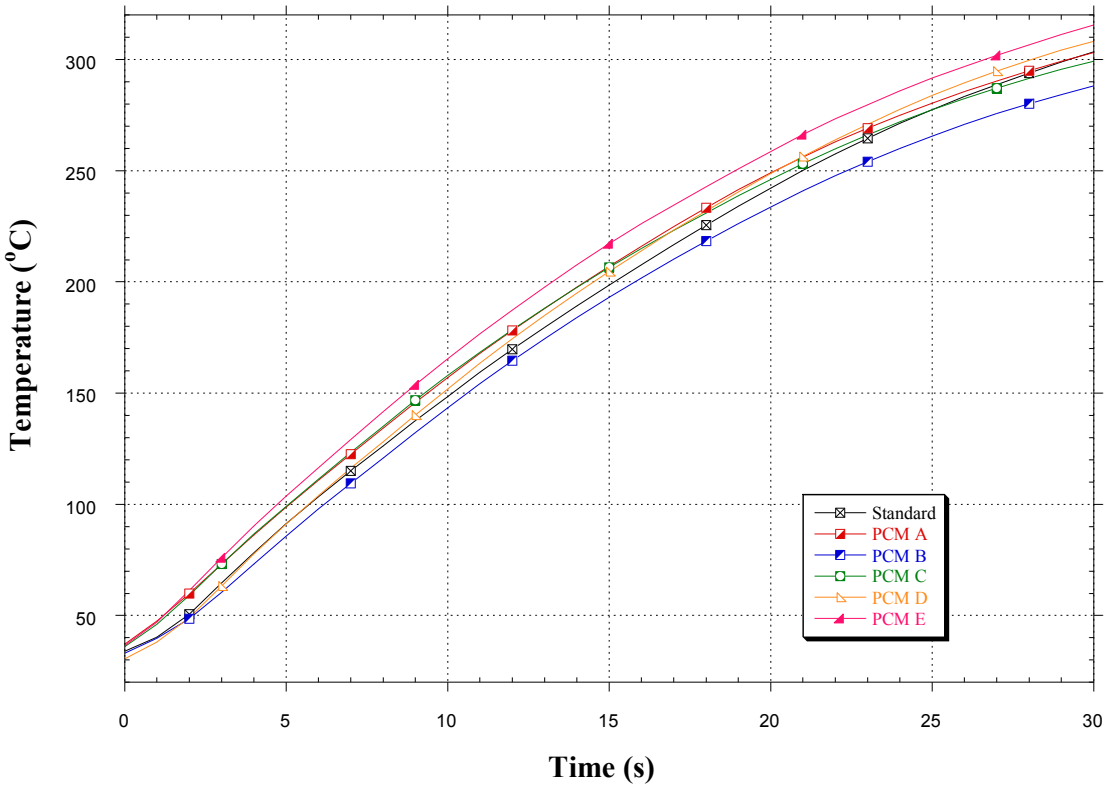

Figure B-9: Series HF – Behind Outer Shell TC Position

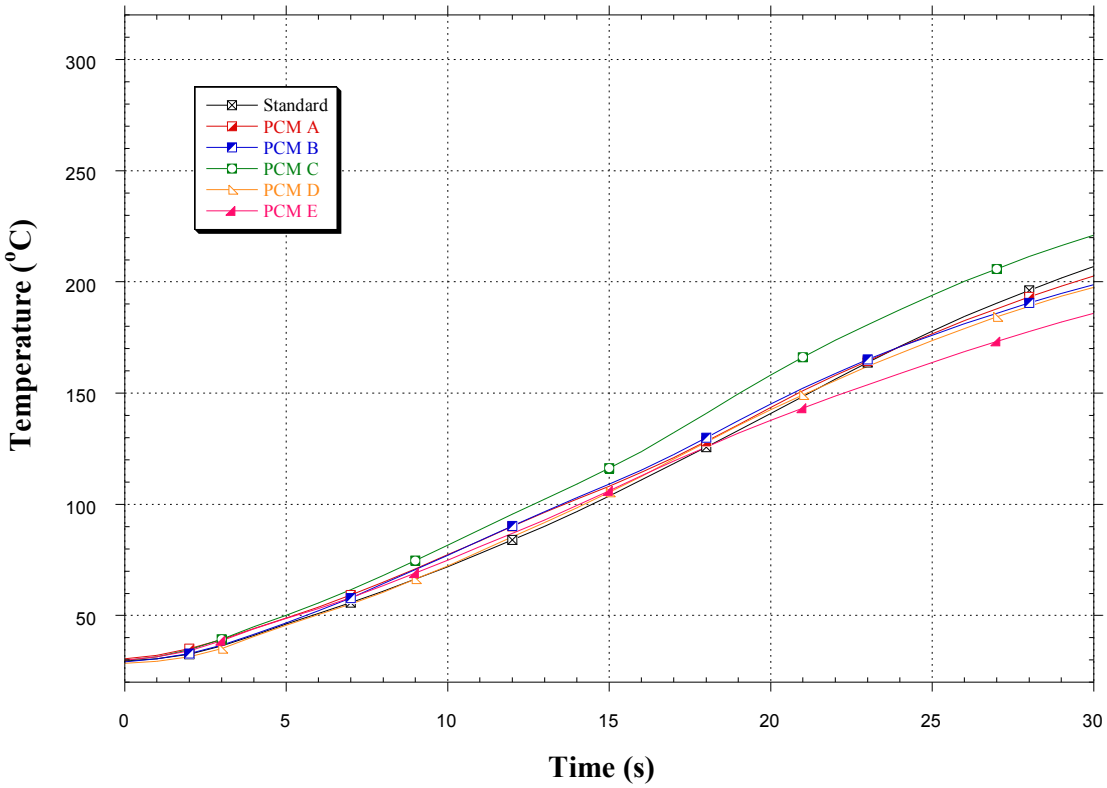

Figure B-10: Series HF – Behind Moisture Barrier TC Position

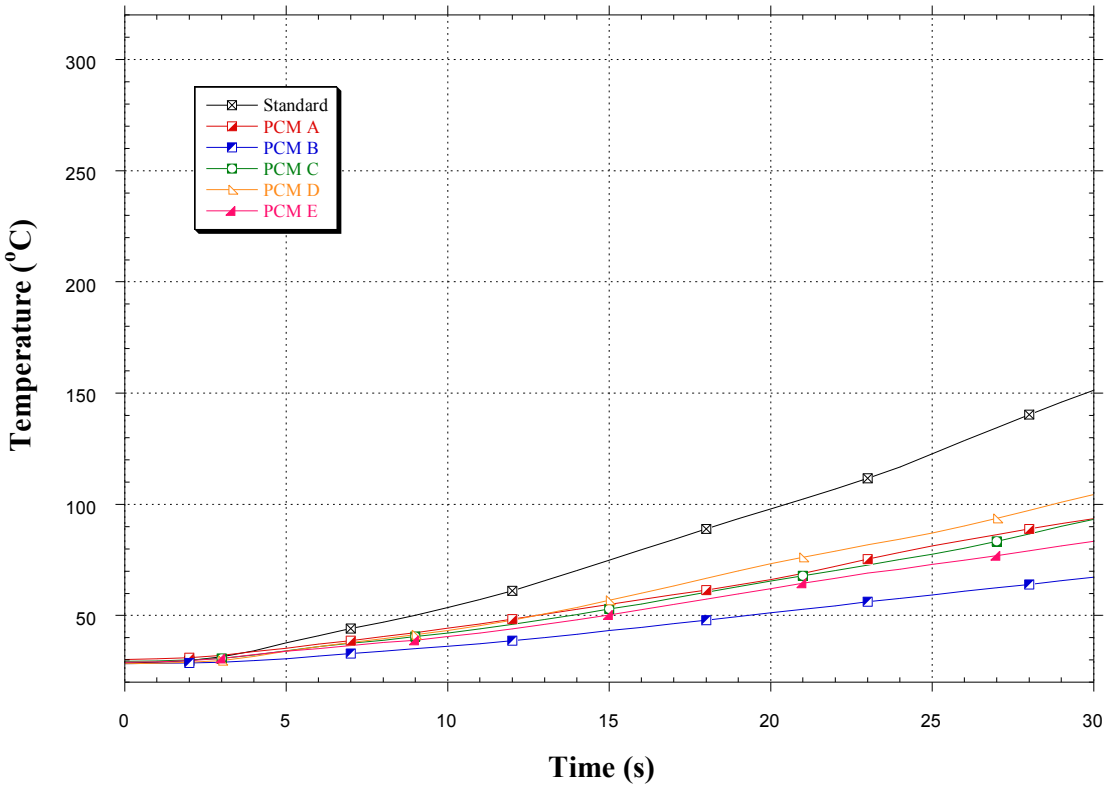

Figure B-11: Series HF – Behind Batting TC Position

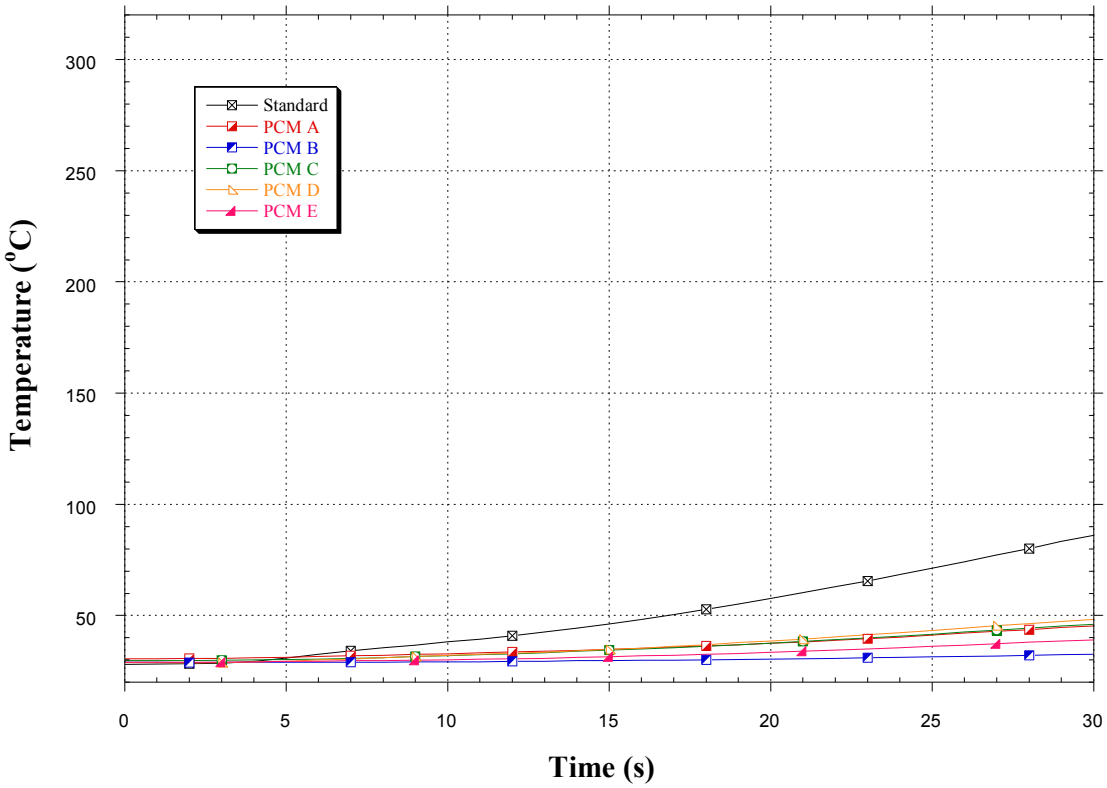

Figure B-12: Series HF – Behind Face Cloth TC Position

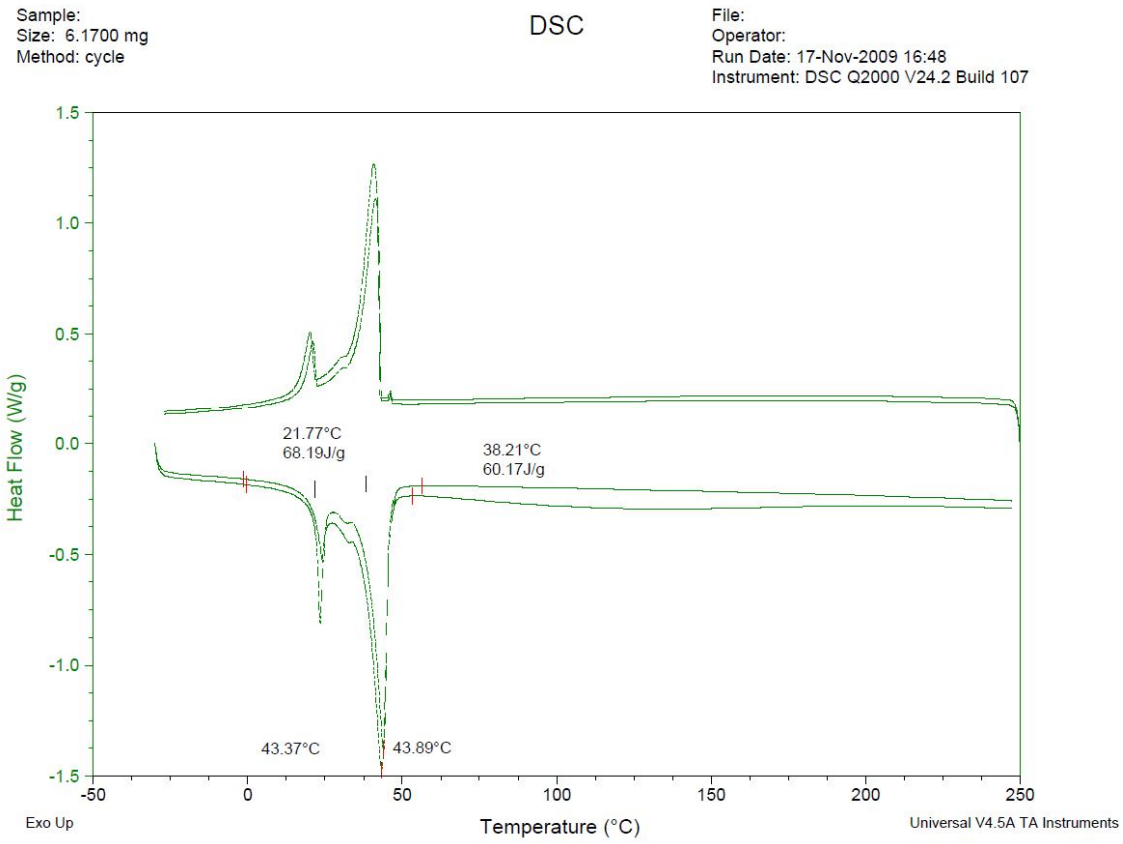

Figure B-13: DSC Results – PCM A

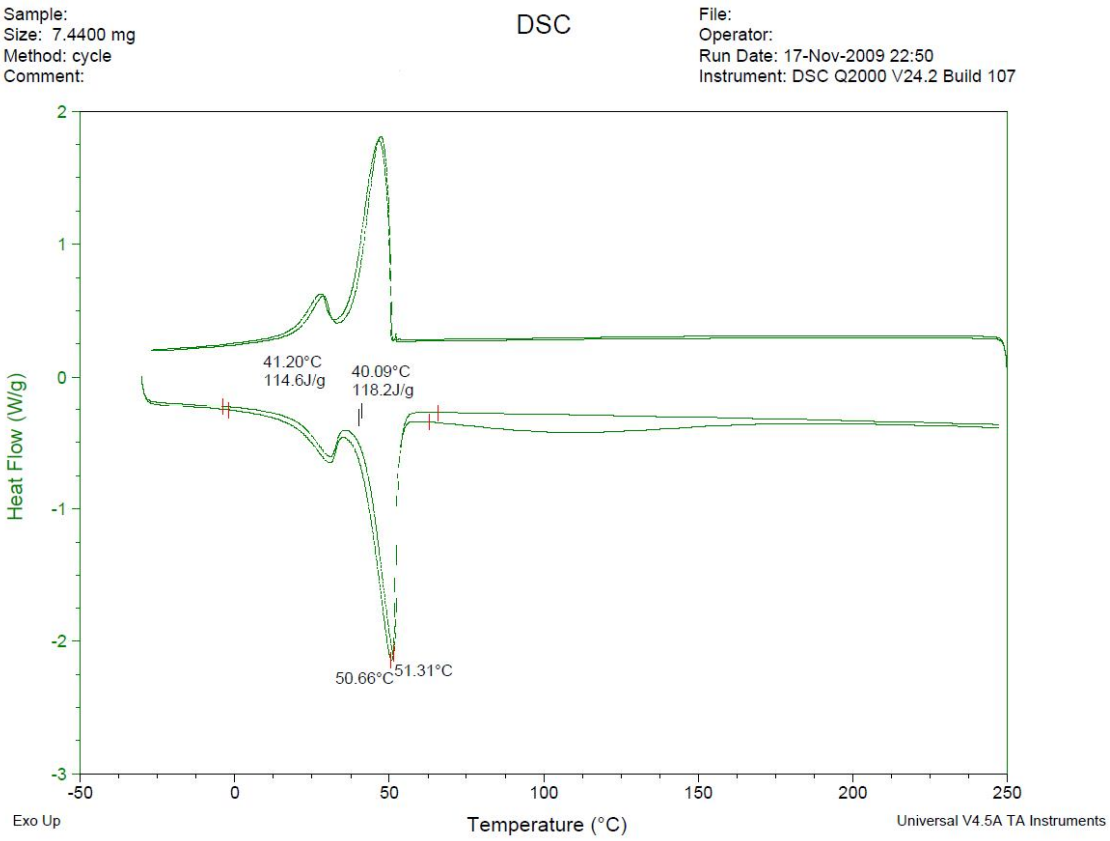

Figure B-14: DSC Results – PCM B

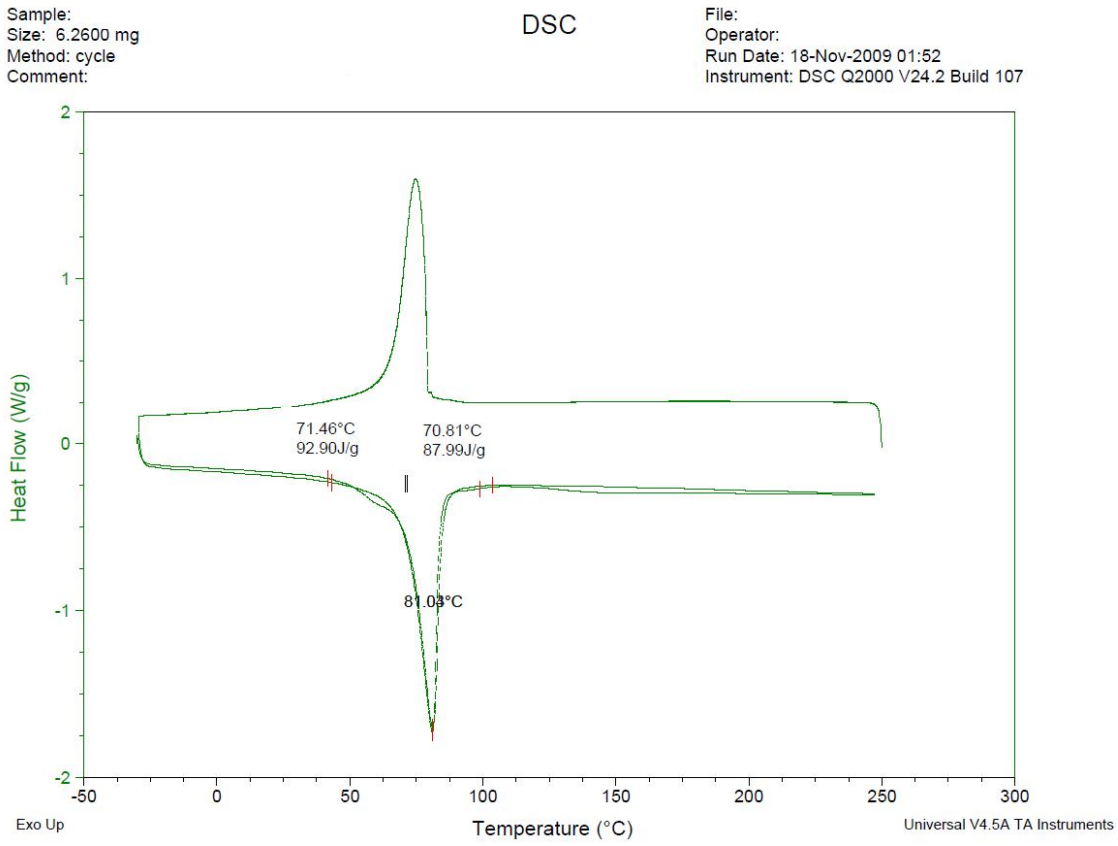

Figure B-15: DSC Results – PCM C

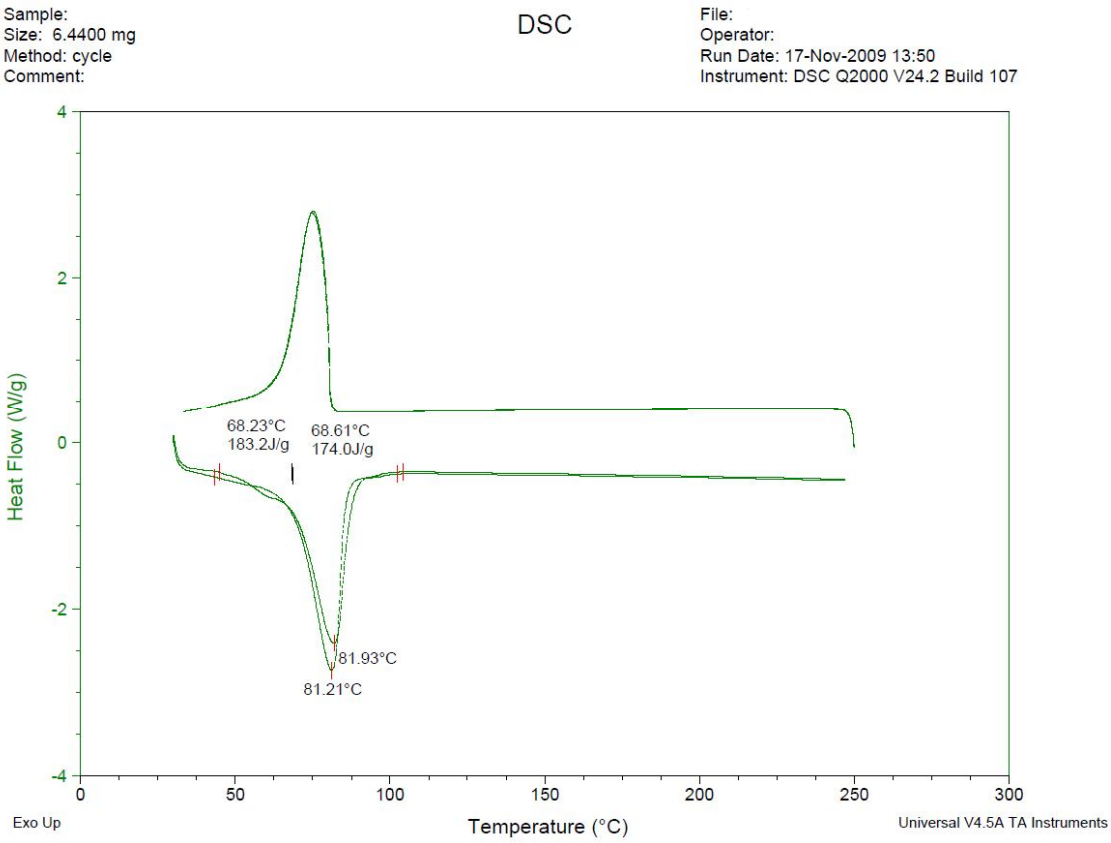

Figure B-16: DSC Results – PCM D

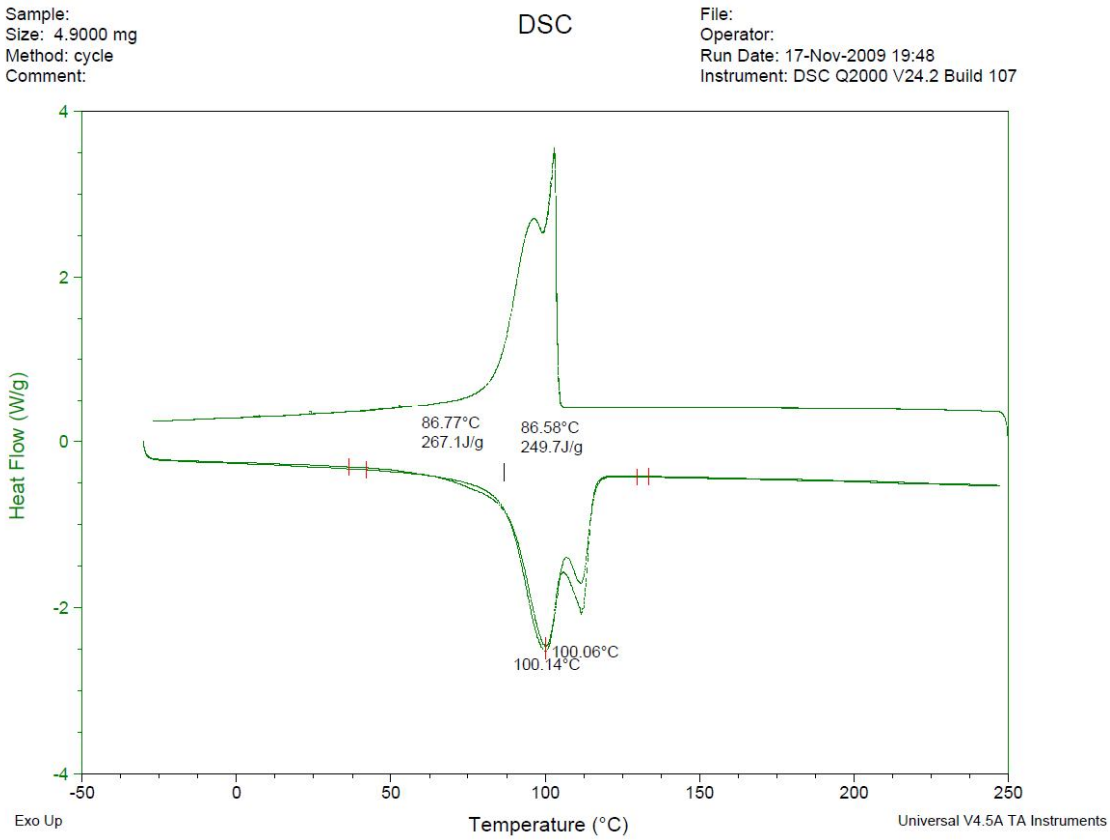

Figure B-17: DSC Results – PCM E

Appendix C

This appendix contains the MATLAB® m-files.

01_FFPC_Single_layer.m

```
%Fire Fighter Protective Clothing Single Layer Assumption
%

clear
clc

% Defining variables
l = 14.8e-3;            % Overall Thickness 14.8 mm
alpha = 15.6e-8;        % Mean value for the Thermal Diffusivity
x1 = 0.46e-3;           % Behind Moisture Barrier 0.46 mm
x2 = 1.26e-3;           % Behind Batting ~ 1.26 mm
x3 = 2.06e-3;           % Behind Face Cloth 2.06 mm
total_t = 300;          % total time for calculation

%Pre-allocating arrays for efficiency
time = zeros(total_t,1);
temp1 = zeros (total_t,1);
temp2 = zeros (total_t,1);
temp3 = zeros (total_t,1);

for t=1:total_t

    time(t) = t;
    temp1(t) = 0;
    temp2(t) = 0;
    temp3(t) = 0;

    for n=1:1000

        temp1(t) = temp1(t) + (1-exp(-
alpha*n^2*pi^2*t/l^2))*(sin(pi*x1*n/l))/(pi*n/2);
        temp2(t) = temp2(t) + (1-exp(-
alpha*n^2*pi^2*t/l^2))*(sin(pi*x2*n/l))/(pi*n/2);
        temp3(t) = temp3(t) + (1-exp(-
alpha*n^2*pi^2*t/l^2))*(sin(pi*x3*n/l))/(pi*n/2);

    end
end

%Plot Labels
hold on
grid on
title('Single Layer, Fixed Temperature Linear Heat Flow Assumption')
ylabel('Dimensionless Temperature, T(x,t)/T_0')
xlabel('Time (s)')

%Plotting T vs t for 3 x positions of interest
plot (time,temp1,'LineWidth',2, 'Color', 'blue')
plot (time,temp2,'LineWidth',2,'Color','red')
plot (time,temp3,'LineWidth',2,'Color','green')
```

TDMA.m

```
%Tridiagonal matrix algorithm - TDMA (Thomas algorithm)
%
% --                        -- --    --  --    --
% | b_1 c_1                  | | T_1 | = | Ti_1 |
% | a_2 b_2 c_2              | | T_2 | = | Ti_2 |
% |     a_3 b_3 c_3          | | T_3 | = | Ti_3 |
% |       .   .   .          | |  .  | = |   .  |
% |           .   .   .      | |  .  | = |   .  |
% |               .   .   . | |  .  | = |   .  |
% |                 a_n b_n | | T_n | = | Ti_n |
% --                       -- --   --   --    --
%
%       Note:   a corresponds to position n-1
%               b corresponds to position n
%               c corresponds position n+1
%               d corresponds to the Temp at position n or Ti_n
%               T is the solution vector.  T is used as a scratch vector in
%               the forward solve replacing "w".
%
%This system can be efficiently solved using LU factorization with backward
%substitution.  Since the coefficient matrix is positive definite, we can
%use LU factorization without pivoting.
%
%    --                        --     --                          --
%    | e_1                      |     |1    f_1                   |
%    | a_2 e_2                  |     |    1    f_2               |
%    |     a_3 e_3              |     |         1    f_3          |
%L = |       .   .              | U = |              .   .        |
%    |           .   .          |     |                  .   .    |
%    |               .   .      |     |                      .   . |
%    |                 a_n e_n  |     |                          1 |
%    --                        --     --                          --
%

function T = TDMA(a,b,c,d)

%Define number of nodes
n = length(d);

%Define e and f in the LU factorization
e = zeros(n,1); f = e;
e(1) = b(1);
f(1) = c(1)/b(1);
for i = 2:n
    e(i) = b(i) - a(i)*f(i-1);
    f(i) = c(i)/e(i);
end

%Forward substitution to solve L*w = d, where w=U*T - note
T(1) = d(1)/e(1);
for i = 2:n
    T(i) = (d(i) - a(i)*T(i-1))/e(i);
end

%Backward substitution to solve U*T = w
for i=(n-1):-1:1
    T(i) = T(i) - f(i)*T(i+1);
End
```

02_FFPC_Single_layer_TriDiagonal.m

```
%Fire Fighter Protective Clothing Single Layer Finite Difference Approx
%
%Approximation of the heat transfer based on a single layer assumption with
%fixed temperatures using a tridiagonal matrix algorithm (Thomas algorithm)
%to solve a Crank-Nicolson finite difference method (CNFDM).
%
%This program requires:
%                       -TDMA.m (tridiagonal matrix algorithm function)
%

% Clear any previously defined variables and the command window.
clear
clc

%% Define initial variables:
dt = 1;                             %Time step (s)
total_t = 300;                      %Total time for calculation (s)
t_steps = total_t/dt;               %Number of time steps

dx = 10e-6;                         %Discretization distance in x-dir (m)
l = 14.8e-3;                        %Overall Thickness (m)
n = round(l/dx);                    %Number of nodes

Initial_T = 0;                      %Initial Temperature (°C)
Max_T = 1;                          %Max Temperature (°C)

alpha = 15.6e-8;                    %Mean value for the Thermal Diffusivity (m²/s)
Fo = alpha*dt/dx^2;                 %Finite difference form of the Fourier number
p1 = round((0.46e-3)/dx);           %Node at x-position behind Moisture Barrier
p2 = round((1.26e-3)/dx);           %Node at x-position behind Batting
p3 = round((2.06e-3)/dx);           %Node at x-position behind Thermal Liner


%% Tridiagonal Matrix Algorithm

%Define intial values of the coeffients CNFDM eqn.  Note that a, b and c
%represent the coefficients on the LHS while d, e, and f represent the
%coefficients on the RHS of the CNFDM eqn.  For the boundary conditions
%(positions 1 and n) the temperatured is fixed, so coefficents on the RHS
%of the RHS of the CNFDM eqn not needed, and the coefficients on the LHS
%are assigned to 0,1,0 respectively.

a = zeros(n,1);
b = zeros(n,1);
c = zeros(n,1);
d = zeros(n,1);
e = zeros(n,1);
f = zeros(n,1);

for i = 1:n
    if (i > 1) && (i < n)

        a(i) = -Fo/2;
        b(i) = (1 + Fo);
        c(i) = -Fo/2;

        d(i) = -a(i);
        e(i) = -b(i) + 2;
```

```
        f(i) = -c(i);
    else
        a(i) = 0;
        b(i) = 1;
        c(i) = 0;
    end
end

%Define inital condition and initial values for T
Ti = zeros(n,1);
T = zeros(n,1);

for i = 1:n
    Ti(i) = Initial_T;
end

for i=2:(n-1)
    T(i) = d(i)*Ti(i-1) + e(i)*Ti(i) + f(i)*Ti(i+1);
end

%Graphics
hold on
grid on
title('Single Layer Finite Difference Method Approximation')
ylabel('Dimensionless Temperature, T(x,t)/T_0')
xlabel('Time (s)')
pause on

%Iterations of CNFDM eqn for each time step
for i = 1:t_steps

    %Define boundary conditions
    T(n) = Initial_T;
    T(1) = Max_T;

    Temp = TDMA(a,b,c,T);
    T_norm = (Temp - Initial_T)/(Max_T - Initial_T);

    %Graphics
    pause(.01);
    plot((i*dt), T_norm(p1), 'b.')
    plot((i*dt), T_norm(p2), 'r.')
    plot((i*dt), T_norm(p3), 'g.')


    for j=2:(n-1)
        T(j) = d(j)*Temp(j-1) + e(j)*Temp(j) + f(j)*Temp(j+1);
    end
end
```

03_FFPC_Multi_Layer.m

```
%
%Fire Fighter Protective Clothing Multi Layer Finite Difference Approx
%
%Approximation of the heat transfer through multiple layers of fire fighter
%protective clothing using a tridiagonal matrix algorithm (Thomas algorithm)
%to solve a Crank-Nicolson finite difference method (CNFDM) equation.
%This program imports actual temperature readings from experimentation for
%the boundary conditions.
%
%This program requires:
%                       -Material Properties ".m" file
%                       -Empirical data ".xls" file
%                       -TDMA.m (tridiagonal matrix algorithm function)
%

% Clear any previously defined variables and the command window.
clear
clc


%% *********         Define initial variables         **********
%

Initial_T = 27;                 %Initial Temperature (°C)
dt = 1;                         %Time step (s)
total_t = 300;                  %Total time for calculation (s)
t_steps = total_t/dt;           %Number of time steps
dx = 10e-6;                     %Discretization distance in x-dir (m)

%
%% *********         Define material properties         **********
%

%Obtain material properties for each layer.  Define the number of nodes
%per layer(N), the nodes at a positions of interest (MB = behind the
%Moisture Barrier, BT = behind the batting, and FC = behind the Face
%Cloth), and the total number of nodes (n).
layers = 0;
n = 1;
stop = 0;
x = 0;

while (stop ~= 1)
    layers = layers + 1;
    [k(layers), rho(layers), Cp(layers), d, x, stop] =
Material_Properties(layers);
    N(layers) = ceil(d/dx);
    n = n + N(layers);

%Assign nodes at positions of interest
    if x ~= 0
        if x == 1;
            MB = n;
        else if x == 2
                BT = n;
            else if x == 3
                    FC = n;
                end
```

```
            end
        end
    end

end

%Define the material properties for each node.
k_n = zeros(n,1);
rho_n = zeros(n,1);
Cp_n = zeros(n,1);
i=1;
j=1;
cnt = 1;

for i=1:layers
    for j = cnt:(cnt + N(i))
        k_n(j) = k(i);
        rho_n(j) = rho(i);
        Cp_n(j) = Cp(i);
    end
     cnt = cnt + N(i) + 1;
end

%Assign Fourier number to each node.
Fo_a = zeros(n,1);
Fo_b = zeros(n,1);
Fo_c = zeros(n,1);

for i = 2:n-1
       Avg = ((rho_n(i)*Cp_n(i) + rho_n(i+1)*Cp_n(i+1))/2);
       Fo_a(i) = (k_n(i)/(Avg))*(dt/dx^2);
       Fo_b(i) = ((k_n(i) + k_n(i+1))/(2*Avg))*(dt/dx^2);
       Fo_c(i) = (k_n(i+1)/(Avg))*(dt/dx^2);
end

%
%% *********         Tridiagonal matrix algorithm         **********
%

%Define initial values of the coefficients CNFDM eqn.  Note that a, b and c
%represent the coefficients on the LHS while d, e, and f represent the
%coefficients on the RHS of the CNFDM eqn.  For the boundary conditions
%(positions 1 and n) the temperature is fixed, so coefficients on the RHS
%of the CNFDM eqn are not needed, and the coefficients on the LHS
%are assigned to 0,1,0 respectively.
a = zeros(n,1);
b = zeros(n,1);
c = zeros(n,1);
d = zeros(n,1);
e = zeros(n,1);
f = zeros(n,1);

for i = 1:n
    if (i > 1) && (i < n)
        a(i) = -Fo_a(i)/2;
        b(i) = (1 + Fo_b(i));
        c(i) = -Fo_c(i)/2;

        d(i) = -a(i);
        e(i) = -b(i) + 2;
        f(i) = -c(i);
```

```
    else
        a(i) = 0;
        b(i) = 1;
        c(i) = 0;
    end
end

%Define initial condition and initial values for T (RHS of CNFDM eqn)
Ti = zeros(n,1);
T = zeros(n,1);

for i = 1:n
    Ti(i) = Initial_T;
end

for i=2:(n-1)
    T(i) = d(i)*Ti(i-1) + e(i)*Ti(i) + f(i)*Ti(i+1);
end

%Import empirical data
Input = xlsread ('input');

%Graphics
hold on
grid on
title('Multi Layer FDM Approximation - Theoretical vs Empirical')
ylabel('Temperature (°C)')
xlabel('Time (s)')
pause on

%Iterations of CNFDM eqn for each time step
for i = 1:t_steps

%Define boundary conditions:
    T(1) = Input(ceil(i*dt),1);
    T(n) = Input(ceil(i*dt),5);

%Tri-diagonal Matrix Algorithm
    Temp = TDMA(a,b,c,T);

%Re-define RHS of CNFDM
    for j=2:(n-1)
        T(j) = d(j)*Temp(j-1) + e(j)*Temp(j) + f(j)*Temp(j+1);
    end

%Graphics
    pause(.01);
    plot((i*dt), Temp(MB), '.b')
    plot((i*dt), Temp(BT), '.b')
    plot((i*dt), Temp(FC), '.b')

    plot((i*dt), Input(i,2), '.g')
    plot((i*dt), Input(i,3), '.g')
    plot((i*dt), Input(i,4), '.g')

end
```

04_FFPC_Multi_Layer_PCMB.m

```
%
%Fire Fighter Protective Clothing Multi Layer Finite Difference Approx
%
%Approximation of the heat transfer through multiple layers of fire fighter
%protective clothing using a tridiagonal matrix algorithm (Thomas algorithm)
%to solve a Crank-Nicolson finite difference method (CNFDM) equation.
%This program imports actual temperature readings from experimentation for
%the boundary conditions.
%
%This program requires:
%                       -Material Properties ".m" file
%                       -Empirical data ".xls" file
%                       -TDMA.m (tridiagonal matrix algorithm function)
%

%Clear any previously defined variables and the command window.
clear
clc


%% *********         Define initial variables         **********
%

Initial_T = 30;                 %Initial Temperature [°C]
dt = 1;                         %Time step [s]
total_t = 300;                  %Total time for calculation [s]
t_steps = total_t/dt;           %Number of time steps
dx = 10e-6;                     %Discretization distance in x-dir [m]

%
%% *********         Define material properties         **********
%

%Obtain material properties for each layer.  Define the number of nodes
%per layer(N), the nodes at a positions of interest (MB = behind the
%Moisture Barrier, BT = behind the batting, and FC = behind the Face
%Cloth), and the total number of nodes (n).
layers = 0;
n = 1;
stop = 0;
x = 0;

while (stop ~= 1)
    layers = layers + 1;
    [k(layers), rho(layers), Cp(layers), d, x, stop] =
Material_Properties(layers);
    N(layers) = ceil(d/dx);
    n = n + N(layers);

%Assign nodes and layers for positions/layers of interest
    if x ~= 0
        if x == 1;
            MB = n;
        else if x == 2
                BT = n;
            else if x == 3
                    FC = n;
                else if x == 4
```

```
                    pcm = layers;
                end
            end
        end
    end
end

%Define the material properties for each node.
k_n = zeros(n,1);
rho_n = zeros(n,1);
Cp_n = zeros(n,1);
i=1;
j=1;
cnt = 1;

for i=1:layers
    for j = cnt:(cnt + N(i))
        k_n(j) = k(i);
        rho_n(j) = rho(i);
        Cp_n(j) = Cp(i);
    end
     cnt = cnt + N(i) + 1;
end

%Assign Fourier number to each node.
Fo_a = zeros(n,1);
Fo_b = zeros(n,1);
Fo_c = zeros(n,1);

for i = 2:n-1
       Avg = ((rho_n(i)*Cp_n(i) + rho_n(i+1)*Cp_n(i+1))/2);
       Fo_a(i) = (k_n(i)/(Avg))*(dt/dx^2);
       Fo_b(i) = ((k_n(i) + k_n(i+1))/(2*Avg))*(dt/dx^2);
       Fo_c(i) = (k_n(i+1)/(Avg))*(dt/dx^2);
end

%
%% *********         Finite Deference Method         **********
%

%Define initial values of the coefficients CNFDM eqn.  Note that a, b and c
%represent the coefficients on the LHS while d, e, and f represent the
%coefficients on the RHS of the CNFDM eqn.  For the boundary conditions
%(positions 1 and n) the temperature is fixed, so coefficients on the RHS
%of the CNFDM eqn are not needed, and the coefficients on the LHS
%are assigned to 0,1,0 respectively.
a = zeros(n,1);
b = zeros(n,1);
c = zeros(n,1);
d = zeros(n,1);
e = zeros(n,1);
f = zeros(n,1);

for i = 1:n
    if (i > 1) && (i < n)
        a(i) = -Fo_a(i)/2;
        b(i) = (1 + Fo_b(i));
        c(i) = -Fo_c(i)/2;
```

```
        d(i) = -a(i);
        e(i) = -b(i) + 2;
        f(i) = -c(i);
    else
        a(i) = 0;
        b(i) = 1;
        c(i) = 0;
    end
end

%Define initial condition and initial values for T (RHS of CNFDM eqn)
Ti = zeros(n,1);
T = zeros(n,1);

for i = 1:n
    Ti(i) = Initial_T;
end

for i=2:(n-1)
    T(i) = d(i)*Ti(i-1) + e(i)*Ti(i) + f(i)*Ti(i+1);
end

%Import empirical data
Input = xlsread ('input');

%Graphics
hold on
grid on
title('Multi Layer FDM Approximation - Theoretical vs Empirical')
ylabel('Temperature (°C)')
xlabel('Time (s)')
pause on

%Define variables for latent heat approximation
 L = 105;                    %Latent heat of PCM [kJ/kg]
 m = rho(pcm)*dx*0.01;       %Mass per CV [kg] (note 0.01 m² is the SA)
 T1 = 44;                    %Starting Melting Temperature [°C]
 T2 = 55;                    %Starting Melting Temperature [°C]
 Tm = (T2 + T1)/2;           %Approximate Melting Temperature [°C]
 Tr = (T2 - T1);            %Range of Melting Temperature [°C]
 T_energy = zeros(n,1);      %Total available latent energy per CV [kJ]
 energy = zeros(n,1);        %Amount of latent energy used[kJ]

for i = 1:n
    T_energy(i) = m*L;
end

%Iterations of CNFDM eqn for each time step
for i = 1:t_steps

%Define boundary conditions:
    T(1) = Input(ceil(i*dt),1);
    T(n) = Input(ceil(i*dt),5);

%Tri-diagonal Matrix Algorithm
    Temp = TDMA(a,b,c,T);

%Re-define RHS of CNFDM with latent heat calculation for the PCM layer.
%
%To remove the latent heat, the node of interest must be:
%           -Within the melting temperature range
```

```
%           -Within the PCM layer
%           -Not completely changed phase
%           -The heat flux across the control volume must be positive
%           -The upper limit of latent heat absorbed is equal to the
%               calculated heat flux.

    for j=2:(n-1)
         if (Temp(j) >= T1) && (Temp(j) <= T2)
             if (j > BT) && (j < (BT + N(pcm)))
                 if energy(j) < T_energy(j)
                     qmax = 0.6*(k(pcm)/(dx)^2*(Temp(j+1)- 2*Temp(j) + Temp(j-
1)))*dt/(rho(pcm) * Cp(pcm));
                     if qmax > 0;
                        q = L*dt/Cp(pcm) * 1.4 *(1-erf(abs((Temp(j)- Tm)/Tr)));
                        if q > qmax
                            q = qmax;
                        end
                        T(j) = d(j)*Temp(j-1)+e(j)*Temp(j)+f(j)*Temp(j+1)-q;
                        energy(j) = energy(j) + q*Cp(pcm)*m;
                     else
                         T(j) = d(j)*Temp(j-1) + e(j)*Temp(j) + f(j)*Temp(j+1);
                     end
                 else
                     T(j) = d(j)*Temp(j-1) + e(j)*Temp(j) + f(j)*Temp(j+1);
                 end
             else
                 T(j) = d(j)*Temp(j-1) + e(j)*Temp(j) + f(j)*Temp(j+1);
             end
         else
            T(j) = d(j)*Temp(j-1) + e(j)*Temp(j) + f(j)*Temp(j+1);
         end
    end

%Graphics
    pause(.01);
    plot((i*dt), Temp(MB), '.b')
    plot((i*dt), Temp(BT), '.b')
    plot((i*dt), Temp(FC), '.b')

    plot((i*dt), Input(i,2), '.g')
    plot((i*dt), Input(i,3), '.g')
    plot((i*dt), Input(i,4), '.g')


end
```

Material_Properties.m

```
%
%This function defines the material properties for each layer.
%
function [k, rho, Cp, d, x, stop] = Material_Properties (layer)
switch layer

%Defining Layer 1 - Air Gap
    case(1)
        k = 0.041e-3;           %(kW/m-K)
        rho = 0.70;             %(kg/m³)
        Cp = 1.03;              %(kJ/kg-K)
        d = 0.75e-3;            %(m)
        x = 0;
        stop = 0;

%Defining Layer 2 - Moisture Barrier
    case(2)
        k = 0.134e-3;           %(kW/m-K)
        rho = 316.8;            %(kg/m³)
        Cp = 2.75;              %(kJ/kg-K)
        d = 0.46e-3;            %(m)
        x = 1;
        stop = 0;

%Defining Layer 3 - Air Gap
    case(3)
        k = 0.041e-3;           %(kW/m-K)
        rho = 0.70;             %(kg/m³)
        Cp = 1.03;              %(kJ/kg-K)
        d = 0.5e-3;             %(m)
        x = 0;
        stop = 0;

%Defining Layer 4 - Batting
    case(4)
        k = 0.088e-3;           %(kW/m-K)
        rho = 54;               %(kg/m³)
        Cp = 3.4;               %(kJ/kg-K)
        d = 0.80e-3;            %(m)
        x = 2;
        stop = 0;

%Defining Layer 5 - Air Gap
    case(5)
        k = 0.041e-3;           %(kW/m-K)
        rho = 0.70;             %(kg/m³)
        Cp = 1.03;              %(kJ/kg-K)
        d = 0.75e-3;               %(m)
        x = 0;
        stop = 0;

%Defining Layer 6 - PCM B
    case(6)
        k = 0.1e-3;             %(kW/m-K)
        rho = 640;              %(kg/m³)
        Cp = 1.6;               %(kJ/kg-K)
        d = 2.45e-3;             %(m)
        x = 4;
```

```
        stop = 0;

%Defining Layer 7 - Face Cloth
    case(7)
        k = 0.14e-3;            %(kW/m-K)
        rho = 316.9;            %(kg/m³)
        Cp = 3.51;              %(kJ/kg-K)
        d = 0.24e-3;            %(m)
        x = 3;
        stop = 0;

%Defining Layer 8 - Air Gap
    case(8)
        k = 0.041e-3;           %(kW/m-K)
        rho = 0.70;             %(kg/m³)
        Cp = 1.03;              %(kJ/kg-K)
        d = 2e-3;            %(m)
        x = 0;
        stop = 0;

%Defining Layer 9 - Calcium Silicate Board
    case(9)
        k = 0.12e-3;            %(kW/m-K)
        rho = 737;              %(kg/m³)
        Cp = 1.26;              %(kJ/kg-K)
        d = 13.02e-3;           %(m)
        x = 0;
        stop = 1;
end
```

References

[1] M.J. Karter Jr, “Patterns of Firefighter Fireground Injuries,” National Fire Protection Association, Quincy, MA, May. 2009.

[2] R.F. Fahy, P.R. LeBlanc, and J. Molis, “Firefighter Fatalities in the United States—2008,” National Fire Protection Association, Quincy, MA, Jul. 2009.

[3] NFPA 1971 Standard on Protective Ensembles for Structural Fire Fighting and Proximity Fire Fighting, 2007 Edition, Quincy, MA: National Fire Protection Association, 2006.

[4] National Institute of Standards and Technology (NIST), “Fire.Gov - Turnout Gear.” Internet: http://www.fire.gov/turnout/index.htm, Feb. 2, 2008 [Dec. 20, 2009]

[5] North Carolina State University College of Textiles, “T-PACC.” Internet: http://www.tx.ncsu.edu/tpacc/general.html [Dec. 20, 2009]

[6] National Institute for Occupational Safety and Health, “NIOSH - NPPTL - The National Personal Protective Technology Laboratory.” Internet: http://www.cdc.gov/niosh/npptl/, Jan. 14, 2010 [Dec. 20, 2009]

[7] W.E. Mell and J.R. Lawson, "A Heat Transfer Model for Fire Fighter's Protective Clothing," NISTIR 6299, National Institute of Standards and Technology, Gaithersburg, MD, 1999.

[8] K. Prasad, W. Twilley, and J.R. Lawson, "Thermal Performance of Fire Fighters’ Protective Clothing. 1. Numerical Study of Transient Heat and Water Vapor Transfer," NISTIR 6881, National Institute of Standards and Technology, Gaithersburg, MD, 2002.

[9] K. Prasad, H.M.H. Dac, and S.R. Kukuck, "Thermal Performance of Fire Fighters’ Protective Clothing. 2. Protective Clothing Performance Simulator-User’s Manual," NISTIR 6901, National Institute of Standards and Technology, Gaithersburg, MD, 2003.

[10] S. Kukuck and K. Prasad, "Thermal Performance of Fire Fighters’ Protective Clothing. 3. Simulating a TPP Test for Single-Layered Fabrics," NISTIR 6993, National Institute of Standards and Technology, Gaithersburg, MD, 2003.

[11] R. Barker, "A Review of Gaps and Limitations in Test Methods for First Responder Protective Clothing and Equipment," Report Presented to National Personal Protection Technology Laboratory, 2005.

[12] N. Keltner, "Evaluating thermal protective performance testing," *Journal of ASTM International*, vol. 2, 2005, pp. 45-56.

[13] "Thermal Capacity of Fire Fighter Protective Clothing," Fire Protection Research Foundation, Quincy, MA, Oct. 2008.

[14] T.S. Fay, "Development of an Improved Fabric Flammability Test," M.S. Thesis, Worcester Polytechnic Institute, MA, 2002.

[15] J.J. Barry and R.W. Hill, "Computational Modeling of Protective Clothing," *International Nonwovens Journal*, vol. 12, Fall. 2003, pp. 25–34.

[16] P. Chitrphiromsri and A.V. Kuznetsov, "Modeling heat and moisture transport in firefighter protective clothing during flash fire exposure," *Heat and Mass Transfer*, vol. 41, 2005, pp. 206–215.

[17] R.C. Heniford, "The Effects of Batting Materials on the Performance of Turnout Thermal Liners," M.S. Thesis, North Carolina State University, NC, 2005.

[18] K. Spangler, "Energy Transport in Firefighter Protective Clothing," M.S. Thesis, University of Maryland, College Park, 2008.

[19] Y. Shin, D.I. Yoo, and K. Son, "Development of thermoregulating textile materials with microencapsulated phase change materials (PCM). II. Preparation and application of PCM microcapsules," *Journal of Applied Polymer Science*, vol. 96, 2005, pp. 2005–2010.

[20] "PCM Thermal Solutions, Inc.," Internet: http://www.pcm-solutions.com/, 2008 [Dec. 20, 2009].

[21] J. Gates, "Phase Change Material Home Page." Internet: http://freespace.virgin.net/m.eckert/, Dec. 29, 2000 [Dec. 20, 2009]

[22] K. Koo, Y. Park, J. Choe, and E. Kim, "The application of microencapsulated phase-change materials to nylon fabric using direct dual coating method," *Journal of Applied Polymer Science*, vol. 108, 2008, pp. 2337–2344.

[23] B. Zalba, J.M. Marín, L.F. Cabeza, and H. Mehling, "Review on thermal energy storage with phase change: materials, heat transfer analysis and applications," *Applied Thermal Engineering*, vol. 23, Feb. 2003, pp. 251-283.

[24] U.S. NASA Center for AeroSpace Information, "Spinoff 2004-COVERED IN COMFORT," Internet: http://www.sti.nasa.gov/tto/Spinoff2004/ch_1.html, Feb. 27, 2009 [Dec. 20, 2009].

[25] B.H. Pause, "New heat protective garment with phase change material," *Performance of protective clothing: issues and priorities for the 21st century*, vol. 7, ASTM STP 1386, 2000.

[26] D.V. Hale, M.J. Hoover, and M.J. ONeill, *Phase change materials handbook*, Lockheed Missiles and Space Co Inc, Huntsville, AL, 1971.

[27] Rubitherm Technologies GmbH, "RUBITHERM GmbH." Internet: http://www.rubitherm.com/english/index.htm [Dec. 28, 2009]

[28] Microtek Laboratories, Inc., "Microtek Laboratories - MicroPCMs," Internet: http://www.microteklabs.com/micropcm.html, 2009 [Dec. 28, 2009]

[29] G.A. Selkirk, T.M. McLellan, and J. Wong, "Active versus passive cooling during work in warm environments while wearing firefighting protective clothing," *Journal of Occupational and Environmental Hygiene*, vol. 1, 2004, pp. 521-531.

[30] S. Sayar, "Heat Transfer During Melting and Solidification in Heterogeneous Materials," M.S. Thesis, Virginia Polytechnic Institute and State University,VA 2000.

[31] F. Li, C. Wu, and Y. Li, "Model of heat and moisture transfer in porous textiles with microencapsulated phase change materials," *Dalian Ligong Daxue Xuebao/Journal of Dalian University of Technology*, vol. 48, 2008, pp. 162-167.

[32] Y. Ding, G.N. Mercer, and A.J. Roberts, "A finite element modeling of thermal conductivity of fabrics embedded with phase change material," *Australia and New Zealand Industrial and Applied Mathematics Journal*, vol. 49, Dec. 2007, pp. C439-C456.

[33] J.A. Gear, M.J. Lachut, and Y. Ding, "Enhanced thermal performance of garments embedded with encapsulated phase change material," *Australia and New Zealand Industrial and Applied Mathematics Journal*, vol. 47, Jul. 2006, pp. C137-C151.

[34] R.M. Rossi and W.P. Bolli, "Phase Change Materials for the Improvement of Heat Protection," *Advanced Engineering Materials*, vol. 7, 2005, pp. 368–374.

[35] G.N. Mercer and H.S. Sidhu, "Mathematical modelling of the effect of fire exposure on a new type of protective clothing," *Australia and New Zealand Industrial and Applied Mathematics Journal*, vol. 49, Dec. 2007, pp. C289-C305.

[36] M.J. Karter Jr and J. Molis, "U.S. Fire Fighter Injuries -2006,"National Fire Protection Association, Quincy, MA, Nov. 2007.

[37] M.K. Donnelly, W.D. Davis, J.R. Lawson, and M.S. Selepak, "Thermal Environment for Electronic Equipment used by First Responders," NIST Technical Note 1474, National Institute of Standards and Technology, Gaithersburg, MD, 1996.

[38] J.R. Lawson, "Fire Facts, Heat Flux & Response," 2nd Edition, National Institute of Standards and Technology, Gaithersburg, MD, Apr. 2007.

[39] British Standards Institution, "BS EN 136:1998. Respiratory protective devices—full face masks—requirements, testing, marking.," London, 1998.

[40] K.A. DeMars, W.P. Henderson, and M. Liu, "Thermal Measurements for Fire Fighters' Protective Clothing," Thermal Measurements: The Foundation of Fire Standards, ASTM STP 1427, L.A. Gritzo and N.J. Alvares, Eds., American Society for Testing Materials, West Conshohocken, PA, 2002.

[41] American Society of Testing and Materials, E162 Standard Test Method for Surface Flammability of Materials Using Radiant Heat Energy Source, *Annual Book of ASTM Standards*, West Conshohocken, PA, 1997.

[42] J. R. Lawson and W.H. Twilley, "Developement of an Apparatus for Measuring the Thermal Performance of Fire Fighters' Protective Clothing," NISTIR 6400, National Institute of Standards and Technology, Gaithersburg, MD, 1999.

[43] R.L. Vettori, W.H. Twilley, and D. Stroup, "Measurement techniques for low heat flux exposures to fire fighters protective clothing," NISTIR 6750, National Institute of Standards and Technology, Gaithersburg, MD, 2001.

[44] H. Brown, "Firefighter Turnout Coat Configurations: Performance Data for Acquisition Decisions," NISTIR 7141, National Institute of Standards and Technology, Gaithersburg, MD 2005.

[45] American Society for Testing and Materials, C 1055, Standard Guide for Heated Systems Surface Conditions That Produce Contact Burn Injuries, *Annual Book of ASTM Standards,* West Conshohocken, PA 1998.

[46] F. Incropera, D. DeWitt, T. Bergman, and A. Lavine, *Fundamentals of Heat and Mass Transfer*, John Wiley & Sons, Inc., Hoboken, NJ, 2007.

[47] J.R. Lawson, W.D. Walton, N.P. Bryner, and F.K. Amon, "Estimates of Thermal Properties for Fire Fighters' Protective Clothing Materials," NISTIR 7282, National Institute of Standards and Technology, Gaithersburg, MD, 2005.

[48] H. Carslaw and J. Jaeger, *Conduction of Heat in Solids*, Second Edition, Oxford University Press, Oxford, 1956.

[49] Omega Engineering Inc., "Revised Thermocouple Reference Tables, Type K," The Temperature Handbook, vol. MM, pp. z218 - z220.